Electronic Supplementary Material (ESI) for Dalton Transactions.

Reduced quenching effect of pyridine ligands in highly luminescent Ln(III) complexes: the role of tertiary amide linkers

Daniel Kocsi, Daniel Kovacs, Jordann A. L. Wells, K. Eszter Borbas*

Department of Chemistry, Ångström Laboratory, Box 523, Uppsala University, 75120, Uppsala, Sweden.

eszter.borbas@kemi.uu.se

Table of contents

General experimental procedures

^{1}H NMR (400 MHz), ^{13}C NMR (101 MHz) and ^{19}F NMR (376 MHz) spectra were recorded on a JEOL 400 MHz instrument. Chemical shifts were referenced to residual solvent peaks and are given as follows: chemical shift (δ, ppm), multiplicity (s, singlet; br, broad; d, doublet, t, triplet; q, quartet; m, multiplet), coupling constant (Hz), integration. LC-MS analysis was carried out using an analytical Dionex UltiMate 3000 HPLC instrument coupled to a Thermo Finnigan LCQ DECA XP MAX mass spectrometer. HR-ESI-MS analyses were performed at the Organisch Chemisches Institut WWU Münster, Germany or at the Stenhagen Analyslab AB, Mölndal. All compounds displayed the expected isotope distribution pattern. Anhydrous CH_2Cl_2 was obtained by distillation from CaH_2 under an Ar atmosphere.

Compounds **1a**, **1b**, **1c**[1] and **3**[2] were synthesised following literature methods. All other chemicals were from commercial sources and used as received.

Paramagnetic ^{1}H NMR. ^{1}H NMR spectra of Eu-complexes were recorded at 400 MHz in D_2O (~2 mM) using the following parameters: relaxation delay: 1 s; number of scans: 128; number of points: 131072; range: –25 to +35 ppm. ^{19}F NMR spectra of Eu-complexes were recorded at 376 MHz in D_2O using the following parameters: relaxation delay: 1 s; number of scans: 128; number of points: 262144; range: –300 to +100 ppm. Variable temperature measurements were recorded at 80 °C using 600 s temperature delay. In all cases chemical shifts were referenced to HDO (4.79 ppm), phase correction and exponential decay as apodization function (1 Hz has been applied) were performed.

Electrochemistry. Cyclic voltammograms (CV) were obtained in an argon atmosphere at room temperature (~20 °C) using an AUTOLAB PGSTAT 204N potentiostat, equipped with a 3 mm glassy carbon (GC) working electrode, a Pt wire auxiliary electrode, and an $Ag/AgCl/KCl_{(sat)}$ as a reference. The solution was allowed to equilibrate for 10 s at the start potential before starting the measurements. A step potential of –0.9 mV was used for 100 mV/s scan rate. Measurements were carried out in acetonitrile solutions in the presence of $TBAPF_6$ (0.2 M) as the supporting electrolyte.

General procedure for CV measurements: the electrolyte solution was added to the electrochemical cell, and the sample was purged with a stream of Ar for 10 min prior to each measurement. The working electrode was polished with 0.05 µm alumina on a polishing pad, washed with water and ethanol, and dried with air. The three electrodes (GC working electrode, Pt wire auxiliary electrode, and $Ag/AgCl/KCl_{(sat)}$ reference electrode) were inserted into the cell setup and a background scan was recorded with a scan rate of 100 mV/s, and four sweeps. The appropriate compound (~1 mM) was added and the resulting solution was purged with argon for 10 min. Scans were recorded at 100 mV/s rate with two sweeps for each measurement.

Chromatography. Preparative chromatography was carried out on silica gel [Normasil 60 chromatographic silica media (40–63 micron)] and aluminum oxide [activated, neutral, Brockmann Activity I, Sigma-Aldrich]. Thin layer chromatography was performed on silica-coated (60G F_{254}) Al plates from Merck and aluminum oxide coated with 254 nm fluorescent indicator Al plates from Sigma-Aldrich. Samples were visualised by UV-light (254 and 365 nm) and permanganate stain.

HPLC-analysis was performed on a Dionex UltiMate 3000 system using a Phenomenex Gemini® C18 TMS end-capped 150 mm×4.6 mm HPLC column with HPLC water (0.05% formic acid): MeCN (0.05% formic acid) eluent system using the methods: (a) 0–10 min: 10%→90% MeCN, 0.5 mL/min; (b) 0–12 min: 10→50%, 12–16 min: 50→90% MeCN, 0.5 mL/min; (c) 0–8 min: 10→20% & 8–12 min: 20% iso & 12–16 min 20→90% MeCN, 0.5 mL/min. UV (UltiMate 3000 Photodiode Array Detector) and ESI-MS detections (LCQ DECA XP MAX) were used.

UV-Vis absorption and emission spectroscopy. All measurements were performed in PIPES-buffered distilled water at pH 6.5 or D_2O. [**LnL**] was nominally 10 µM, however, small quantities of Ln salts may diminish this. Glycerol was of 99.9+% purity. Quartz cells with 1 cm optical pathlengths were used for the room temperature measurements. The absorbance spectra were measured by a Varian Cary 100 Bio UV-Visible spectrophotometer. The emission and excitation spectra, lifetimes, time-resolved spectra and quantum yields were recorded on a Horiba FluoroMax-4P. All emissions were corrected by the wavelength sensitivity (correction function) of the spectrometer. All measurements were performed at room temperature unless stated otherwise.

Quantum yields were measured at room temperature, using quinine sulfate (QS) in H_2SO_4 0.05 M (Φ_{ref} = 0.59) as reference.[3] Quantum yields were calculated according to Eq. S1, with Φ_s the quantum yield of the sample, Φ_{ref} the quantum yield of the reference, I the integrated corrected emission intensity of the sample (s) and of the reference (ref), f_A the absorption factor of the sample (s) and of the reference (ref) at the excitation wavelength and n the refractive indexes of the sample (s) and of the reference (ref). The concentration of the complexes was adjusted to obtain an absorbance around the maxima of the antennae matching that of the QS fluorescence standard. The excitation wavelength where the absorption factors of the samples and of the reference were the same was chosen (i.e. where the absorptions are identical). The corrected emission spectra of the sample and reference standard were then measured under the same conditions over the 315–800 nm spectral range as well as blank samples containing only the solvent (i.e. PIPES-buffered aqueous solutions). The appropriate blanks were subtracted from their respective spectra, and the antenna fluorescence and Ln(III) luminescence were separated by fitting the section of the antenna emission overlapping the Ln(III) emission with an exponential decay or with a scaled emission spectrum from the corresponding Gd(III) complexes. The quantum yields were then calculated according to Eq. S1. The given relative error on the quantum yields ($\delta\Phi = \Delta\Phi/\Phi$, where $\Delta\Phi$ is the absolute error) take into account the accuracy of the spectrometer and of the integration procedure [$\delta(I_s/I_{ref}) < 2\%$], an error of 0.59 ±0.01 on the quantum yield of the reference QS [$\delta(\Phi_{ref}) < 2\%$], an error on the ratio of the absorption factors [$\delta(f_{Aref}/f_{As}) < 5\%$, relative to the fixed absorption factor of the reference QS] and an error on the ratio of the squared refractive indexes [$\delta(n_s^2/n_{ref}^2) < 1\%$, < 0.25% around 1.333 for H_2O[4] on each individual refractive index], which sums to a total estimated relative error that should be $\delta\Phi_s < 10\%$. A limit value of 10% is thus chosen.

$$\Phi_s = \frac{I_s}{I_{ref}} \cdot \frac{f_{Aref}}{f_{As}} \cdot \frac{(n_s)^2}{(n_{ref})^2} \cdot \Phi_{ref} \qquad \text{Eq. S1}$$

Low temperature measurements were done in quartz capillaries (0.2 cm optical pathlength) at 77 K by immersion in a liquid N_2-filled quartz Dewar and with addition of glycerol (1 drop) to the solutions (9 drops) measured at room temperature.

Lifetimes were recorded 0.05 ms after pulsed excitation at the excitation maxima (λ_{exc}) of 329, 331 and 342 nm of **LnL^{t,Me}**, **LnL^{t,MOM}** and **LnL^{t,CF3}**, respectively, by measuring the decay of the lanthanide

main emission peak (614 nm for Eu and 543 nm for Tb). The increments after the initial delay were adjusted between 0.2–20 μs depending on the lifetime in order to have a good sampling of the decay. The obtained data were fitted by single and double exponential decay models in OriginPro 9, and the most reliable value was chosen according to the adjusted R^2 value and the shape of the residuals. A relative error of 10% is typically found among a series of measurements on the same sample.

Hydration numbers (q) were obtained by measuring the lifetimes of the same quantity of complex in a PIPES-buffered solution in H_2O and in D_2O and fitting the difference according to the model of Horrocks et al.,[5] and Beeby et al.[6]

Photostability experiments were performed on a Horiba FluoroMax-4P fluorimeter in quartz cuvettes (1 cm optical pathlengths) by continuously irradiating the whole volume (3 mL) of the sample in a Horiba FluoroMax-4P (150 W Xenon lamp) set at the maximum excitation wavelength of the sample with the excitation slit at 2 nm (Tb) or 3 nm (Eu), respectively. Samples were dissolved at [**LnL**] = 10 μM in PIPES-buffered distilled water at pH 6.5. The sample was continuously irradiated for 4 h. The steady-state Ln(III) emission was recorded every 30 min over a 4 h-period upon continuous irradiation. Measurements were performed over the 450–750 nm spectral range using 395 nm filter for Tb and 550–800 nm spectral range using 500 nm filter for Eu, respectively. Integrated emission intensities of the whole spectral range were normalised to the value at t_0.

Crystallography. Measurements were performed using graphite-monochromatised Mo K_α radiation at 170 K using a Bruker D8 APEX-II equipped with a CCD camera. The structure was solved by direct methods (SHELXS-2014) and refined by full-matrix least-squares techniques against F^2 (SHELXL-2018). The non-hydrogen atoms were refined with anisotropic displacement parameters. The H atoms of the CH_2 / CH groups were refined with common isotropic displacement parameters for the H atoms of the same group, and idealised geometry. The H atoms of the methyl groups were refined with common isotropic displacement parameters for the H atoms of the same group, and idealised staggered geometry. Both solid-state structures incorporate $LnCl_3$ as a fully hydrated Ln^{3+} ion with chloride ligands in the crystal lattice. The Ln^{3+} ion acts as a bridging ligand between two **LnLt^{t,Me}** molecular units. The inclusion of the

$[Ln(OH_2)_6]^{3+}$ "node" was not intentional and is likely due to the excess amounts of Ln precursor used during the synthesis. The Cl atom locations were determined crystallographically by initially allocating density to O atoms which were allowed to freely refine. The impact of changing O to Cl on either the statistics (e.g. R1) or the shape and size of ellipsoids was monitored to establish which sites may correspond to Cl atom positions. This was employed in order to conserve the charge balance in the unit cell/asymmetric unit. The 'real' situation may be more akin to multiple Cl sites of low occupancy in the solvent lattice, making them near indistinguishable from disordered lattice solvent (water) molecules.

Specific for **GdLt^{t,Me}**: Disorder of the carbostyril antenna was modelled over two sites. A third disordered position may also be present; however, no stable refinement could be reached upon modelling. The occupancy of Gd2 was set to 75%. Several of the Gd2-bound water ligands are disordered, but the occupancy of these ligands was set such that the sum of the parts equals 1 (i.e. 100% occupancy). Residual density about Gd2 (two Q peaks) could be ascribed to a disordered water molecule which resides over two sites with approximately equal occupancy (12.5%), however attempts to model this led to unstable refinement. This was addressed by placing an oxygen atom with 25% occupancy in the same site as Gd2 using the EXYZ command. The H atoms of the lattice solvent water molecules were located on the difference map where possible. The O-H and intramolecular H-H bond lengths were set to 0.84 Å and 1.34 Å, respectively, using AFIX and DANG instructions. The lattice solvent H atoms which could not be found on the difference map or which led to unstable refinement were omitted from the model.

Specific for **TbLt^{t,Me}**: Disorder of the carbostyril antenna was modelled over two sites. The secondary Tb centre is split over two sites, with the sum of occupancies of Tb2 and Tb3 equalling 76%. Some of the Tb2-bound water ligands are disordered, but the occupancies of these ligands was set such that the sum of the parts equals 1 (i.e. 100% occupancy). Residual density about Tb2 could be ascribed to a disordered water molecule with occupancy (15%), however attempts to model this led to unstable refinement. This was addressed by placing an oxygen atom with 15% occupancy in the same site as Tb2 using the EXYZ command. The H atoms of the lattice solvent water molecules were located on the difference map where possible. The O-H and

intramolecular H-H bond lengths were set to 0.84 Å and 1.34 Å, respectively, using AFIX and DANG instructions

CCDC 2102702–2102703 contain the supplementary crystallographic data for this paper. The data can be obtained free of charge from The Cambridge Crystallographic Data Centre via www.ccdc.cam.ac.uk/structures.

Table S1. Crystal data and structure refinement.

Compound	**GdLt^{t,Me}**	**TbLt^{t,Me}**
Chemical formula	$(C_{34}H_{34}N_7O_8Gd)()$ ·1.125(Cl)·11.025(H_2O)	$(C_{34}H_{34}N_7O_8Tb)(2.35(H_2O)Tb_{0.425})$ ·1.275(Cl)·7.8(H_2O)
M_r	1155.99	1122.24
Crystal system, space group	Monoclinic *C2/c*	Monoclinic *C2/c*
Temperature (K)	170	170
***a*, *b*, *c* (Å)**	22.3377 (6) 26.9746 (6) 16.0949 (4)	22.2162 (18) 26.8066 (18) 16.0827 (12)
β (°)	101.168 (2)	101.195 (2)
***V* (Å^3)**	9514.3 (4)	9395.7 (12)
Z	8	8
Radiation type	Mo K_α	Mo K_α
μ (mm^{-1})	2.05	2.41
Crystal size (mm)	0.6 × 0.4 × 0.2	0.7 × 0.2 × 0.1
Diffractometer	Bruker D8 APEX-II	Bruker D8 APEX-II
Absorption correction	Multi-scan	Multi-scan
T_{min}, T_{max}	0.660, 0.746	0.608, 0.746
No. of measured, independent and observed [I > 2s(I)] reflections	155499 10892 8622	131933 11693 8795
R_{int}	0.049	0.083
(sin θ/λ)$_{max}$ (Å^{-1})	0.649	0.668
R*[F^2 > 2σ(F^2)], *wR*(F^2), *S	0.040, 0.118, 1.14	0.058, 0.156, 1.14
No. of parameters	851	844
No. of restraints	802	657
H-atom treatment	Riding and independent	Riding
Δ⟩$_{max}$, Δ⟩$_{min}$ (e Å^{-3})	1.46, –0.92	1.28, –1.36
CCDC No.	2102702	2102703

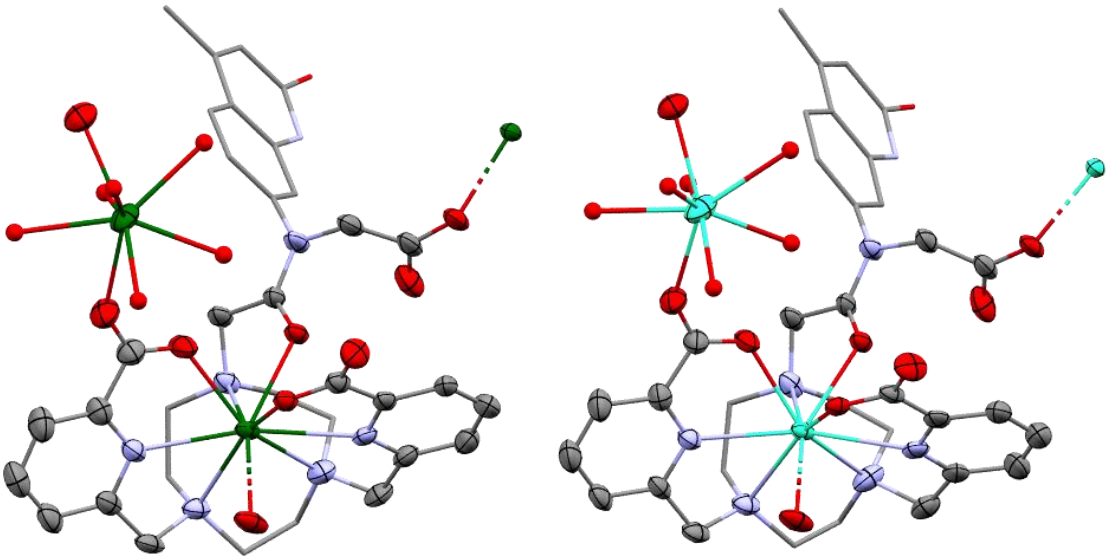

Figure S1. Solid-state structures of Gd (left) and Tb (right). H atoms, non-coordinating Cl^- counterions and water molecules omitted, triazacyclonane C atoms and antenna displayed as capped sticks and Ln2 co-ligands displayed as ball and stick for clarity. Ellipsoids displayed at 35% probability. Only major occupancy disordered sites shown.

Selected Ln-O, Ln-N and Ln-X distances (where X denotes the Cl/H_2O ligands) are displayed in Table S2, and follow the convention outlined in Figure S2.

Table S2. Selected bond lengths (Å) and angles (°) for **GdLt^{t,Me}** and **TbLt^{t,Me}**. The distance of the Ln centre to the relevant plane (not the plane centroid) are reported. [a]Average bond distance to account for multiple positions of the same atom (disorder).

Parameter	**GdLt^{t,Me}**	**TbLt^{t,Me}**
Ln1-O1	2.425(3)	2.414(3)
Ln1-O2	2.414(9)[a]	2.390(13)[a]
Ln1-O4	2.439(3)	2.442(4)
Ln1-O6	2.274(3)	2.258(5)
Ln1-N1	2.593(4)	2.576(6)
Ln1-N2	2.680(5)	2.68(3)[a]
Ln1-N3	2.665(4)	2.658(5)
Ln1-N4	2.532(8)	2.528(12)[a]
Ln1-N5	2.565(4)[a]	2.547(5)
Ln2-O5	2.426(4)	2.449(8)[a]
Ln2-OH_2	2.350(19)–2.485(12)	2.19(2)–2.577(15)
NNO_{PL}-Yb1-NNN_{PL}	115.1(3)[a]	116.8(6)[a]
Yb1-NNO_{PL}	0.312(3)[a]	0.328(6)[a]
Yb1-NNN_{PL}	2.044(3)	2.024(8)[a]

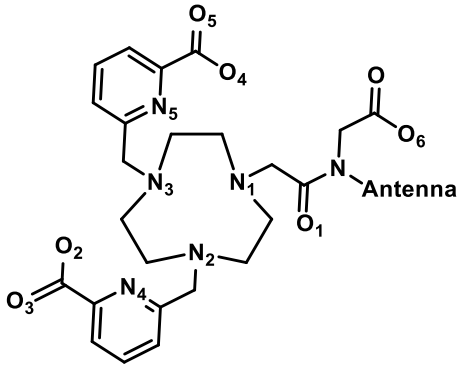

Figure S2. Numbering convention for Table S2.

While the asymmetric units of the crystallographically characterised complexes only contain one repeating unit of the polymeric molecule, the unit cells consist of eight repeating units. The space groups determined for the lanthanide complexes contains inversion centres, so any chirality seen in the asymmetric unit is lost when translated to the unit cell, giving a racemic mixture of Δ and Λ isomers in the unit cell.

Additional synthetic procedures

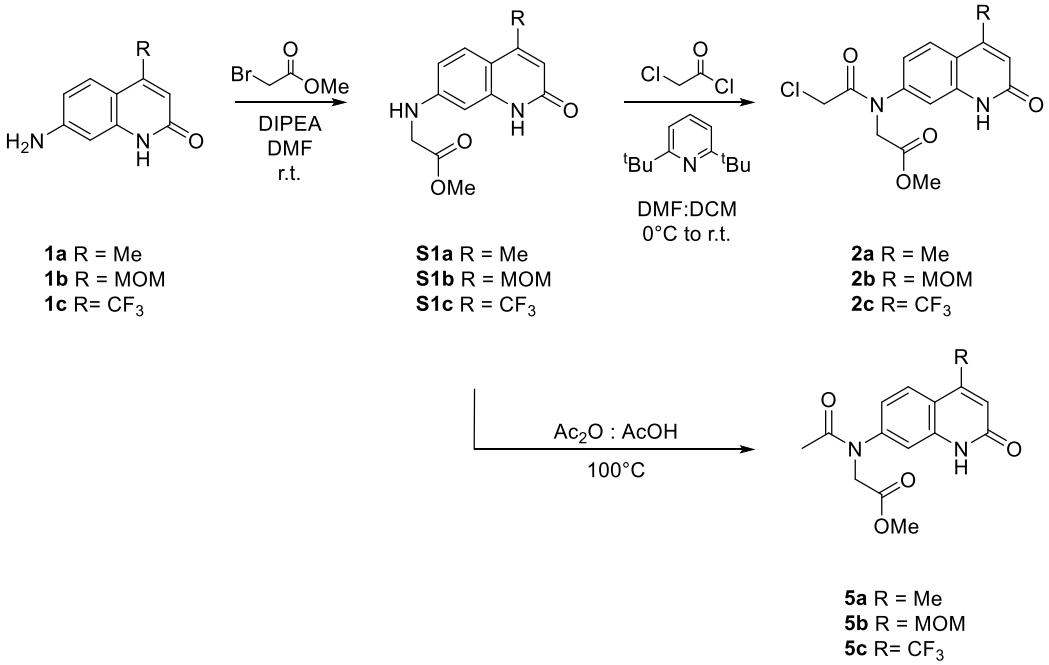

1a R = Me
1b R = MOM
1c R= CF_3

S1a R = Me
S1b R = MOM
S1c R = CF_3

2a R = Me
2b R = MOM
2c R= CF_3

5a R = Me
5b R = MOM
5c R= CF_3

Scheme S1. Preparation of **2a**, **2b**, **2c**, **5a**, **5b** and **5c** respectively.

Methyl-, methoxymethyl- and trifluoromethyl-carrying antennae **1a**, **1b** and **1c** were alkylated in the presence of DIPEA at room temperature. Further alkylation of **S1a**, **S1b** and **S1c** was performed in the

presence of 2,6-Di-*tert*-butylpyridine to afford tertiary-amide core **2a**, **2b** and **2c**, respectively. Acetylation in a mixture of acetic anhydride and acetic acid (1:4) yielded **5a**, **5b** and **5c**.

Synthetic procedures and characterization data

General procedure for the alkylation of 7-aminocarbostyrils:

A sample of the appropriate 7-aminocarbostyril compound (**1a**, **1b**, **1c**, 1.00 mmol) was dissolved in DMF (4 mL). DIPEA (4.5 mmol) was added to the solution, followed by methyl bromoacetate (3.6 mmol). The resulting mixture was stirred at room temperature for 24 hours. The mixture was separated between EtOAc and water; the aqueous phase was further extracted with EtOAc. The combined organic phase was dried over $MgSO_4$, filtered, and the filtrate was evaporated. The crude product was purified by column chromatography. Elution with DCM:Et_2O:^{i}PrOH = 90:10:0 → 80:20:0 → 80:15:5 (**S1a**), DCM:Et_2O:^{i}PrOH = 60:40:0 → 60:35:5 → 60:30:10 (**S1b**) or DCM:EtOAc:^{i}PrOH = 60:40:0 → 60:35:5 → 60:15:25 (**S1c**) resulted the products as beige solids.

S1a (1.08 g, quant.): ^{1}H NMR (400 MHz, DMSO-d_6) δ ppm 11.15 (s, 1H), 7.40 (d, J = 9.0 Hz, 1H), 6.71 (t, J = 6.5 Hz, 1H), 6.53 (dd, J_1 = 9.0 Hz, J_2 = 2.0 Hz, 1H), 6.29 (d, J = 2.0 Hz, 1H), 6.00 (s, 1H), 3.94 (d, J = 6.5 Hz, 2H), 3.66 (s, 3H), 2.29 (s, 3H); ^{13}C NMR (101 MHz, DMSO-d_6) δ ppm 171.3 (O=C–O_{Me}), 162.2 (O=C–$NH_{carbostyril}$), 150.0 (C_{Ar}), 147.9 (C_q), 140.7 (C_{Ar}), 125.5 (CH_{Ar}), 115.3 (CH), 110.9 (C_{Ar}), 109.2 (CH_{Ar}), 95.0 (CH_{Ar}), 51.7 (CH_3–O_{ester}), 44.2 (CH_2-COOMe), 18.4 (CH_3); RP-HPLC t_R = 5.07 min (method (a)); ESI-MS obsd 247.60, calcd 247.10 $(M + H)^+$; HR-ESI-MS obsd 247.1092, calcd 247.1077 [$(M + H)^+$, M = $C_{13}H_{14}N_2O_3$].

S1b (3.35 g, 83%): ^{1}H NMR (400 MHz, DMSO-d_6) δ ppm 11.26 (s, 1H), 7.37 (d, J = 9.0 Hz, 1H), 6.74 (t, J = 6.0 Hz, 1H), 6.52 (dd, J_1 = 9.0, J_2 = 2.5 Hz, 1H), 6.30 (d, J = 2.5 Hz, 1H), 6.13 (s, 1H), 4.54 (s, 2H), 3.94 (d, J = 6.5 Hz, 2H), 3.66 (s, 3H), 3.35 (s, 3H); ^{13}C NMR (101 MHz, DMSO-d_6) δ ppm 171.2 (O=C–O_{Me}), 162.2 (O=C–$NH_{carbostyril}$), 150.0 (C_{Ar}), 147.3 (C_q), 141.0 (C_{Ar}), 124.9 (CH_{Ar}), 113.4 (CH), 109.3 (CH_{Ar}), 108.7 (C_{Ar}), 95.1 (CH_{Ar}), 70.5 (CH_2–MOM), 58.0 (CH_3–MOM), 51.8 (CH_3–O_{ester}), 44.2 (CH_2-COOMe); RP-HPLC t_R = 4.97 min (method (a)); ESI-MS obsd 277.80, calcd 277.10 $(M + H)^+$; HR-ESI-MS obsd 277.1181, calcd 277.1183 [$(M + H)^+$, M = $C_{14}H_{16}N_2O_4$].

S1c (831 mg, 28%): ^{1}H NMR (400 MHz, DMSO-d_6) δ 11.83 (s, 1H), 7.40 (dd, J_1 = 9.0 Hz, J_2 = 2.5 Hz, 1H), 7.10 (t, J = 6.5 Hz, 1H), 6.66 (dd, J_1 = 9.0 Hz, J_2 = 2.5 Hz, 1H), 6.49 (s, 1H), 6.38 (d, J = 2.5 Hz, 1H), 3.99 (d, J = 6.5 Hz, 2H), 3.67 (s, 3H); ^{13}C NMR (101 MHz, DMSO-d_6) δ 170.9 ($O{=}C{-}O_{Me}$), 160.8 ($O{=}C{-}NH_{carbostyril}$), 150.8 (C_{Ar}), 142.1 (C_{Ar}), 136.7 (C_q, q, J = 31 Hz), 124.2 (CH_{Ar}), 122.9 (CF_3, q, J = 276 Hz), 114.4 (CH, d, J = 6 Hz), 110.9 (CH_{Ar}), 104.1 (C_{Ar}), 95.1 (CH_{Ar}), 51.8 ($CH_3{-}O_{ester}$), 44.0 (CH_2); ^{19}F NMR (376 MHz, DMSO-d_6) δ ppm –62.3 (s, 3F); RP-HPLC t_R = 5.93 min (method (a)); ESI-MS obsd 301.18, calcd 301.07 $(M + H)^+$; HR-ESI-MS obsd 301.0793, calcd 301.0795 [$(M + H)^+$, M = $C_{13}H_{11}F_3N_2O_3$].

General procedure for the acylation of alkylated 7-aminocarbostyrils:

A sample of the alkylated 7-aminocarbostyril (**S1a**, **S1b**, **S1c**, 1.0 mmol) was dissolved in a mixture of DMF (4 mL) and DCM (4 mL). To this solution 2,6-di-*tert*-butyl-pyridine (3.0 mmol) was added, and the mixture was cooled down to 0 °C in an ice bath. Chloroacetyl chloride (1.2 mmol) was added in one portion, and the reaction mixture was allowed warm up slowly to room temperature over the course of 3 h while being stirred. Typically, at this point TLC analysis showed full conversion of the starting materials, and the reaction mixture was poured into a separation funnel containing water and EtOAc. The phases were separated, and the aqueous phase was extracted with EtOAc once more. The combined organic phase was dried over $MgSO_4$, filtered, and the filtrate was concentrated under reduced pressure. The crude product was either recrystallized from chloroform (**2b**, light peach coloured solid) or purified by column chromatography. Elution with DCM:Et_2O:^{i}PrOH = 90:10:0 → 80:20:0 → 80:15:5 → 80:5:15 (**2a**), or $CHCl_3$:Et_2O = 60:40 → 50:50 (**2c**) resulted the products as off-white (**2a**) and yellow (**2c**) solids.

2a (3.34 g, 87%): ^{1}H NMR (400 MHz, DMSO-d_6) δ ppm 11.70 (s, 1H), 7.78 (d, J = 8.5 Hz, 1H), 7.35 (s, 1H), 7.24 (d, J = 8.5 Hz, 1H), 6.43 (s, 1H), 4.44 (s, 2H), 4.15 (s, 2H), 3.68 (s, 3H), 2.42 (s, 3H); ^{13}C NMR (101 MHz, DMSO-d_6) δ ppm 169.1 ($O{=}C{-}O_{Me}$), 165.9 ($O{=}C{-}CH_2{-}Cl$), 161.6 ($O{=}C{-}NH_{carbostyril}$), 147.5 (C_q), 142.6 (C_{Ar}), 139.4 (C_{Ar}), 126.3 (CH_{Ar}), 121.5 (CH), 120.9 (CH_{Ar}), 114.2 (CH_{Ar}), 52.1 ($CH_3{-}O_{ester}$), 51.4 (CH_2-COOMe), 41.9 ($CH_2{-}Cl$), 18.5 (CH_3); RP-HPLC t_R = 5.30 min (method (a)); ESI-MS obsd 323.08, calcd 323.07 $(M + H)^+$; HR-ESI-MS obsd 323.0792, calcd 323.0793 [$(M+H)^+$, M = $C_{15}H_{15}ClN_2O_4$].

2b (1.47 g, 82%): ^{1}H NMR (400 MHz, DMSO-d_6) δ 11.82 (s, 1H), 7.74 (d, J = 8.5 Hz, 1H), 7.37 (s, 1H), 7.23 (d, J = 8.0 Hz, 1H), 6.53 (s, 1H), 4.66 (s, 2H), 4.44 (s, 2H), 4.16 (s, 2H), 3.68 (s, 3H), 3.39 (s, 3H); ^{13}C NMR (101 MHz, DMSO-d_6) δ 169.1 (O=C–O_{Me}), 165.9 (O=C–CH_2–Cl), 161.6 (O=C–$NH_{carbostyril}$), 146.8 (C_q), 142.6 (C_{Ar}), 139.7 (C_{Ar}), 125.8 (CH_{Ar}), 121.0 (CH_{Ar}), 119.9 (CH), 117.3 (C_{Ar}), 114.4 (CH_{Ar}), 70.2 (CH_2–MOM), 58.2 (CH_3–MOM), 52.1 (CH_3–O_{ester}), 51.4 (CH_2-COOMe), 41.9 (CH_2–Cl); RP-HPLC t_R = 5.27 min (method (a)); ESI-MS obsd 353.13, calcd 353.08 $(M + H)^+$; HR-ESI-MS obsd 375.0731, calcd 375.0718 [$(M+Na)^+$, M = $C_{16}H_{17}N_2O_5Cl$].

2c (484 mg, 52%): ^{1}H NMR (400 MHz, DMSO-d_6) δ ppm 12.42 (s, 1H), 7.76 (d, J = 9.0, 1H), 7.49 (s, 1H), 7.37 (d, J = 9.0, 1H), 7.03 (s, 1H), 4.48 (s, 2H), 4.22 (s, 2H), 3.69 (s, 3H); ^{13}C NMR (101 MHz, DMSO-d_6) δ ppm 169.1 (O=C–O_{Me}), 165.9 (O=C–CH_2–Cl), 160.0 (O=C–$NH_{carbostyril}$), 143.7 (C_{Ar}), 140.6 (C_{Ar}), 136.1 (C_q, q, J = 31 Hz), 125.7 (CH_{Ar}), 122.6 (CH, d, J = 5 Hz), 122.4 (CF_3, q, J = 276 Hz), 122.2 (CH_{Ar}), 115.3 (CH_{Ar}), 112.7 (C_{Ar}), 52.2 (CH_3–O_{ester}), 51.3 (CH_2-COOMe), 42.0 (CH_2–Cl); ^{19}F NMR (376 MHz, DMSO-d_6) δ ppm –62.5 (s, 3F); RP-HPLC t_R = 6.17 min (method (a)); ESI-MS obsd 377.07, calcd 377.04 $(M + H)^+$; HR-ESI-MS obsd 399.0328, calcd 399.0330 [$(M + Na)^+$, M = $C_{15}H_{12}ClF_3N_2O_4$].

General procedure for the acetylation of alkylated 7-aminocarbostyrils:

A sample of the alkylated 7-aminocarbostyril (**S1a**, **S1b**, **S1c**, 0.1 mmol) was dissolved in a mixture of Ac_2O (75 µL) and AcOH (225 µL). The mixture was stirred at 100 °C until TLC and LC-MS analyses showed full conversion of the starting material (typically 4–6 h). The mixture cooled to room temperature, and poured onto a silica chromatography column. Elution with 0→5% MeOH in DCM, followed by evaporation of the solvents yielded **5a**, **5b** and **5c** as off-white solids, respectively.

5a (24 mg, 83%.): ^{1}H NMR (400 MHz, DMSO-d_6) δ ppm 11.66 (s, 1H), 7.76 (d, J = 8.5 Hz, 1H), 7.29 (s, 1H), 7.19 (d, J = 8.1 Hz, 1H), 6.42 (s, 1H), 4.38 (s, 2H), 3.66 (s, 3H), 2.42 (s, 3H), 1.87 (s, 3H); ^{13}C NMR (101 MHz, DMSO-d_6) δ ppm 169.6 (O=C–O_{Me}), 169.4 (O=C-CH_3), 161.7 (O=C–$NH_{carbostyril}$), 147.6 (C_q), 144.4 (C_{Ar}), 139.3 (C_{Ar}), 126.2 (CH_{Ar}), 121.2 (CH), 120.9 (CH_{Ar}), 118.9 (C_{Ar}), 114.0 (CH_{Ar}), 52.0 (CH_3–O_{ester}), 50.7 (CH_2-COOMe), 22.0 (CH_3), 18.5 (CH_3); HR-ESI-MS obsd 289.1180, calcd 289.1183 [$(M + H)^+$, M = $C_{15}H_{16}N_2O_4$].

5b (20 mg, 63%): ^{1}H NMR (400 MHz, DMSO-d_6) δ ppm 11.78 (s, 1H), 7.73 (d, J = 8.5 Hz, 1H), 7.31 (s, 1H), 7.18 (d, J = 8.3 Hz, 1H), 6.52 (s, 1H), 4.67 (s, 2H), 4.38 (s, 2H), 3.66 (s, 3H), 3.39 (s, 3H), 1.88 (s, 3H); ^{13}C NMR (101 MHz, DMSO-d_6) δ ppm 169.6 (O=C–O_{Me}), 169.4 (O=C-CH_3), 161.6 (O=C–$NH_{carbostyril}$), 146.8 (C_q), 144.4 (C_{Ar}), 139.6 (C_{Ar}), 125.6 (CH_{Ar}), 121.0 (CH_{Ar}), 119.6 (CH), 116.7 (C_{Ar}), 114.1 (CH_{Ar}), 70.2 (CH_2–MOM), 58.1 (CH_3–MOM), 51.9 (CH_3–O_{ester}), 50.6 (CH_2-COOMe), 22.0 (CH_3); HR-ESI-MS obsd 319.1282, calcd 319.1288 [$(M + H)^+$, M = $C_{16}H_{18}N_2O_5$].

5c (32 mg, 94%): ^{1}H NMR (400 MHz, DMSO-d_6) δ 12.37 (s, 1H), 7.75 (dd, J_1 = 8.7 Hz, J_2 = 2.1, 1H), 7.42 (d, J = 2.1 Hz, 1H), 7.32 (d, J = 8.0, 1H), 7.01 (s, 1H), 4.42 (s, 2H), 3.67 (s, 3H), 1.92 (s, 3H); ^{13}C NMR (101 MHz, DMSO-d_6) δ 169.6 (O=C–O_{Me}), 169.5 (O=C-CH_3), 160.0 (O=C–$NH_{carbostyril}$), 145.5 (C_{Ar}), 140.5 (C_{Ar}), 136.1 (C_q, q, J = 31 Hz), 125.5 (CH_{Ar}), 122.4 (CF_3, q, J = 276 Hz), 122.2 (CH), 122.2 (CH_{Ar}), 114.8 (CH_{Ar}), 112.1 (C_{Ar}), 52.0 (CH_3–O_{ester}), 50.7 (CH_2), 22.1 (CH_3); ^{19}F NMR (376 MHz, DMSO-d_6) δ ppm –62.5 (s, 3F); HR-ESI-MS obsd 343.0910, calcd 343.0900 [$(M + H)^+$, M = $C_{13}H_{11}F_3N_2O_3$].

General procedure for the Me-ester protected ligand:

A sample of **3** (400 mg, 0.936 mmol) was dissolved in acetonitrile (11.3 mL), and the solution was transferred into a microwave reaction vessel. Et_3N (392 µL, 2.81 mmol) was added, and the reaction mixture was stirred for a few minutes, after which a sample of **2a, 2b,** and **2c** (0.936 mmol) were added. The vessel was sealed, and was placed into an oil bath pre-heated to 70 °C. After stirring the reaction mixture overnight, the initial suspension became a transparent solution. TLC and LCMS analysis showed full conversion of the starting materials. The reaction mixture was concentrated under reduced pressure. The residue was dissolved in a minimal amount of DCM, and this solution was loaded directly onto an alumina chromatography column. Elution with DCM:Acetone:MeOH (100:0:0 → 99:0.5:0.5 → 98:1:1→ 97:1.5:1.5 → 90:5:5) mixture resulted the title compounds as light brown (**4a**, **4b**) and yellow (**4c**) solids.

4a (376 mg, 56%): ^{1}H NMR (400 MHz, DMSO-d_6) δ 11.60 (s, 1H), 7.96–7.84 (m, 4H), 7.72 (d, J = 8.5 Hz, 1H), 7.68 (d, J = 7.0 Hz, 2H), 7.28 (s, 1H), 7.18 (d, J = 8.0 Hz, 1H), 6.39 (s, 1H), 4.36 (s, 2H), 3.85 (s, 6H), 3.74 (s, 4H), 3.66 (s, 3H), 3.28 (s, 2H), 2.67–2.60 (m, 12H), 2.40 (s, 3H); ^{13}C NMR (101 MHz, DMSO-d_6) δ 170.5 (O=C–N), 169.6 (O=C–O_{Me}), 165.3 (O=C–O_{MePy}), 161.6 (O=C–$NH_{carbostyril}$),

160.9 (C_{ArPy}), 147.5 (C_{Ar}), 146.6 (C_{ArPy}), 160.9 (C_{ArPy}), 147.5 (C_q), 143.7 (C_{Ar}), 139.3 (C_{Ar}), 137.6 (CH_{ArPy}), 126.3 (CH_{ArPy}), 126.0 (CH_{Ar}), 123.1 (CH_{ArPy}), 121.1 (CH), 120.8 (CH_{Ar}), 118.8 (C_{Ar}), 113.7 (CH_{Ar}), 63.5 (CH_{2Py}), 59.0 (CH_2–N_{cyc}), 55.5 (CH_{2cyc}), 55.0 (CH_{2cyc}), 52.3 (CH_3–$O_{esterPy}$), 51.9 (CH_3–O_{ester}), 51.1 (CH_2-COOMe), 18.5 (CH_3); RP-HPLC t_R = 6.98 min (method (b)); ESI-MS obsd 714.50, calcd 714.32 $(M + H)^+$; HR-ESI-MS obsd 714.3262, calcd 714.3246 [$(M + H)^+$, M = $C_{37}H_{43}N_7O_8$].

4b (303 mg, 44%): ^{1}H NMR (400 MHz, DMSO-*d*$_6$) δ 11.71 (s, 1H), 7.98–7.82 (m, 4H), 7.77–7.61 (m, 3H), 7.30 (s, 1H), 7.17 (d, *J* = 7.5 Hz, 1H), 6.50 (s, 1H), 4.65 (s, 2H), 4.37 (s, 2H), 3.86 (s, 6H), 3.75 (s, 4H), 3.66 (s, 3H), 3.38 (s, 3H), 3.28 (s, 2H), 2.92–2.53 (m, 12H); ^{13}C NMR (101 MHz, DMSO-*d*$_6$) δ 170.5 (O=C–N), 169.6 (O=C–O_{Me}), 165.3 (O=C–O_{MePy}), 161.5 (O=C–$NH_{carbostyril}$), 160.9 (C_{ArPy}), 146.8 (C_q), 146.6 (C_{ArPy}), 143.7 (C_{Ar}), 139.6 (C_{Ar}), 137.6 (CH_{ArPy}), 126.3 (CH_{ArPy}), 125.5 (CH_{Ar}), 123.1 (CH_{ArPy}), 120.9 (CH_{Ar}), 119.5 (CH), 116.7 (C_{Ar}), 113.9 (CH_{Ar}), 70.2 (CH_2–MOM), 63.5 (CH_{2Py}), 59.0 (CH_2–N_{cyc}), 58.1 (CH_3–MOM), 55.4 (CH_{2cyc}), 55.0 (CH_{2cyc}), 52.3 (CH_3–$O_{esterPy}$), 51.9 (CH_3–O_{ester}), 51.0 (CH_2-COOMe); RP-HPLC t_R = 6.97 min (method (b)); ESI-MS obsd 744.54, calcd 744.34 $(M + H)^+$; HR-ESI-MS obsd 744.3372, calcd 744.3352 [$(M + H)^+$, M = $C_{38}H_{45}N_7O_9$].

4c (203 mg, 28%): ^{1}H NMR (400 MHz, DMSO-*d*$_6$) δ ppm 12.26 (s, 1H), 7.95–7.85 (m, 4H), 7.70 (d, *J* = 9.0 Hz, 1H), 7.67 (d, *J* = 7.0 Hz, 2H), 7.41 (s, 1H), 7.31 (d, *J* = 8.5 Hz, 1H), 6.98 (s, 1H), 4.42 (s, 2H), 3.86 (s, 6H), 3.74 (s, 4H), 3.66 (s, 3H), 3.33 (s, 2H), 2.81–2.56 (m, 12H); ^{13}C NMR (101 MHz, DMSO-*d*$_6$) δ ppm 170.5 (O=C–N), 169.6 (O=C–O_{Me}), 165.3 (O=C–O_{MePy}), 160.8 (C_{ArPy}), 160.0 (O=C–$NH_{carbostyril}$), 146.6 (C_{ArPy}), 144.9 (C_{Ar}), 140.5 (C_{Ar}), 137.6 (CH_{ArPy}), 136.0 (C_q, q, *J* = 31 Hz), 126.3 (CH_{ArPy}), 125.4 (CH_{Ar}), 122.4 (CF_3, q, *J* = 276 Hz), 123.1 (CH_{ArPy}), 121.9 (CH_{Ar}), 121.9 (CH), 114.4 (CH_{Ar}), 112.0 (C_{Ar}), 63.5 (CH_{2Py}), 59.4 (CH_2–N_{cyc}), 55.3 (CH_{2cyc}), 55.0 (CH_{2cyc}), 52.3 (CH_3–$O_{esterPy}$), 52.0 (CH_3–O_{ester}), 51.0 (CH_2-COOMe); ^{19}F NMR (376 MHz, DMSO-*d*$_6$) δ ppm –62.5 (s, 3F); RP-HPLC t_R = 8.45 min (method (b)); ESI-MS obsd 768.44, calcd 768.30 $(M + H)^+$; HR-ESI-MS obsd 768.2970, calcd 768.2963 [$(M + H)^+$, M = $C_{37}H_{40}N_7O_8F_3$].

General procedure of the synthesis of the free ligands:

A sample of **4a**, **4b**, **4c** (0.300 mmol, 1.0 equiv) were dissolved in acetonitrile (2.3 mL) and H_2O (1.4 mL). A precipitate formed after 1 min, however, a transparent solution was obtained upon the

addition of aqueous 1 M NaOH solution (4.5 equiv, 0.9 mL H_2O). The reaction mixture was stirred for 1 h at room temperature. When TLC and HPLC-MS analysis showed full conversion, the solution was directly loaded onto a silica gel column. Elution with ACN:H_2O mixture (75:25→70:30) yielded white solids after the evaporation of the solvents under reduced pressure.

$Lt^{t,Me}$ (213 mg, 69%): ^{1}H NMR (400 MHz, CD_3CN:D_2O (1:1)) δ ppm 7.76–7.71 (m, 3H), 7.63 (t, J = 7.5 Hz, 2H), 7.33 (d, J = 2.0 Hz, 1H), 7.26 (d, J = 7.5 Hz, 2H), 7.01 (dd, J_1 = 8.5 Hz, J_2 = 2.0 Hz, 1H), 6.46 (s, 1H), 4.16 (s, 2H), 3.67 (s, 4H), 3.28 (m, 2H), 2.40 (s, 3H), 2.66–2.13 (m, 12H); ^{13}C NMR (101 MHz, CD_3CN:D_2O (1:1)) δ ppm 177.4 (CH_2COO^-), 176.2 (O=C–N), 172.8 (COO^-), 171.8 (O=C–$NH_{carbostyril}$), 158.5 (C_{ArPy}), 154.2 (C_{ArPy}), 149.7 (C_{Ar}), 146.8 (C_q), 143.1 (C_{Ar}), 138.9 (CH_{ArPy}), 126.3 (CH_{Ar}), 126.2 (CH_{ArPy}), 123.4 (C_{Ar}), 123.3 (CH_{ArPy}), 123.0 (CH_{Ar}), 120.2 (CH_{Ar}), 120.2 (CH), 63.9 (CH_{2Py}), 60.9 (CH_2-N_{cyc}), 54.9 (CH_2COO^-), 52.9 (CH_{2cyc}), 52.8 (CH_{2cyc}), 52.2 (CH_{2cyc}), 18.7 (CH_3); RP-HPLC t_R = 4.57 min (method (b)); ESI-MS obsd 672.93, calcd 672.28 $(M + H)^+$; HR-ESI-MS obsd 708.20902, calcd 708.21003 $[(M – 3H + Ca)^-$, M = $C_{34}H_{34}N_7O_8$].

$Lt^{t,MOM}$ (130 mg, 55%): ^{1}H NMR (400 MHz, CD_3CN:D_2O (1:1)) δ ppm 7.67–7.78 (m, 3H), 7.63 (t, J = 7.5 Hz, 2H), 7.37 (d, J = 2.0 Hz, 1H), 7.27 (d, J = 7.5 Hz, 2H), 7.03 (dd, J_1 = 8.5 Hz, J_2 = 2.0 Hz, 1H), 6.58 (s, 1H), 4.69 (s, 2H), 4.15 (s, 2H), 3.68 (s, 4H), 3.37 (s, 3H), 3.29 (m, 2H), 1.97–2.92 (m, 12H); ^{13}C NMR (101 MHz, CD_3CN:D_2O (2:1)) δ ppm 176.2 (CH_2COO^-), 173.4 (O=C–N), 172.8 (COO^-), 171.6 (O=C–$NH_{carbostyril}$), 158.5 (C_{ArPy}), 154.2 (C_{ArPy}), 150.2 (C_{Ar}), 144.8 (C_q), 143.2 (C_{Ar}), 138.9 (CH_{ArPy}), 126.2 (CH_{ArPy}), 125.9 (CH_{Ar}), 123.3 (CH_{Ar}), 123.3 (CH_{ArPy}), 121.3 (C_{Ar}), 120.5 (CH_{Ar}), 119.5 (CH), 72.0 (CH_2-MOM), 63.9 (CH_{2Py}), 60.9 (CH_2-N_{cyc}), 58.7 (CH_3-MOM), 54.9 (CH_2COO^-), 53.0 (CH_{2cyc}), 52.8 (CH_{2cyc}), 52.2 (CH_{2cyc}); RP-HPLC t_R = 4.58 min (method (b)); ESI-MS obsd 702.98, calcd 702.29; $(M + H)^+$; HR-ESI-MS obsd 738.21911, calcd 738.22059 $[(M – 3H + Ca)^-$, M = $C_{35}H_{36}N_7O_9$].

$Lt^{t,CF3}$ (84 mg, 63%): ^{1}H NMR (400 MHz, CD_3CN:D_2O (1:1)) δ ppm 7.81–7.70 (m, 3H), 7.63 (t, J = 7.5 Hz, 2H), 7.46 (d, J = 2.0 Hz, 1H), 7.27 (d, J = 7.5 Hz, 2H), 7.10 (dd, J_1 = 9.0 Hz, J_2 = 2.0 Hz, 1H), 6.92 (s, 1H), 4.20–4.03 (m, 2H), 3.69 (s, 4H), 3.30 (s, 2H), 2.85–2.05 (m, 12H); ^{13}C NMR (101 MHz, CD_3CN:D_2O (2:1)) δ ppm 176.0 (CH_2COO^-), 173.4 (O=C–N), 172.8 (COO^-), 170.4 (O=C–$NH_{carbostyril}$), 158.9 (C_{ArPy}), 154.2 (C_{ArPy}), 151.1 (C_{Ar}), 143.9 (C_{Ar}), 138.9 (CH_{ArPy}), 135.9 (C_q, q, J = 31 Hz), 126.1

(CH_{ArPy}), 126.0 (CH_{Ar}), 124.4 (CF_3, q, J = 274 Hz), 123.9 (CH_{Ar}), 123.3 (CH_{ArPy}), 121.4 (CH), 116.9 (CH_{Ar}), 113.4 (C_{Ar}), 63.9 (CH_{2Py}), 61.0 (CH_2-N_{cyc}), 54.8 (CH_2COO^-), 53.0 (CH_{2cyc}), 52.8 (CH_{2cyc}), 52.2 (CH_{2cyc}); ^{19}F NMR (376 MHz, DMSO-d_6) δ ppm –62.2 (s, 3F); RP-HPLC t_R = 6.50 min (method (b)); ESI-MS obsd 726.82, calcd 726.25 $(M + H)^+$; HR-ESI-MS obsd 762.18062, calcd 762.18231 [$(M – 3H + Ca)^-$, M = $C_{34}H_{34}N_7O_8F_3$].

General procedure for lanthanide complexation:

Sample of the ligand (1.0 equiv.) and anhydrous $LnCl_3$ (2.4 equiv.) were placed in a vial. A stirring bar was added, followed by a mixture of H_2O and EtOH (1:1, 0.05 M). The vial was sealed, and was placed in a pre-heated alumina bath (45 °C). The mixture was stirred overnight. HPLC-MS and TLC analysis indicated that the reactions reached full conversion after 16 h, and a white precipitate was observed in the mixture. The mixture was diluted with ^{i}PrOH, and the sample was loaded onto a silica gel column. Elution with ^{i}PrOH:H_2O as eluent (90:10→85:15→80:20→60:40) yielded the complexes as white solids after the evaporation of the solvents.

GdLt^{t,Me} (49 mg, quant.) RP-HPLC t_R = 1.75, 4.27 min (method (c)); ESI-MS obsd 827.32, calcd 827.18 $(M + H)^+$; HR-ESI-MS obsd 827.17946, calcd 827.17881 [$(M + H)^+$, M = $C_{34}H_{34}N_7O_8Gd$].

TbLt^{t,Me} (49 mg, quant.) RP-HPLC t_R = 1.75, 4.12 min (method (c)); ESI-MS obsd 828.30, calcd 828.18 $(M + H)^+$; HR-ESI-MS obsd 828.17985, calcd 828.18005 [$(M + H)^+$, M = $C_{34}H_{34}N_7O_8Tb$].

EuLt^{t,Me} (49 mg, quant.) RP-HPLC t_R = 1.73, 4.27 min (method (c)); ESI-MS obsd 822.53 calcd 822.18 $(M + H)^+$; HR-ESI-MS obsd 822.17691, calcd 822.17594 [$(M + H)^+$, M = $C_{34}H_{34}N_7O_8Eu$].

GdLt^{t,MOM} (36 mg, quant.) RP-HPLC t_R = 1.75, 4.28 min (method (c)); ESI-MS obsd 857.14, calcd 757.19 $(M + H)^+$; HR-ESI-MS obsd 857.18993, calcd 857.18938 [$(M + H)^+$, M = $C_{35}H_{36}N_7O_9Gd$].

TbLt^{t,MOM} (36 mg, quant.) RP-HPLC t_R = 1.73, 4.02 min (method (c)); ESI-MS obsd 858.82, calcd 858.19 $(M + H)^+$; HR-ESI-MS obsd 858.19034, calcd 858.19062 [$(M + H)^+$, M = $C_{35}H_{36}N_7O_9Tb$].

EuLt^{t,MOM} (36 mg, quant.) RP-HPLC t_R = 1.72, 4.30 min (method (c)); ESI-MS obsd 852.68 calcd 852.19 $(M + H)^+$; HR-ESI-MS obsd 852.18679, calcd 852.18650 [$(M + H)^+$, M = $C_{35}H_{36}N_7O_9Eu$].

GdLt^{t,CF3} (23 mg, 96%) RP-HPLC t_R = 8.35 min (method (c)); ESI-MS obsd 881.41, calcd 881.15 (M + H)$^+$; HR-ESI-MS obsd 881.15113, calcd 881.15055 [(M + H)$^+$, M = $C_{34}H_{31}N_7O_8F_3Gd$].

TbLt^{t,CF3} (22 mg, 92%) RP-HPLC t_R = 8.30 min (method (c)); ESI-MS obsd 882.80, calcd 882.15 (M + H)$^+$; HR-ESI-MS obsd 882.15147, calcd 882.15179 [(M + H)$^+$, M = $C_{34}H_{31}N_7O_8F_3Tb$].

EuLt^{t,CF3} (22 mg, 92%) RP-HPLC t_R = 8.37 min (method (c)); ESI-MS obsd 876.78 calcd 876.15 (M + H)$^+$; HR-ESI-MS obsd 876.14785, calcd 876.14767 [(M + H)$^+$, M = $C_{34}H_{31}N_7O_8F_3Eu$].

Paramagnetic ^{1}H NMR spectroscopy

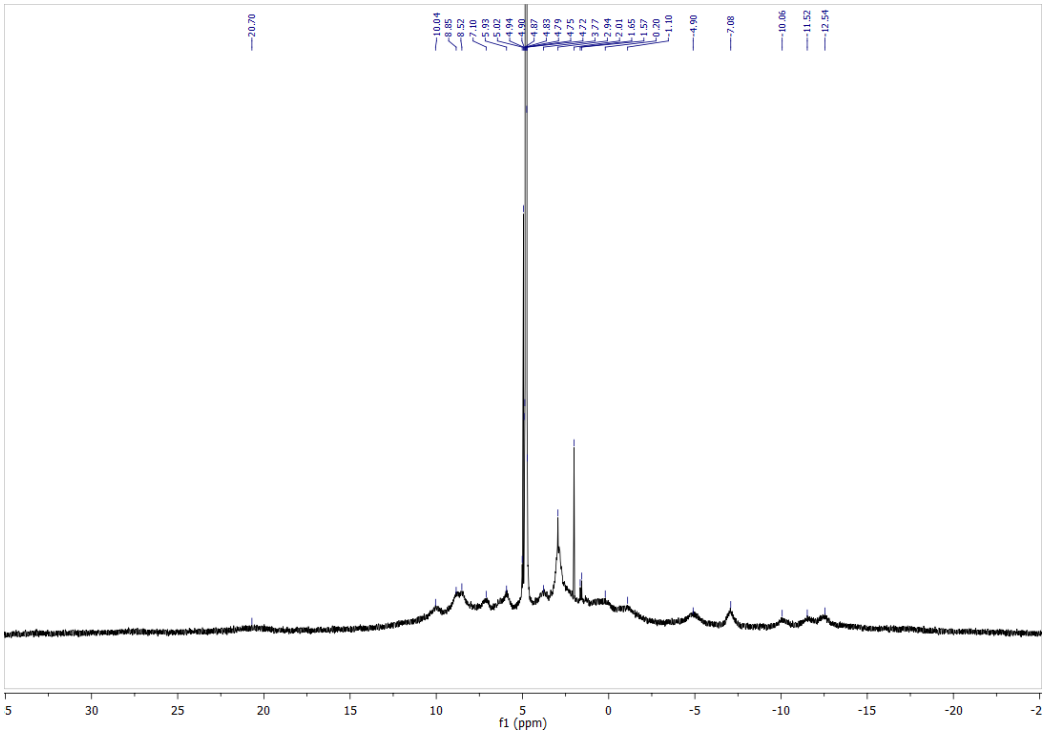

Figure S3. ^{1}H NMR spectrum of **EuLt^{s,Me}** recorded at 298 K. Chemical shifts were referenced to D_2O.

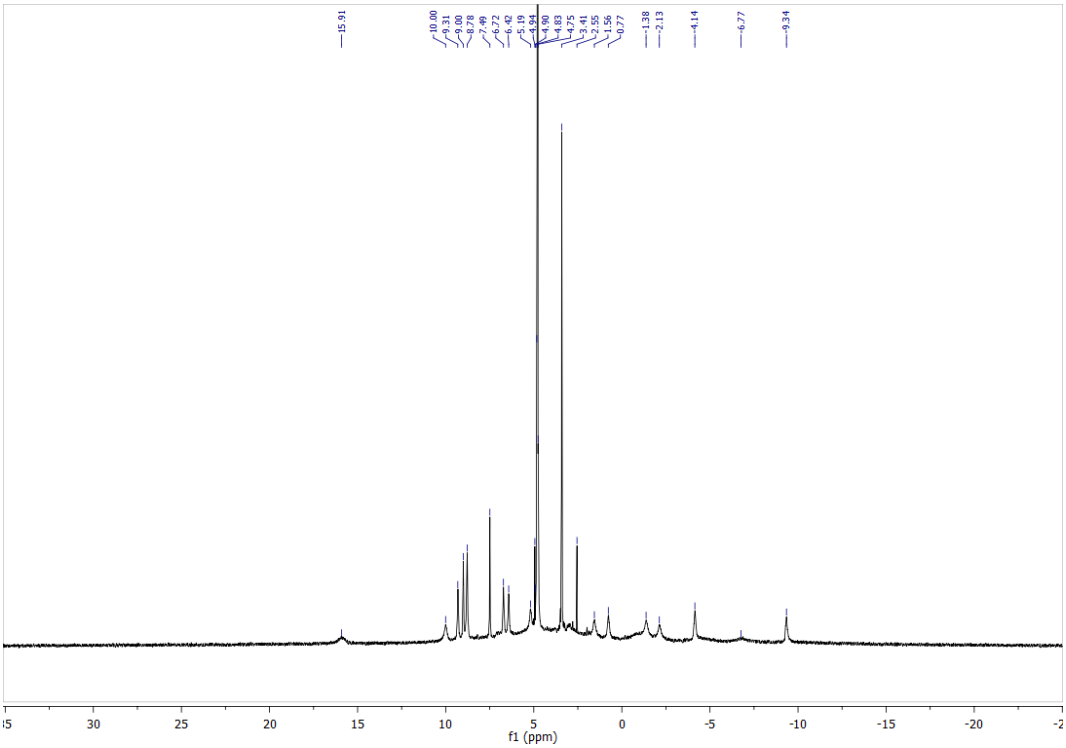

Figure S4. ^{1}H NMR spectrum of **EuLt^{s,Me}** recorded at 353 K. Chemical shifts were referenced to D_2O.

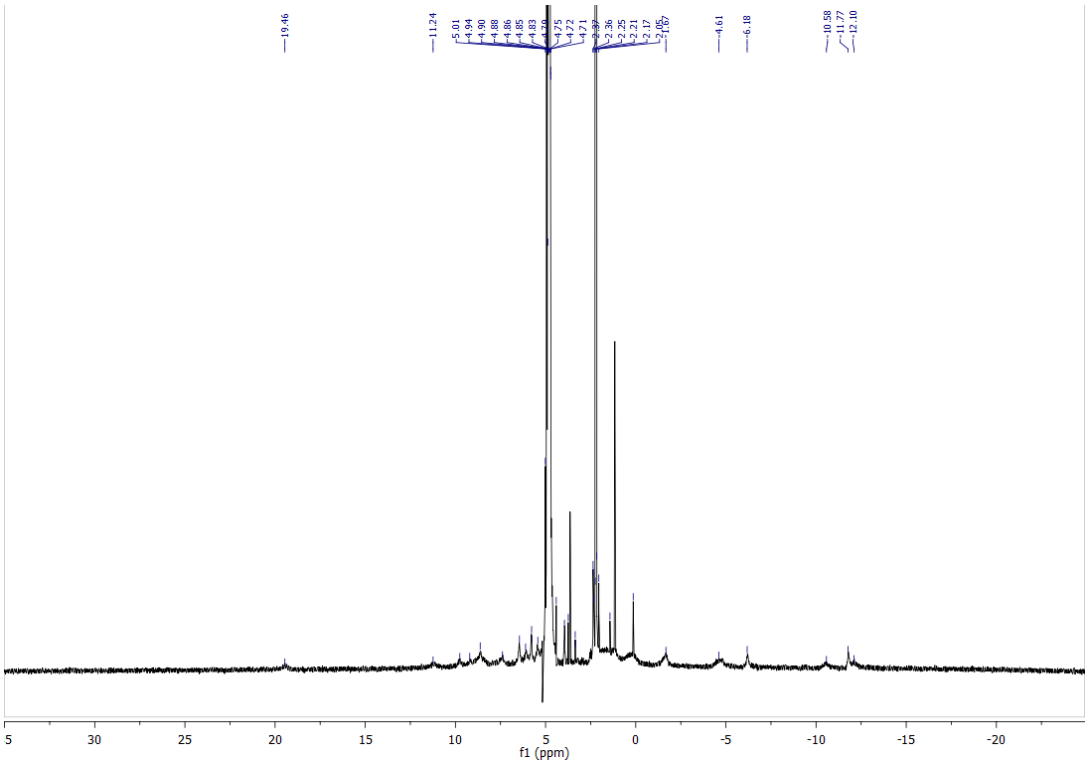

Figure S5. ^{1}H NMR spectrum of **EuLt^{t,Me}** recorded at 298 K. Chemical shifts were referenced to D_2O.

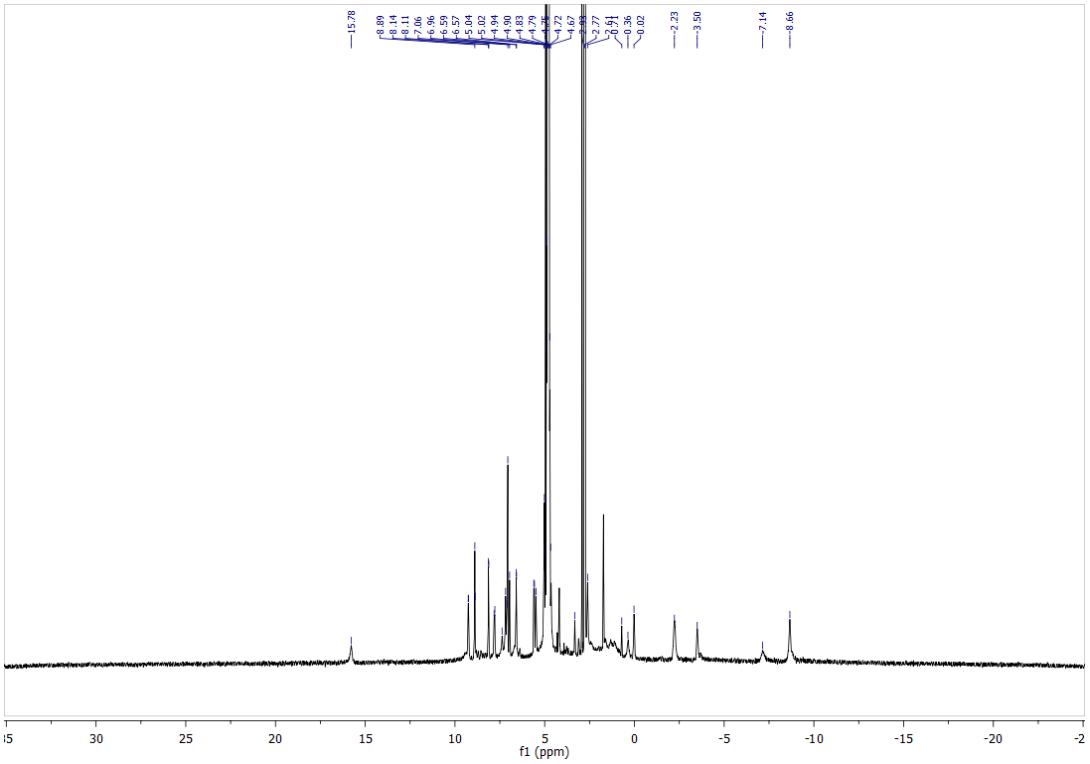

Figure S6. ^{1}H NMR spectrum of **EuLt^{t,Me}** recorded at 353 K. Chemical shifts were referenced to D_2O.

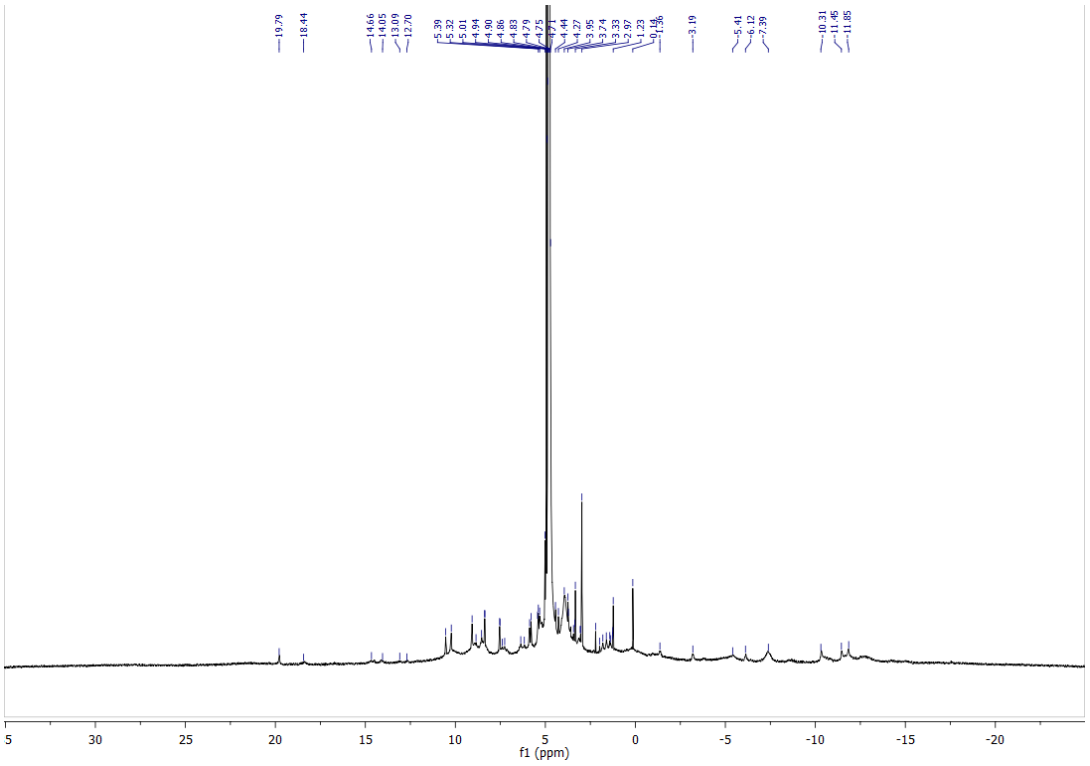

Figure S7. ^{1}H NMR spectrum of **EuLt^{s,MOM}** recorded at 298 K. Chemical shifts were referenced to D_2O.

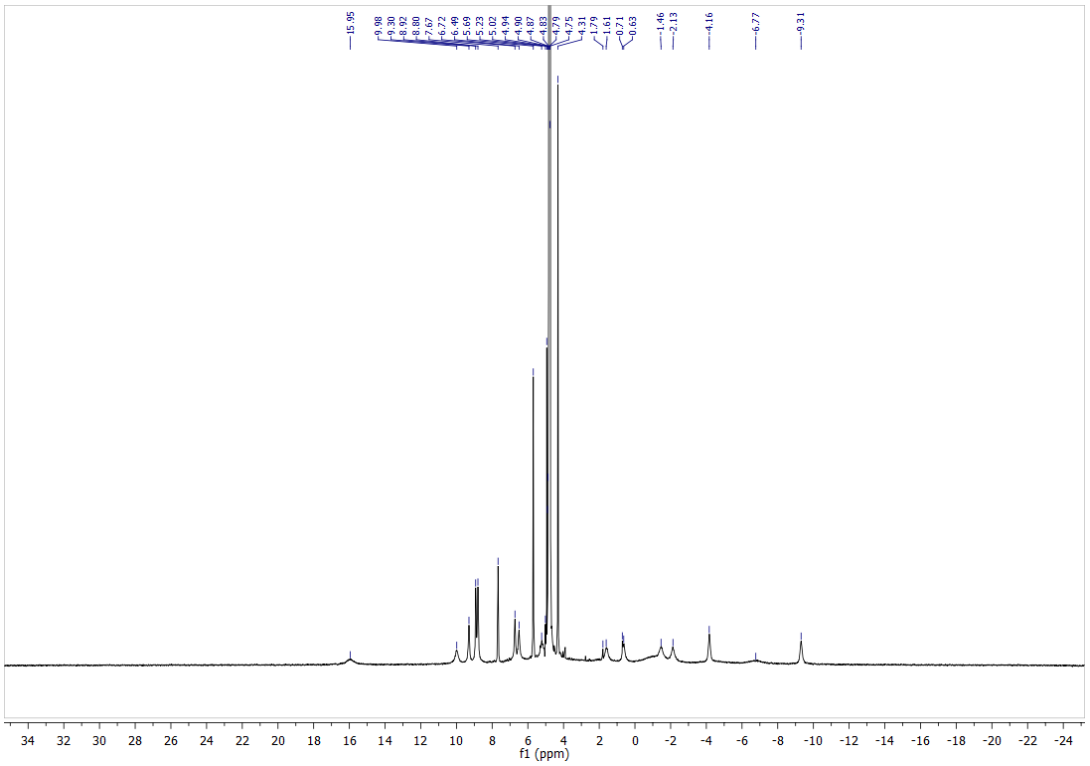

Figure S8. ^{1}H NMR spectrum of **EuLt^{s,MOM}** recorded at 353 K. Chemical shifts were referenced to D_2O.

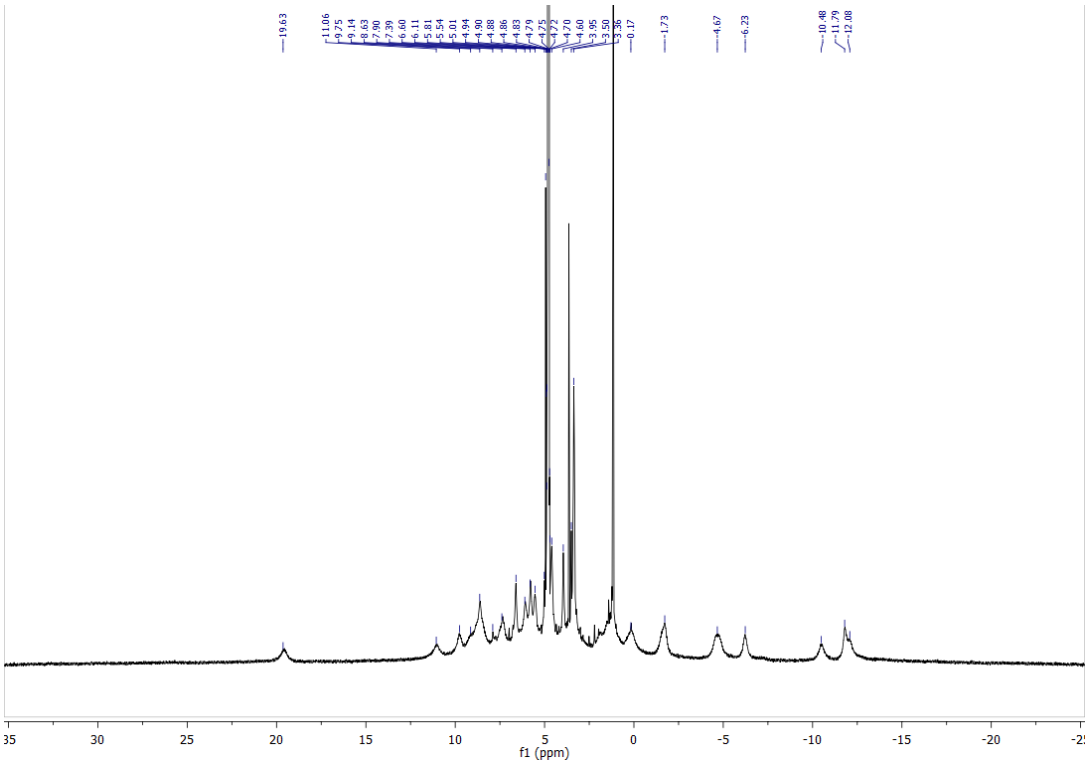

Figure S9. ^{1}H NMR spectrum of **EuLt^{t,MOM}** recorded at 298 K. Chemical shifts were referenced to D_2O.

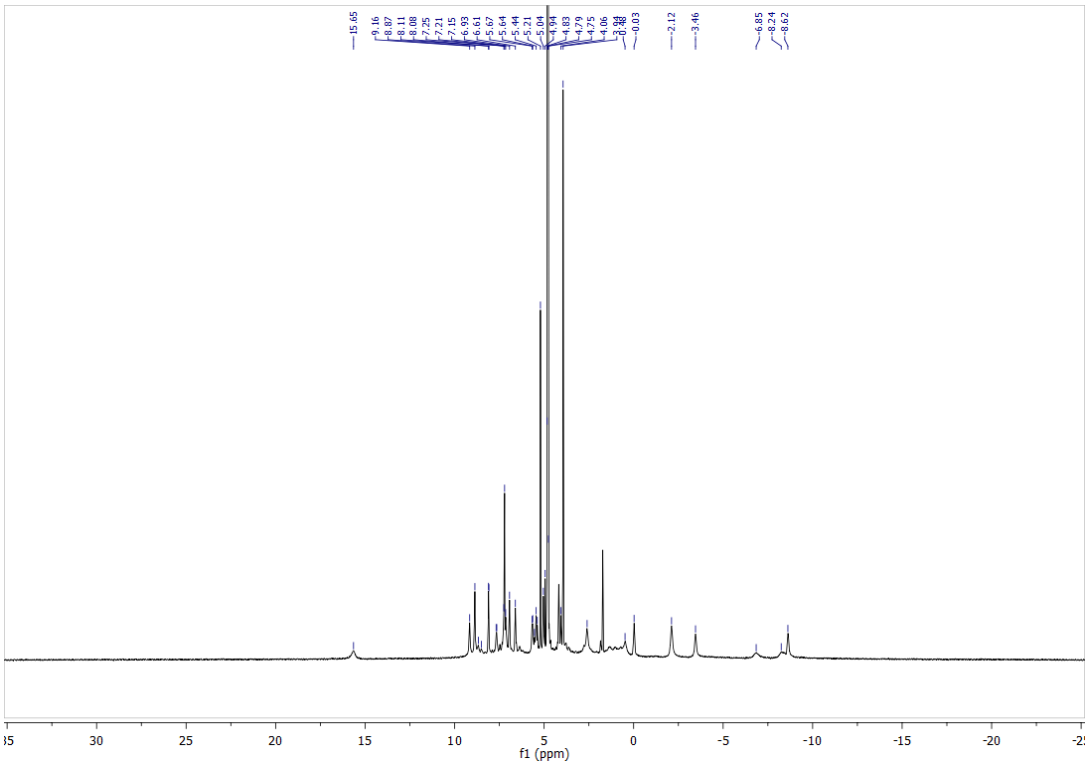

Figure S10. ^{1}H NMR spectrum of **EuLt^{t,MOM}** recorded at 353 K. Chemical shifts were referenced to D_2O.

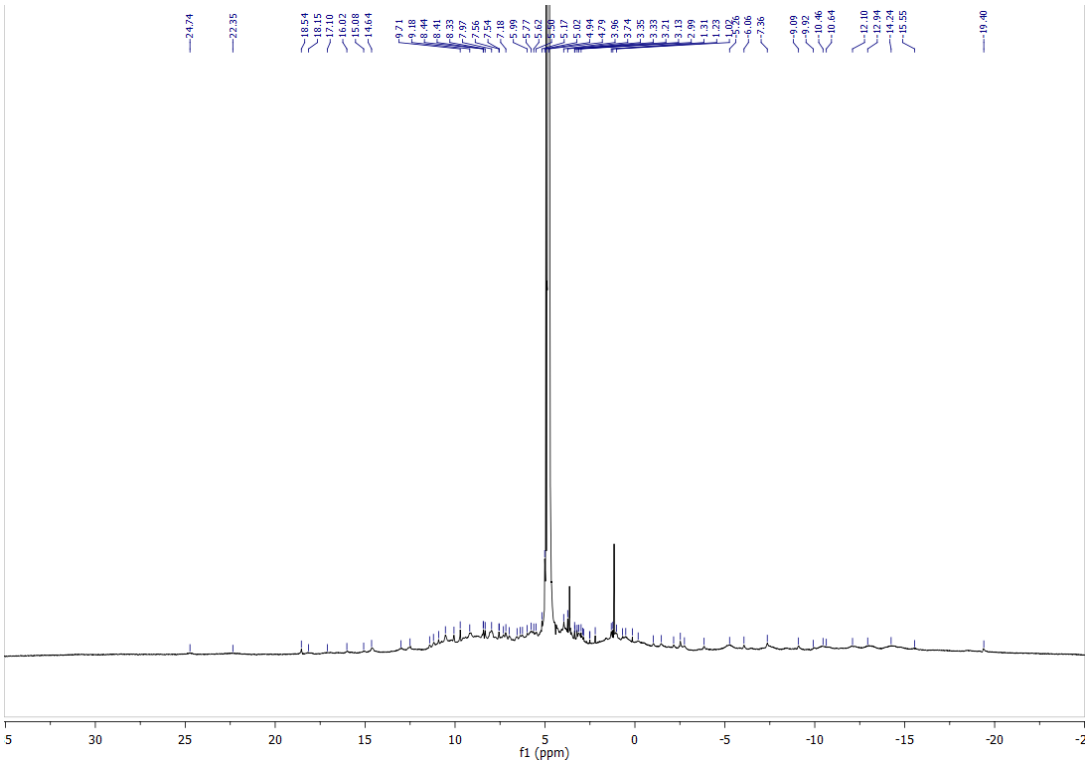

Figure S11. ^{1}H NMR spectrum of **EuLt^{s,CF3}** recorded at 298 K. Chemical shifts were referenced to D_2O.

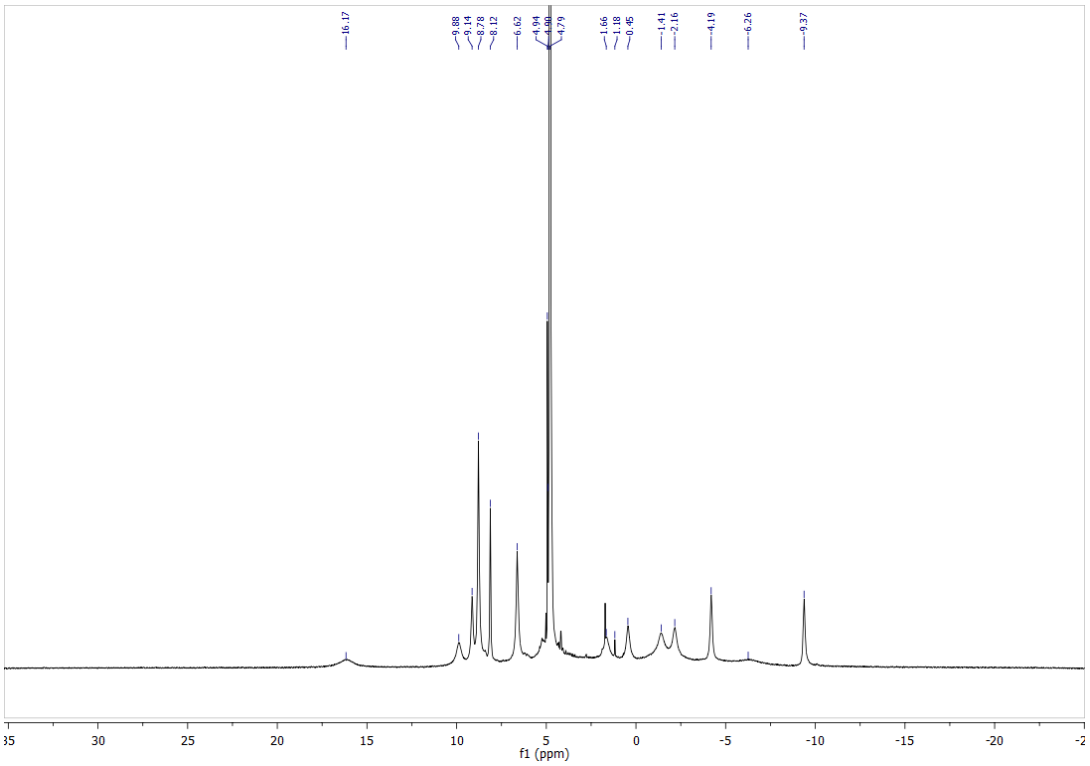

Figure S12. ^{1}H NMR spectrum of **EuLt^{s,CF3}** recorded at 353 K. Chemical shifts were referenced to D_2O.

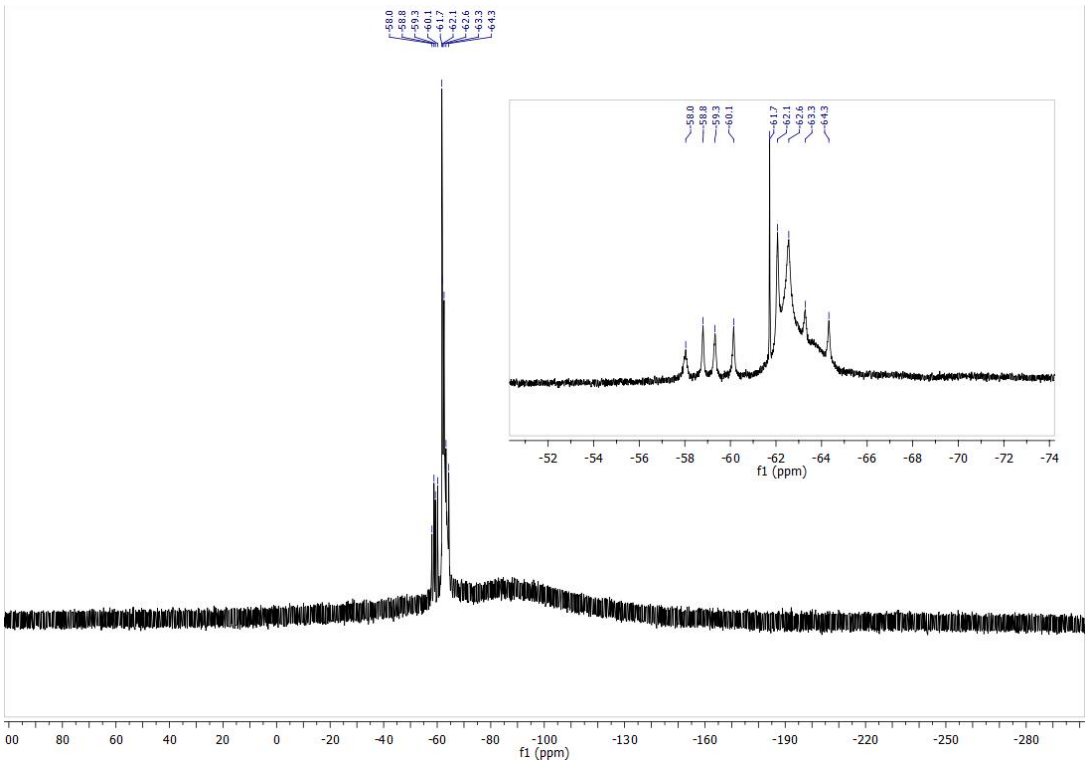

Figure S13. ^{19}F NMR spectrum of **EuLt^{s,CF3}** recorded at 298 K in D_2O.

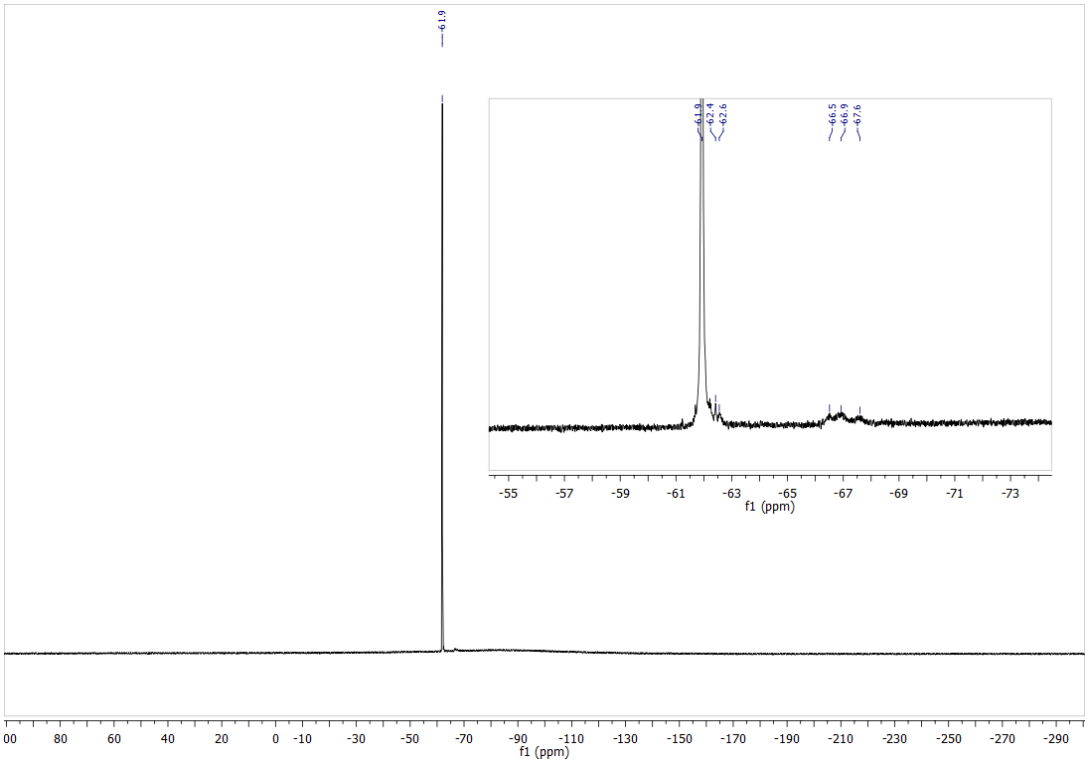

Figure S14. ^{19}F NMR spectrum of **EuLt^{s,CF3}** recorded at 353 K in D_2O.

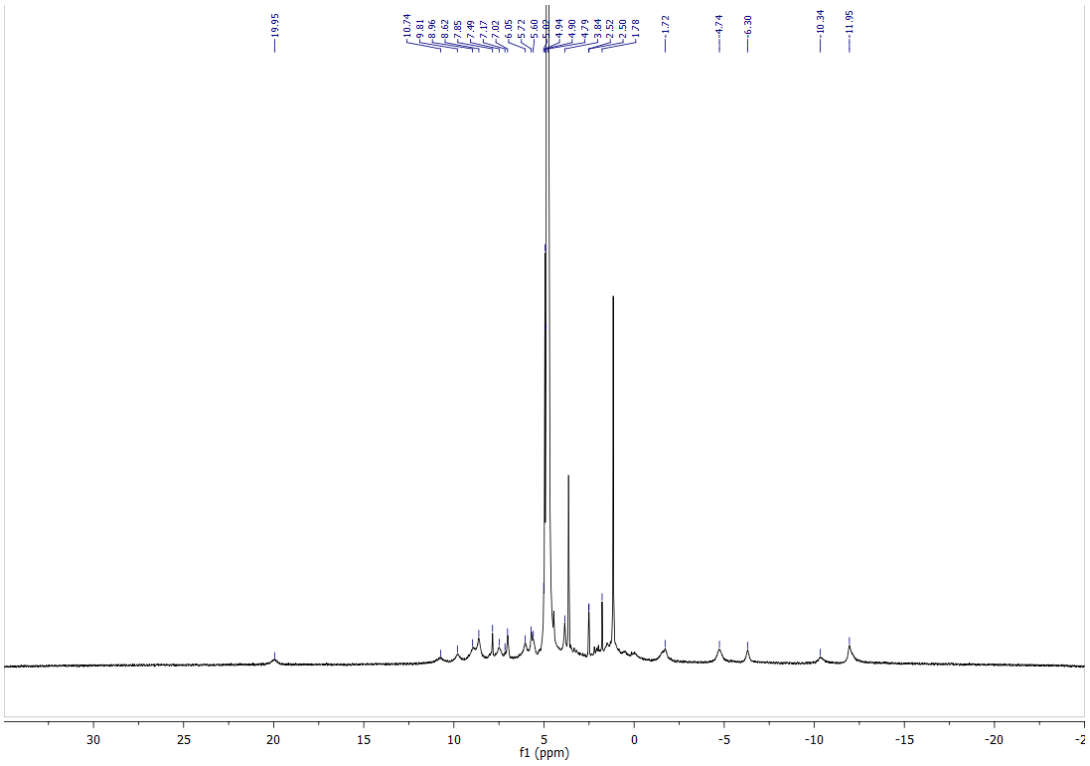

Figure S15. ^{1}H NMR spectrum of **EuLt^{t,CF3}** recorded at 298 K. Chemical shifts were referenced to D_2O.

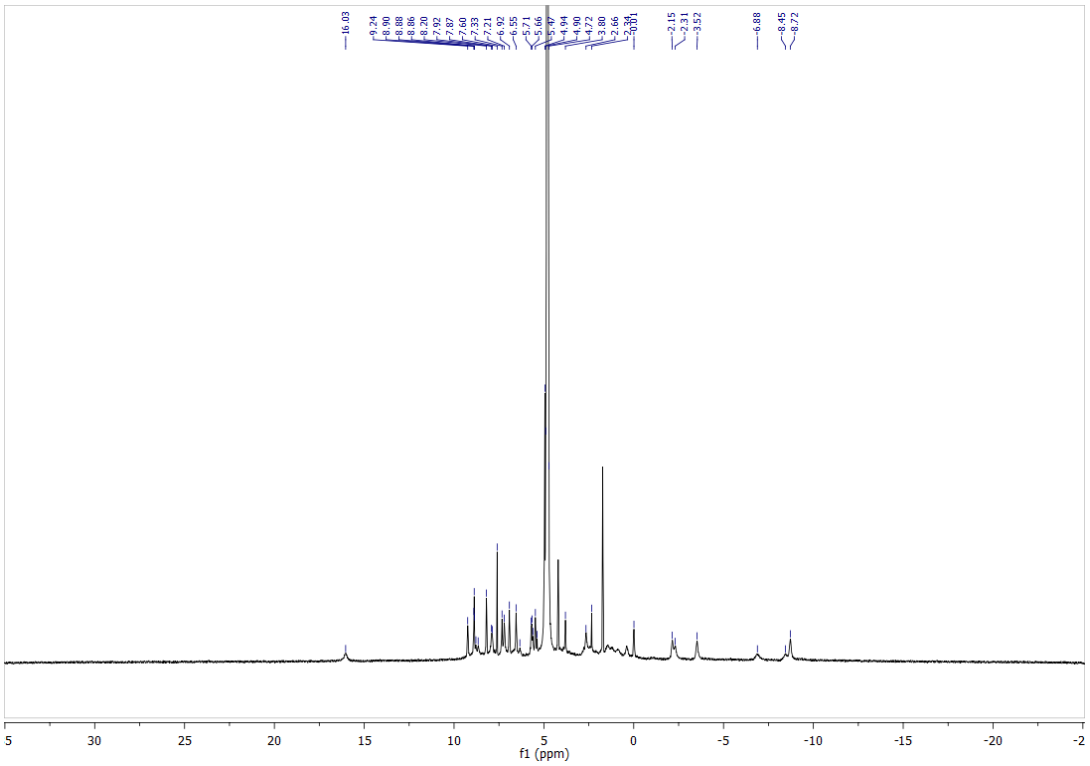

Figure S16. ^{1}H NMR spectrum of **EuLt^{t,CF3}** recorded at 353 K. Chemical shifts were referenced to D_2O.

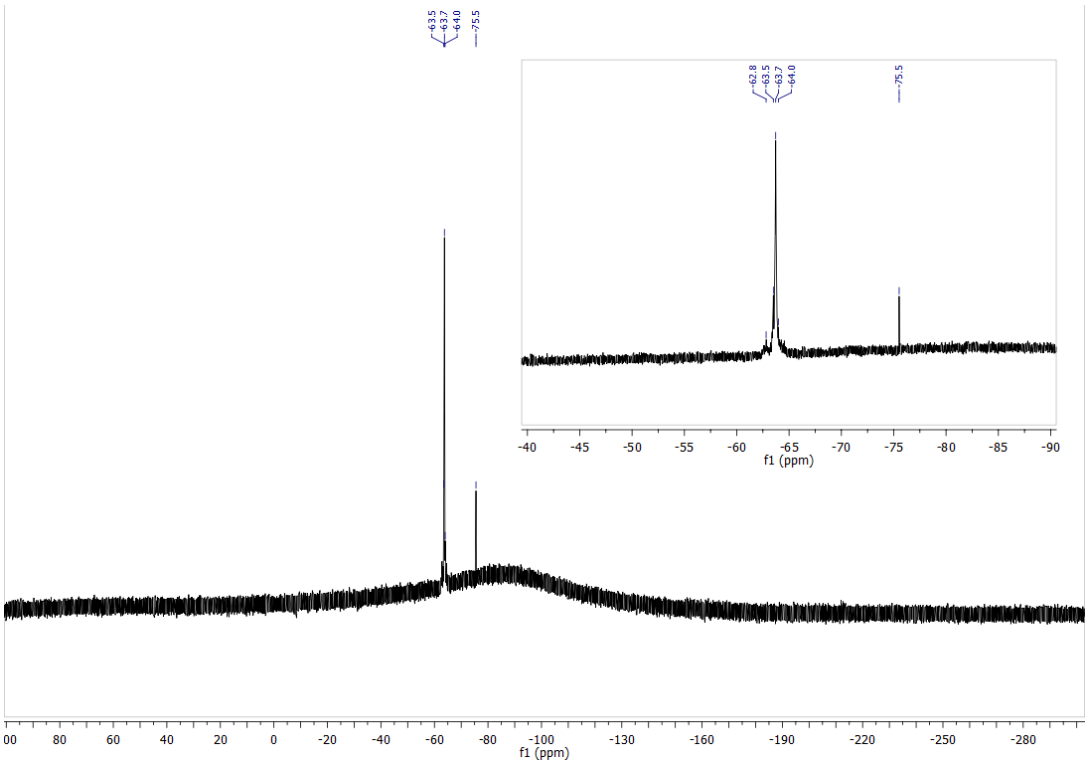

Figure S17. ^{19}F NMR spectrum of **EuLt^{t,CF3}** recorded at 298 K in D_2O.

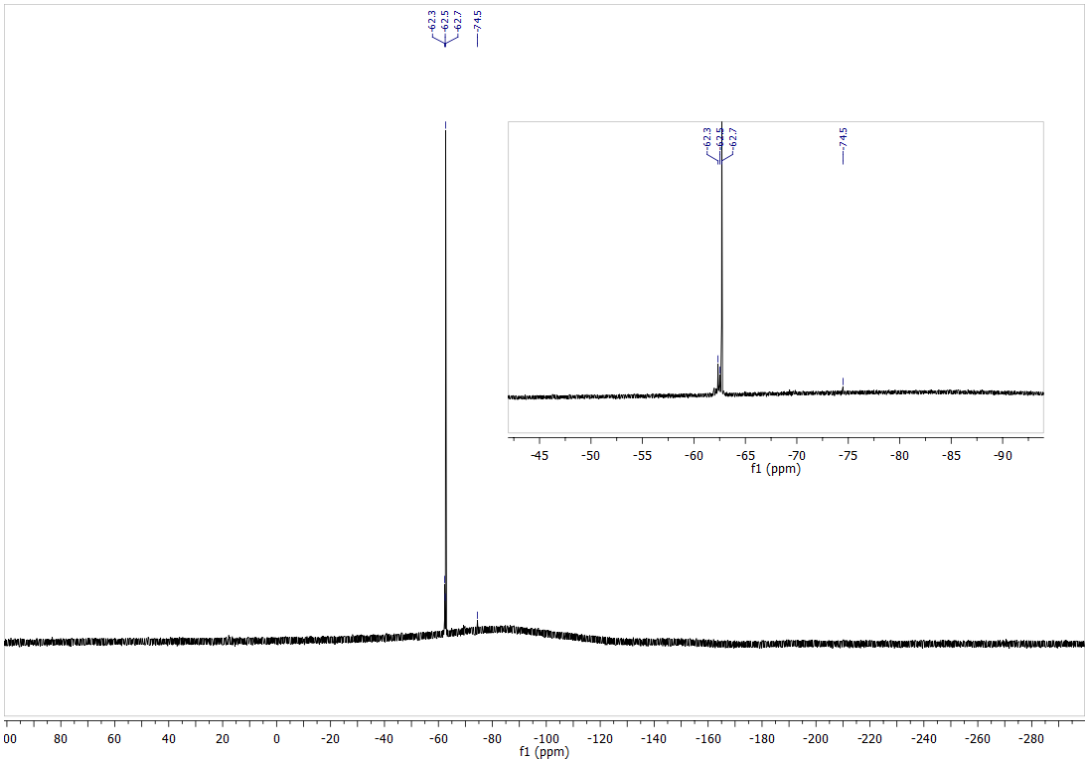

Figure S18. ^{19}F NMR spectrum of **EuLt^{t,CF3}** recorded at 353 K in D_2O.

Electrochemical characterization

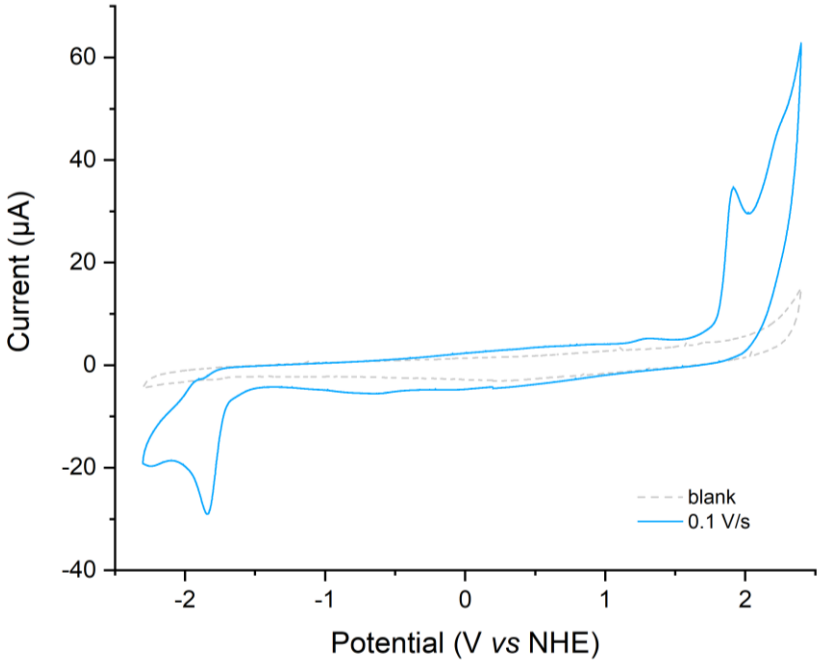

Figure S19. Cyclic voltammogram of **5a** (1mM) with $TBAPF_6$ (200 mM) as supporting electrolyte in MeCN under Ar using a glassy carbon working electrode.

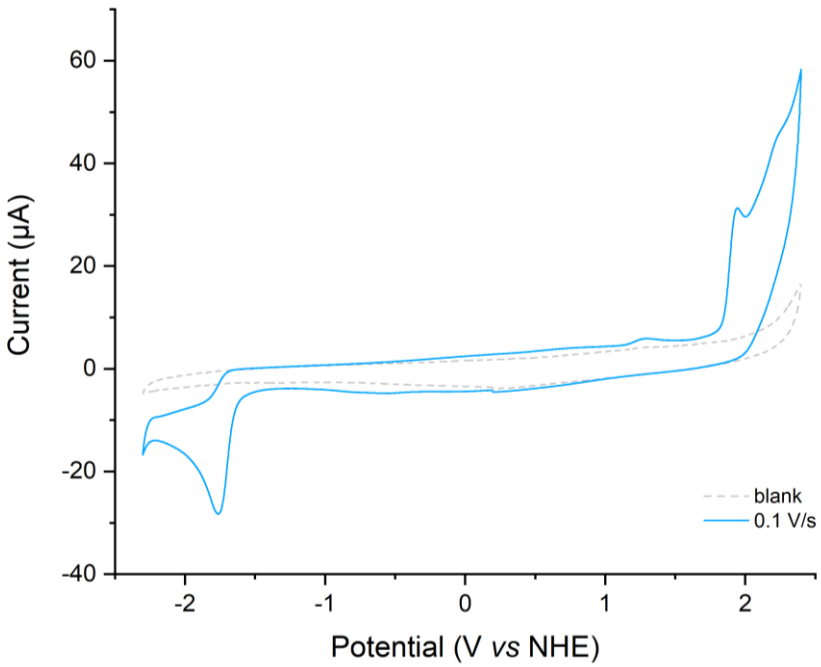

Figure S20. Cyclic voltammogram of **5b** (1mM) with $TBAPF_6$ (200 mM) as supporting electrolyte in MeCN under Ar using a glassy carbon working electrode.

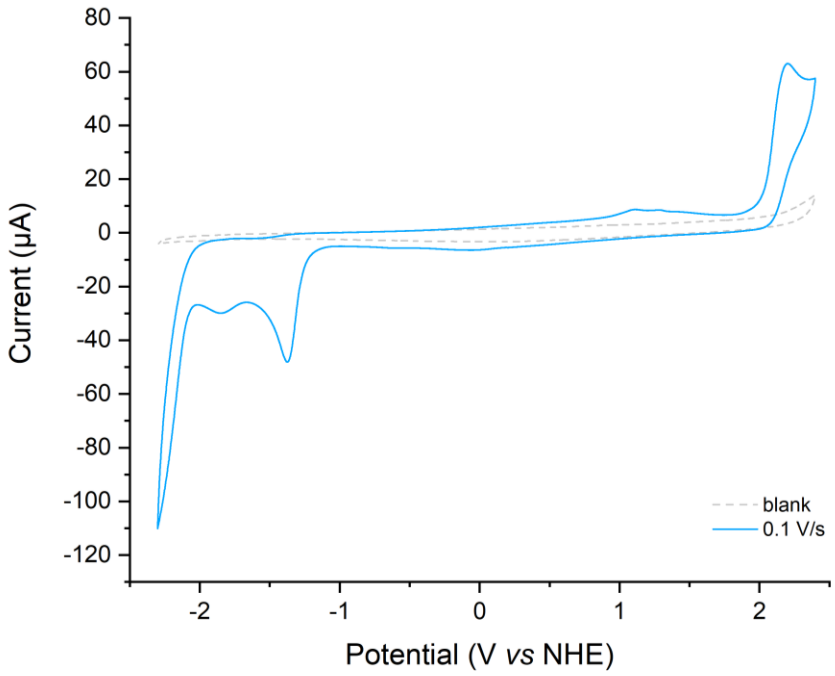

Figure S21. Cyclic voltammogram of **5c** (1mM) with $TBAPF_6$ (200 mM) as supporting electrolyte in MeCN under Ar using a glassy carbon working electrode.

Photophysical characterization

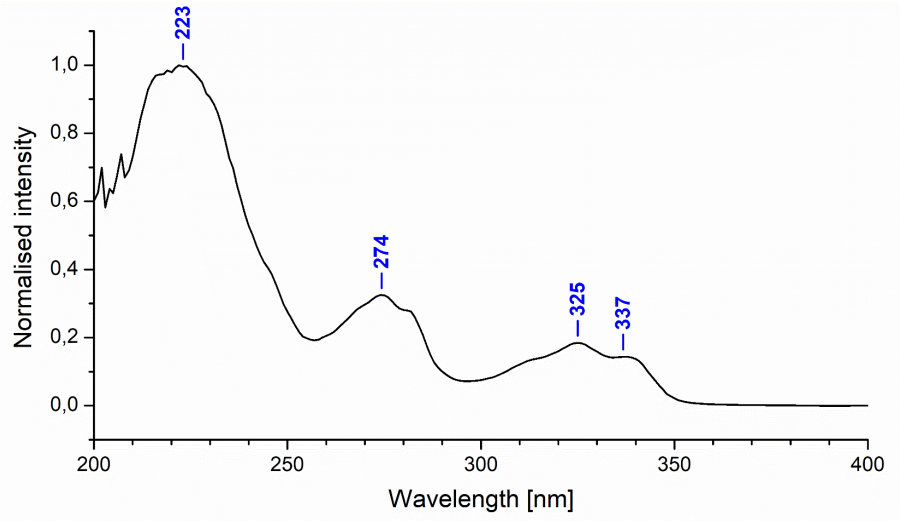

Figure S22. Normalized absorption spectrum of **GdLt^{t,Me}** in 0.01 M PIPES-buffered aqueous solution, pH 6.5. Blue numbers show local maxima of the spectra.

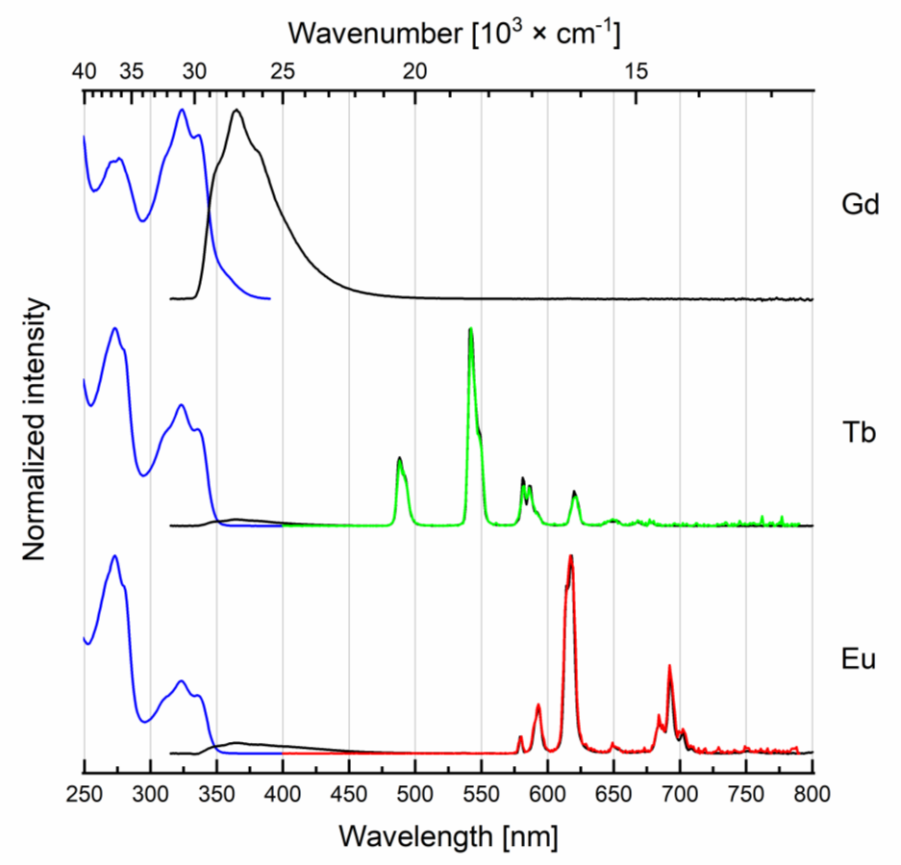

Figure S23. Excitation spectra of the Ln-centered emissions (**TbLt^{t,Me}** λ_{em} = 542 nm, **EuLt^{t,Me}** λ_{em} = 618 nm) and of the ligand centered emission (**GdLt^{t,Me}** 405 nm) at 298 K (blue lines). Steady-state emission spectra of **LnLt^{t,Me}** at 298 K (black lines) and time-resolved emission spectra showing the Ln-centered

emissions (Tb (green), Eu (red), 298 K, colored lines). Excitation at λ_{ex} = 325 nm; [**LnLt^{t,Me}**] = 10 µM, PIPES-buffered aqueous solutions 10 mM, pH 6.5.

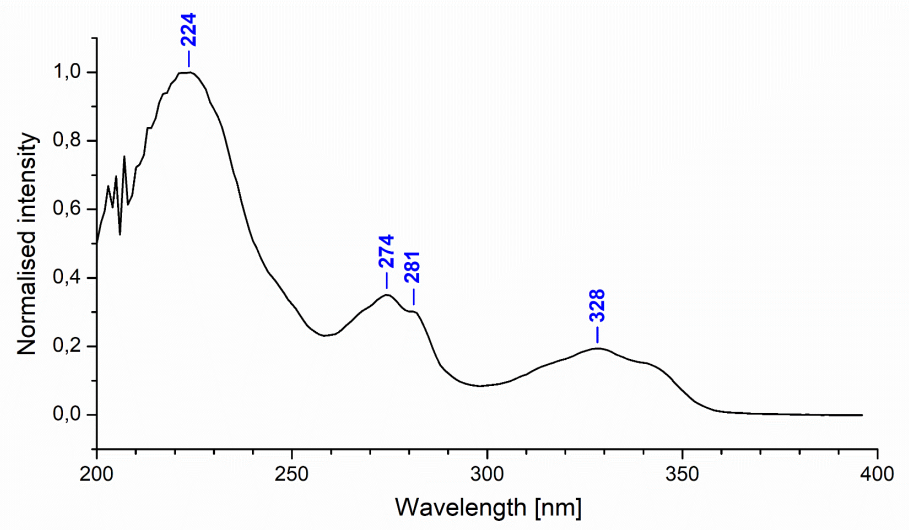

Figure S24. Normalized absorption spectrum of **GdLt^{t,MOM}** in 0.01 M PIPES-buffered aqueous solution, pH 6.5. Blue numbers show local maxima of the spectra.

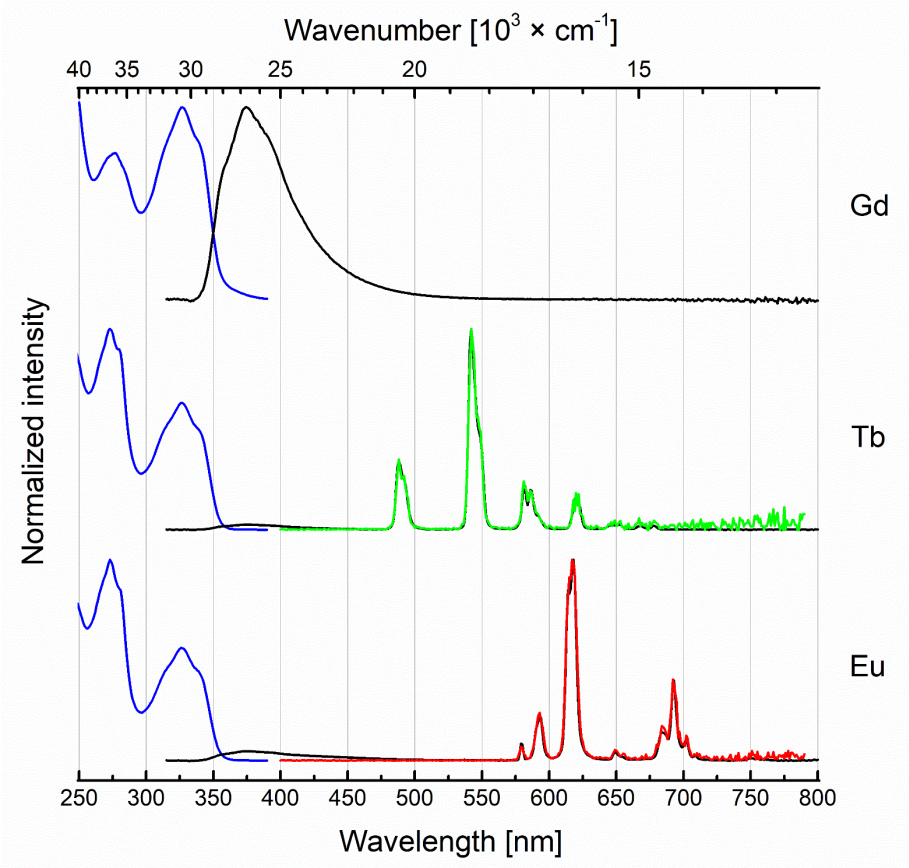

Figure S25. Excitation spectra of the Ln-centered emissions (**TbLt^{t,MOM}** λ_{em} = 542 nm, **EuLt^{t,MOM}** λ_{em} = 618 nm) and of the ligand centered emission (**GdLt^{t,MOM}** 405 nm) at 298 K (blue lines). Steady-state emission spectra of **LnLt^{t,MOM}** at 298 K (black lines) and time-resolved emission spectra showing the

Ln-centered emissions (Tb (green), Eu (red), 298 K, colored lines). Excitation at λ_{ex} = 328 nm; [**LnLt^{t,MOM}**] = 10 µM, PIPES-buffered aqueous solutions 10 mM, pH 6.5.

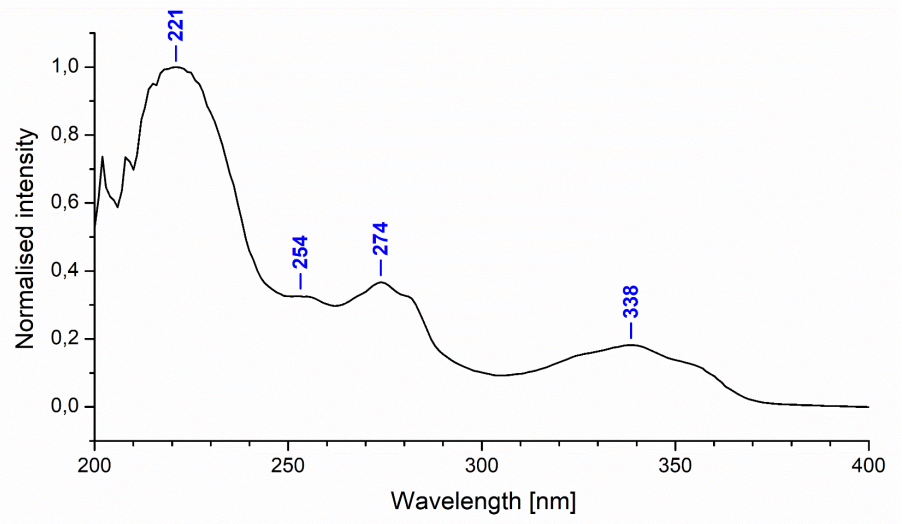

Figure S26. Normalized absorption spectrum of **GdLt^{t,CF3}** in 0.01 M PIPES-buffered aqueous solution, pH 6.5. Blue numbers show local maxima of the spectra.

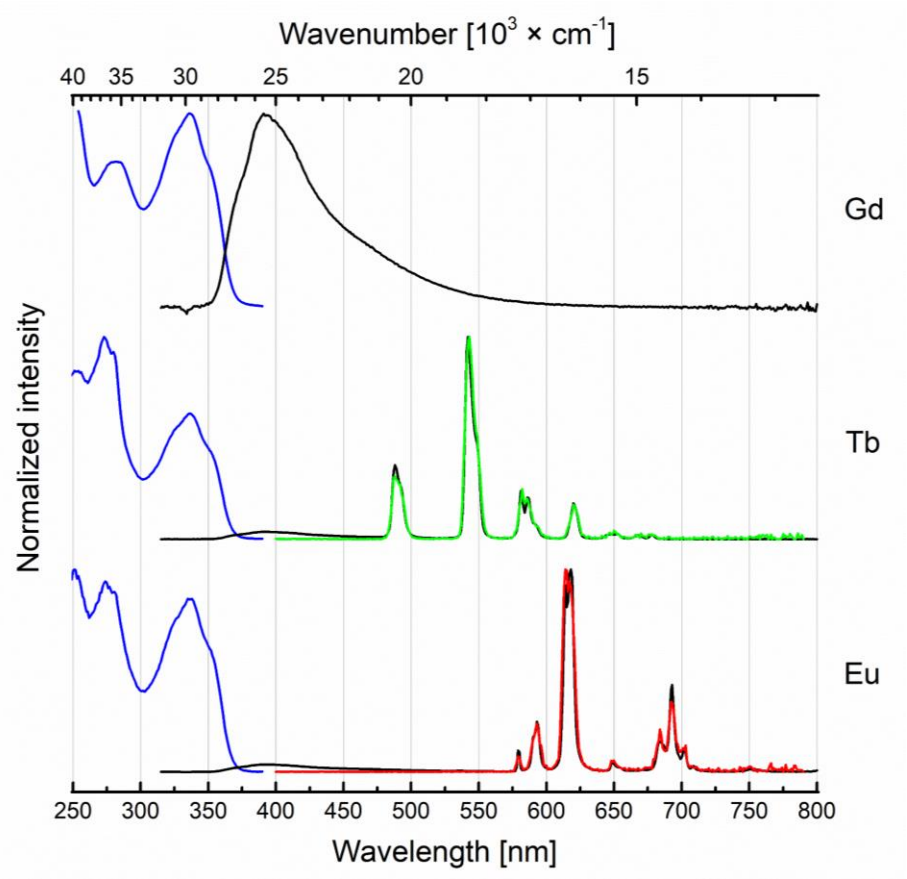

Figure S27. Excitation spectra of the Ln-centered emissions (**TbLt^{t,CF3}** λ_{em} = 542 nm, **EuLt^{t,CF3}** λ_{em} = 618 nm) and of the ligand centered emission (**GdLt^{t,CF3}** 405 nm) at 298 K (blue lines). Steady-state emission spectra of **LnLt^{t,CF3}** at 298 K (black lines) and time-resolved emission spectra showing the Ln-

centered emissions (Tb (green), Eu (red), 298 K, colored lines). Excitation at λ_{ex} = 330 nm; [**LnLt^{t,CF3}**] = 10 µM, PIPES-buffered aqueous solutions 10 mM, pH 6.5.

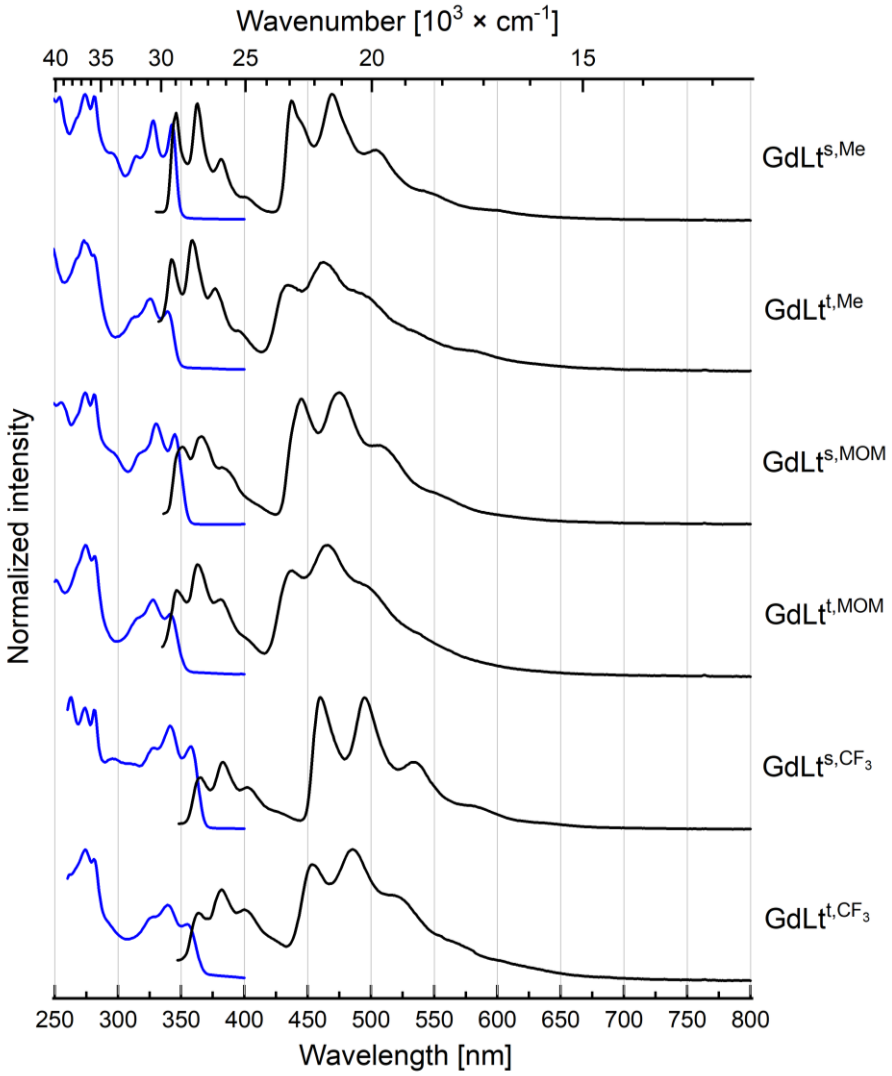

Figure S28. Steady-state phosphorescence spectra of the Gd complexes (**GdLt^{s,Me}** λ_{ex} = 330 nm, **GdLt^{t,Me}** λ_{ex} = 325 nm, **GdLt^{s,MOM}** λ_{ex} = 335 nm, **GdLt^{t,MOM}** λ_{ex} = 328 nm, **GdLt^{s,CF3}** λ_{ex} = 341 nm, **GdL1^{t,CF3}** λ_{ex} = 338 nm) at 77 K with 10% glycerol added to the 10 mM PIPES-buffered aqueous solutions at pH 6.5, [**GdL**] = 10 µM.

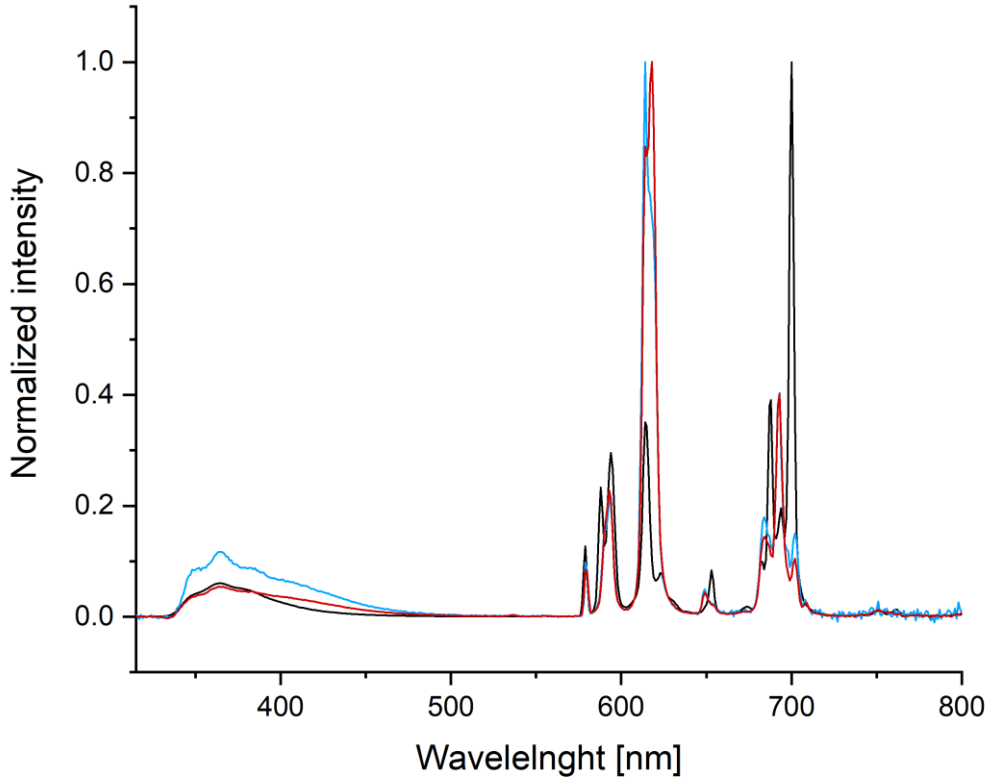

Figure S29. Comparison of the steady-state emission spectra of **EuLt^{s,Me}** (blue),[2] **EuLt^{t,Me}** (red), and **EuLc^{t,Me}** (black).[7]

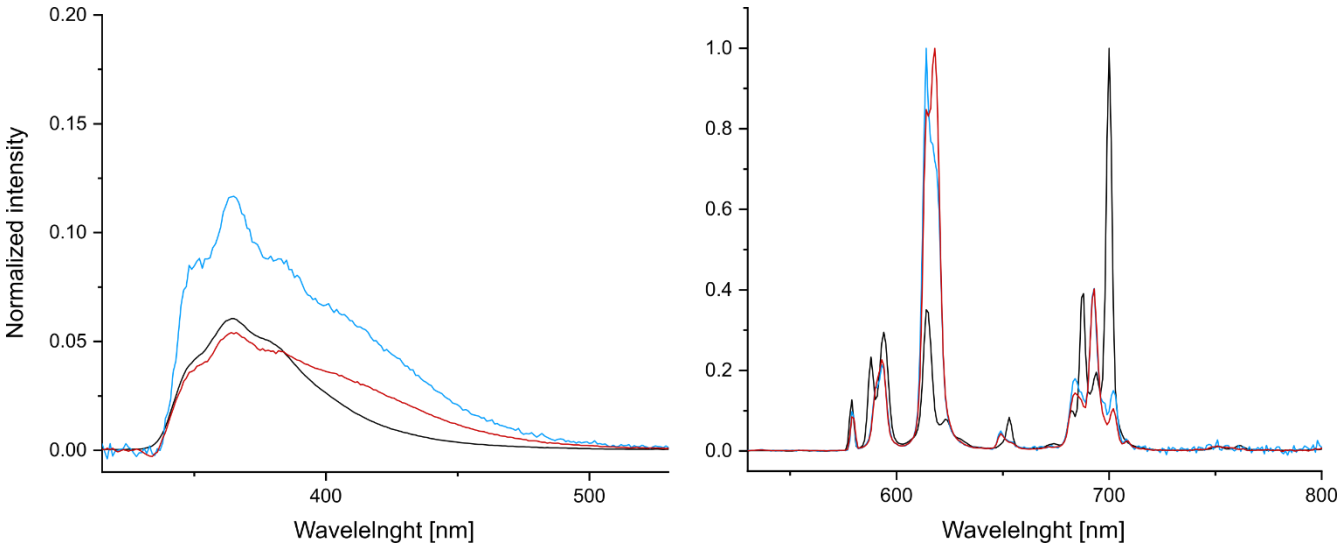

Figure S30. Comparison of steady-state emission spectra of antennae (left) and metal (right), **EuLt^{s,Me}** (blue),[2] **EuLt^{t,Me}** (red), and **EuLc^{t,Me}** (black).[7]

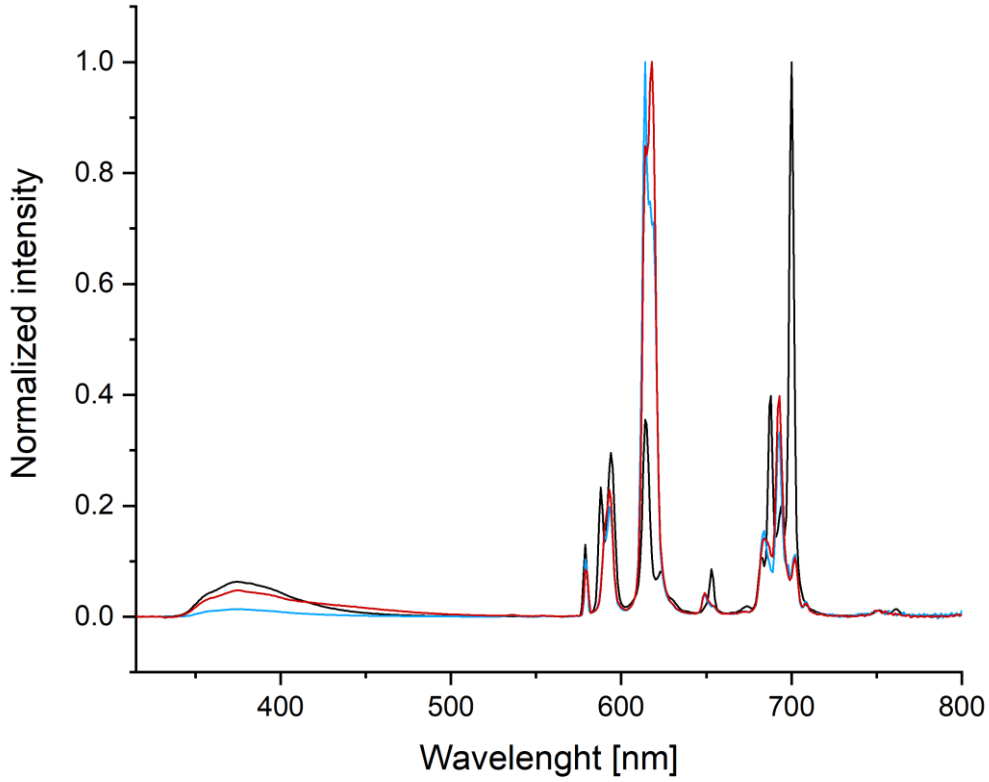

Figure S31. Comparison of the steady-state emission spectra of **EuLt^{s,MOM}** (blue),[2] **EuLt^{t,MOM}** (red), and **EuLc^{t,MOM}** (black).[7]

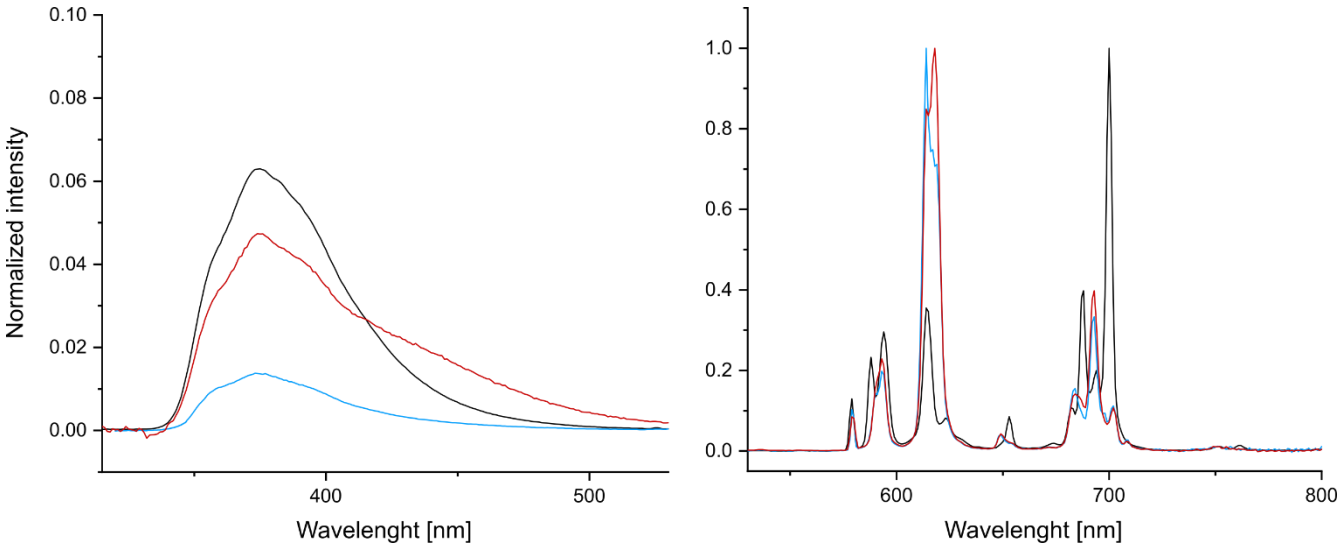

Figure S32. Comparison of steady-state emission spectra of antennae (left) and metal (right), **EuLt^{s,MOM}** (blue),[2] **EuLt^{t,MOM}** (red), and **EuLc^{t,MOM}** (black).[7]

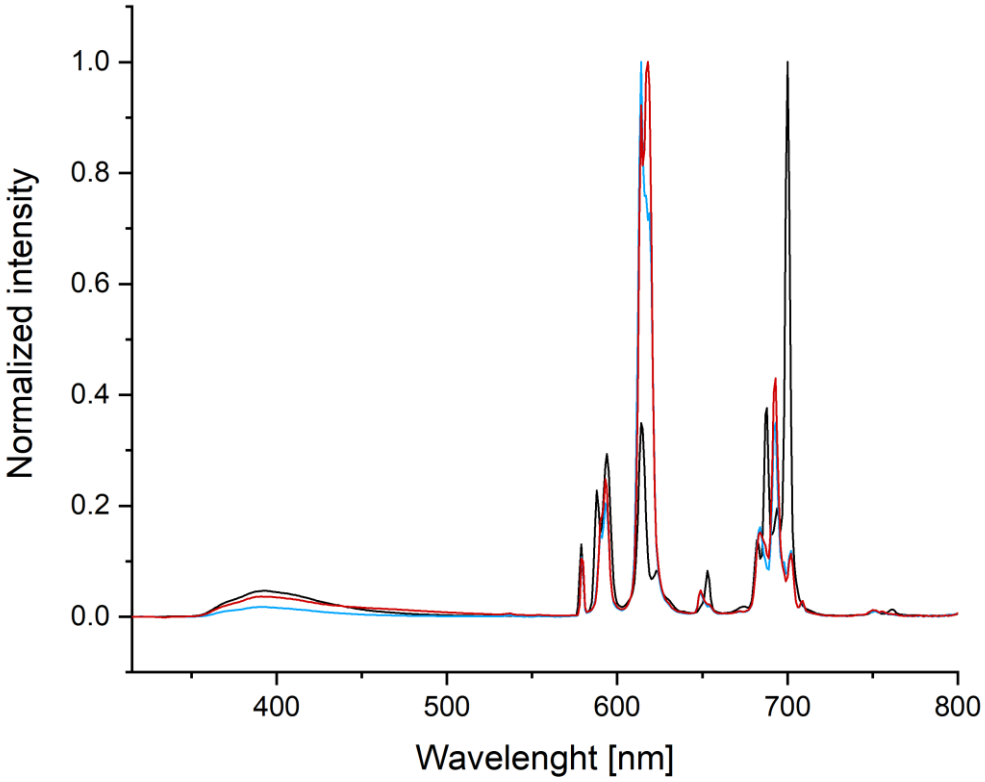

Figure S33. Comparison of the steady-state emission spectra of **EuLt^{s,CF3}** (blue),[2] **EuLt^{t,CF3}** (red), and **EuLc^{t,CF3}** (black).[7]

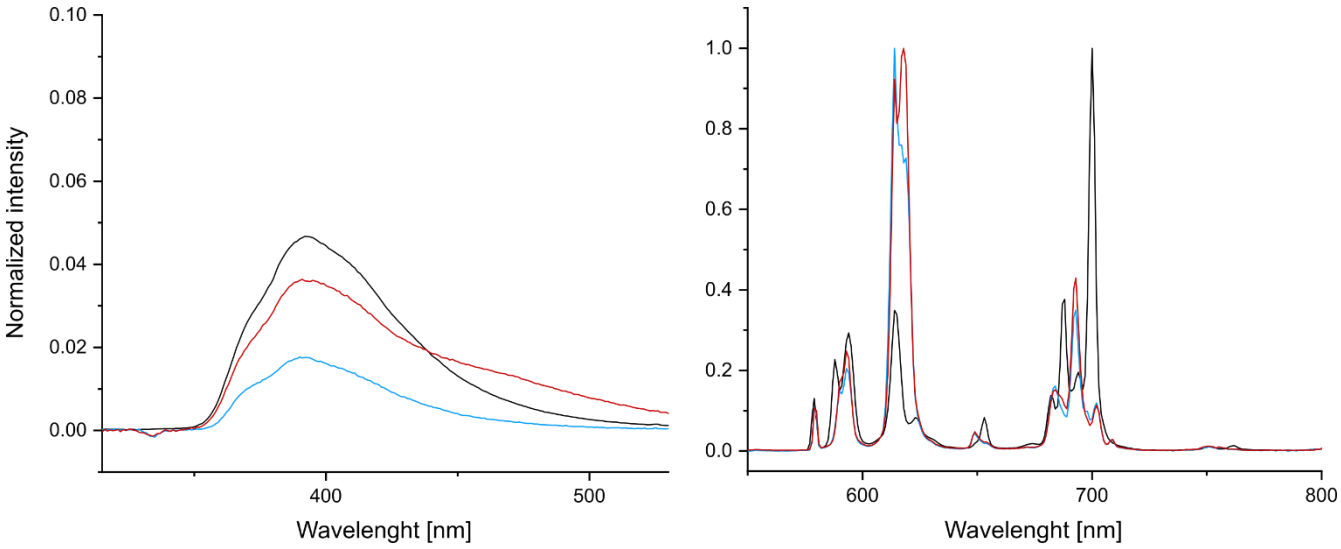

Figure S34. Comparison of steady-state emission spectra of antennae (left) and metal (right), **EuLt^{s,CF3}** (blue),[2] **EuLt^{t,CF3}** (red), and **EuLc^{t,CF3}** (black).[7]

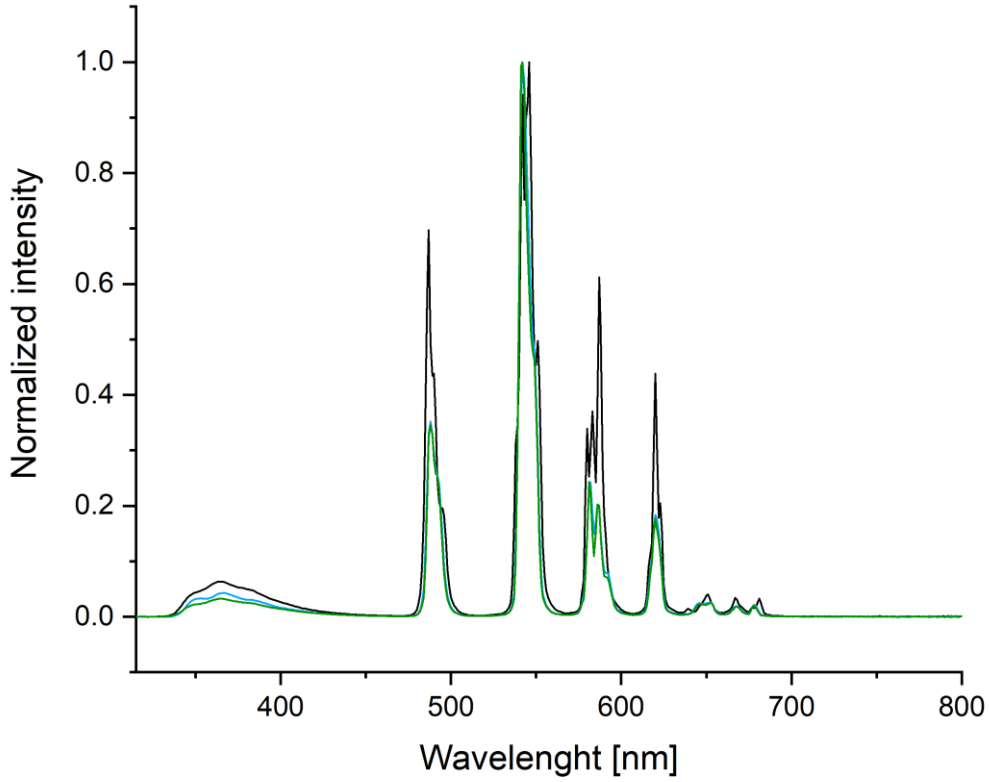

Figure S35. Comparison of the steady-state emission spectra of **TbLt^{s,Me}** (blue),[2] **TbLt^{s,Me}** (green), and **TbLc^{t,Me}** (black).[7]

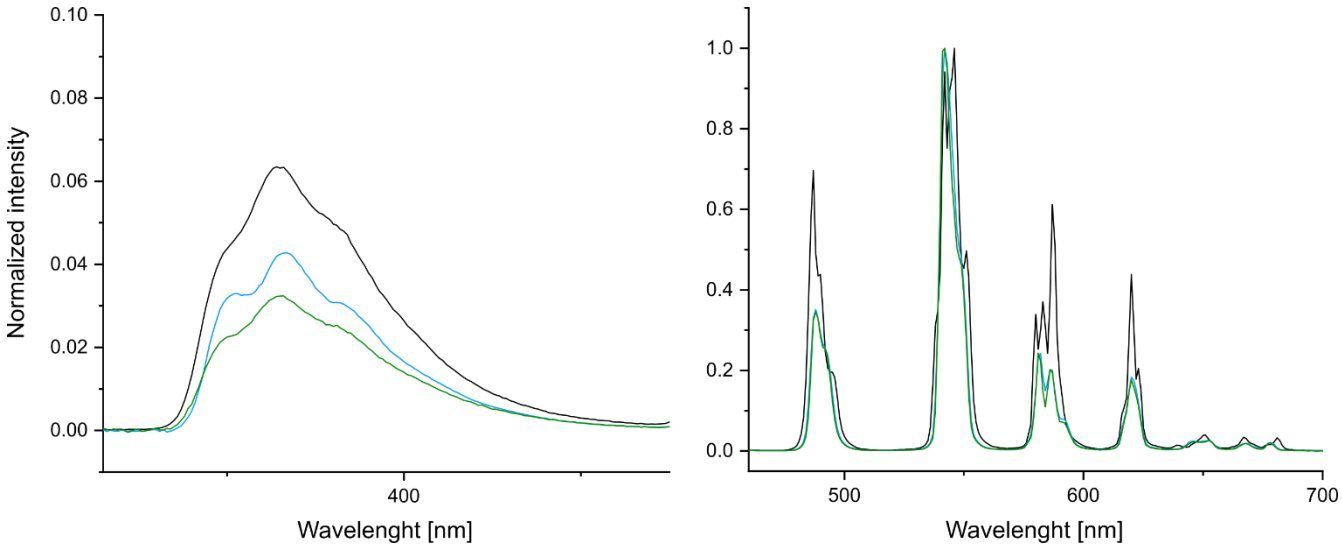

Figure S36. Comparison of steady-state emission spectra of antennae (left) and metal (right), **TbLt^{s,Me}** (blue),[2] **TbLt^{t,Me}** (green), and **TbLc^{t,Me}** (black).[7]

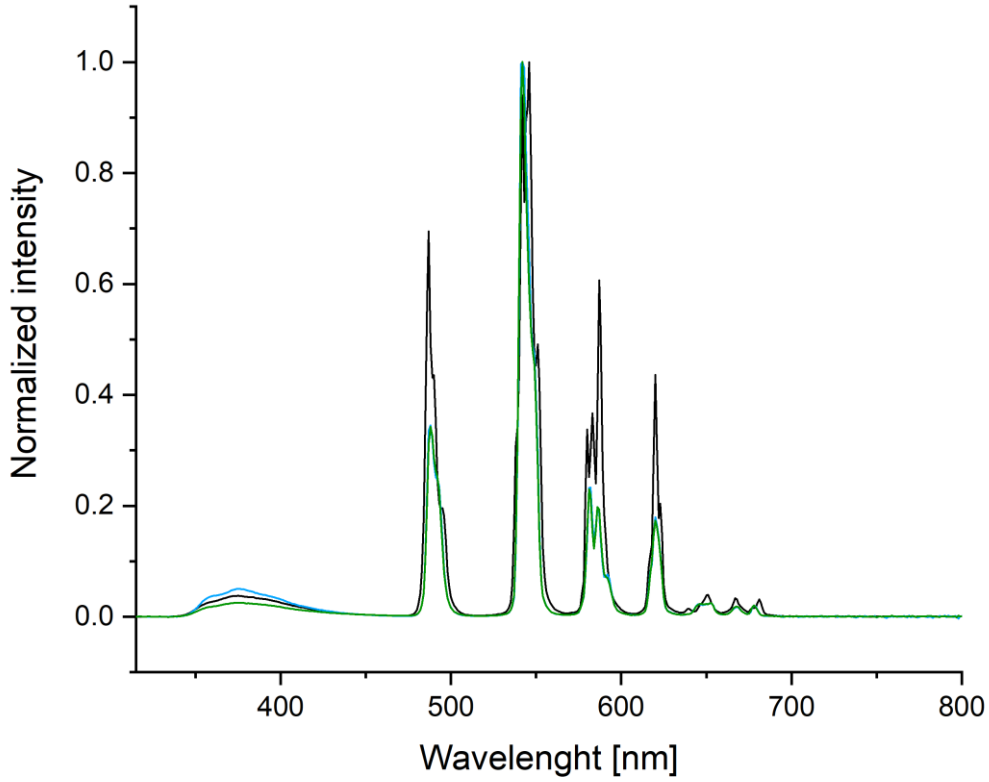

Figure S37. Comparison of the steady-state emission spectra of **TbLt^{s,MOM}** (blue),[2] **TbLt^{t,MOM}** (green), and **TbLc^{t,MOM}** (black).[7]

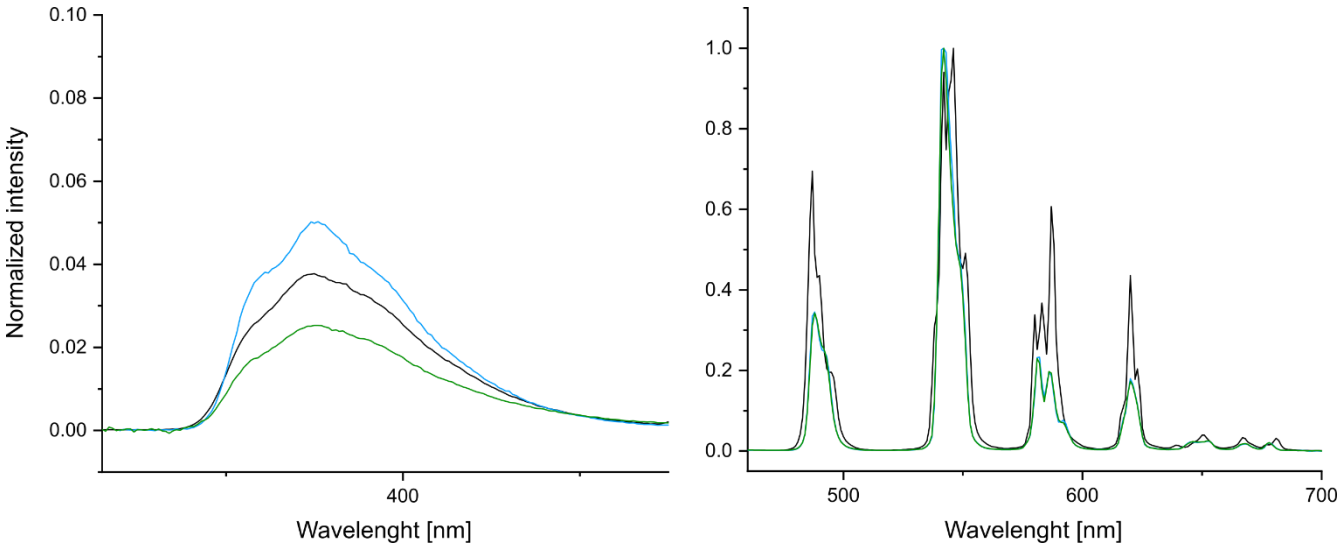

Figure S38. Comparison of steady-state emission spectra of antennae (left) and metal (right), **TbLt^{s,MOM}** (blue),[2] **TbLt^{t,MOM}** (green), and **TbLc^{t,MOM}** (black).[7]

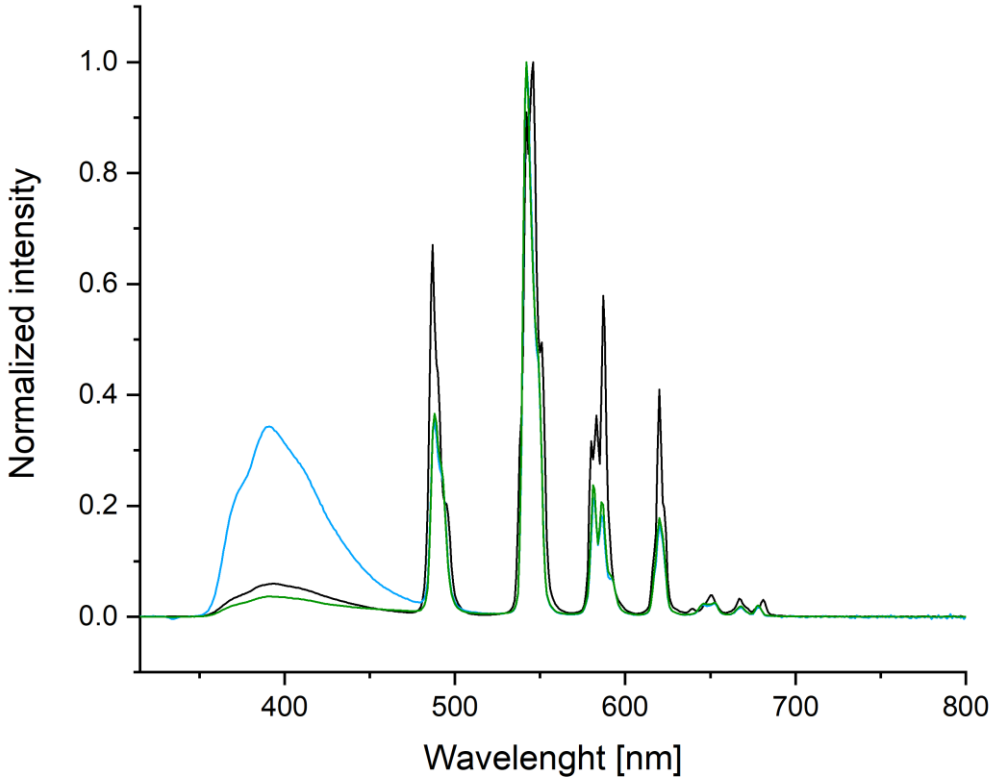

Figure S39. Comparison of the steady-state emission spectra of **TbLt^{s,CF3}** (blue),[2] **TbLt^{t,CF3}** (green), and **TbLc^{t,CF3}** (black).[7]

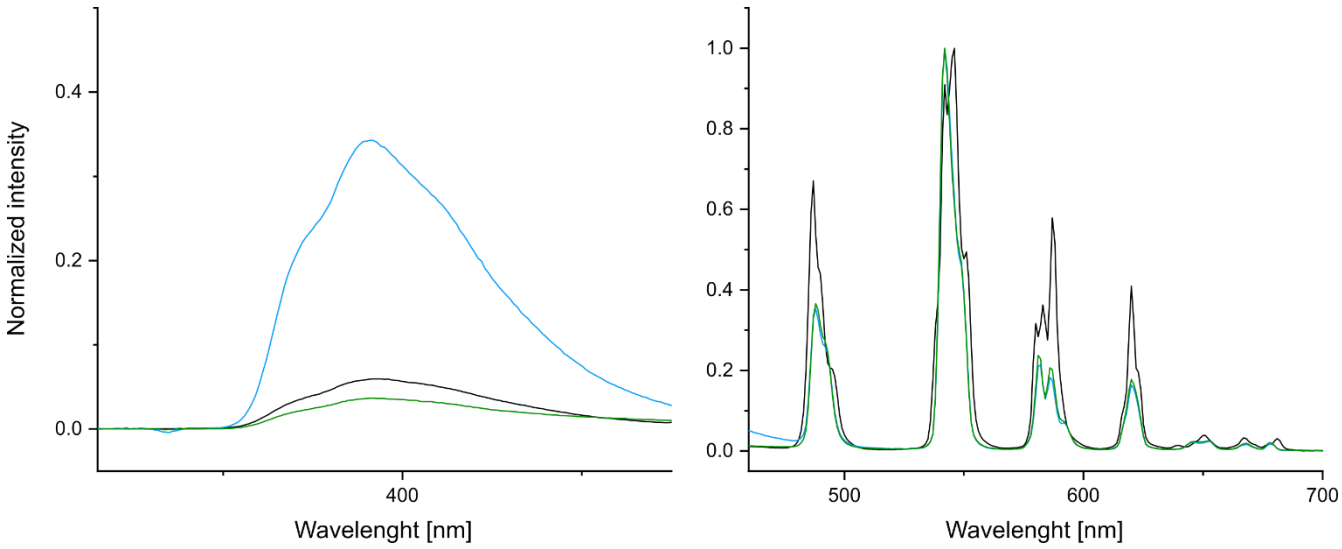

Figure S40. Comparison of steady-state emission spectra of antennae (left) and metal (right), **TbLt^{s,CF3}** (blue),[2] **TbLt^{t,CF3}** (green), and **TbLc^{s,CF3}** (black).[7]

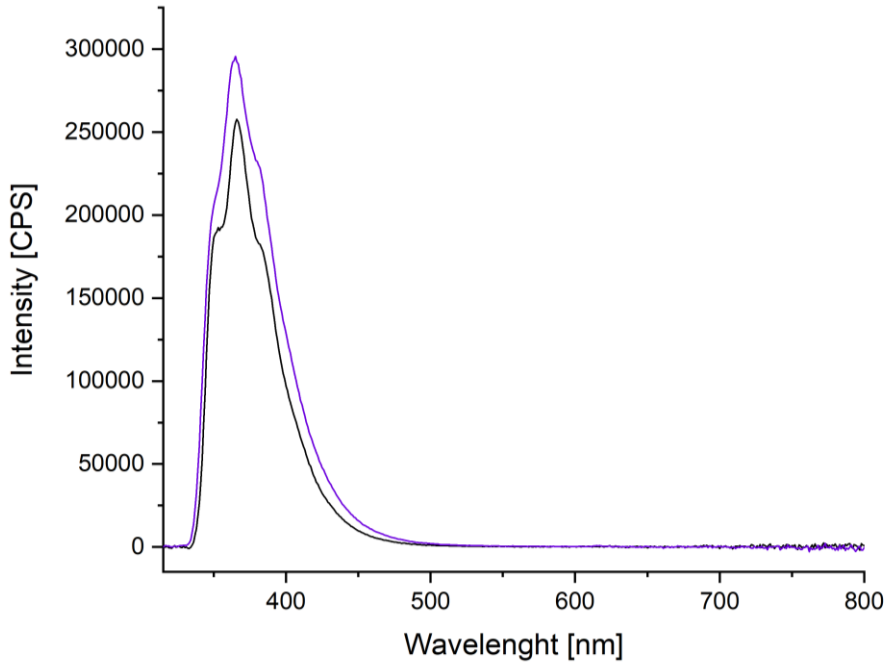

Figure S41. Comparison of the steady-state emission spectra of **GdLt^{s,Me}** (black, λ_{ex} = 328 nm),[2] **GdLt^{t,Me}** (purple, λ_{ex} = 325 nm), [**GdL**] = 10 μM.

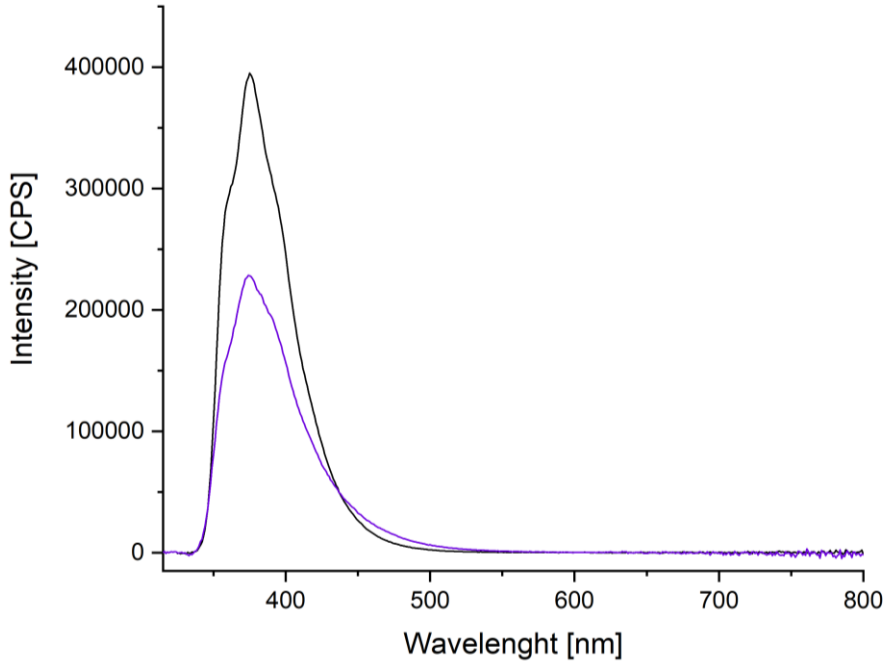

Figure S42. Comparison of the steady-state emission spectra of **GdLt^{s,MOM}** (black, λ_{ex} = 328 nm),[2] **GdLt^{t,MOM}** (purple, λ_{ex} = 328 nm), [**GdL**] = 10 μM.

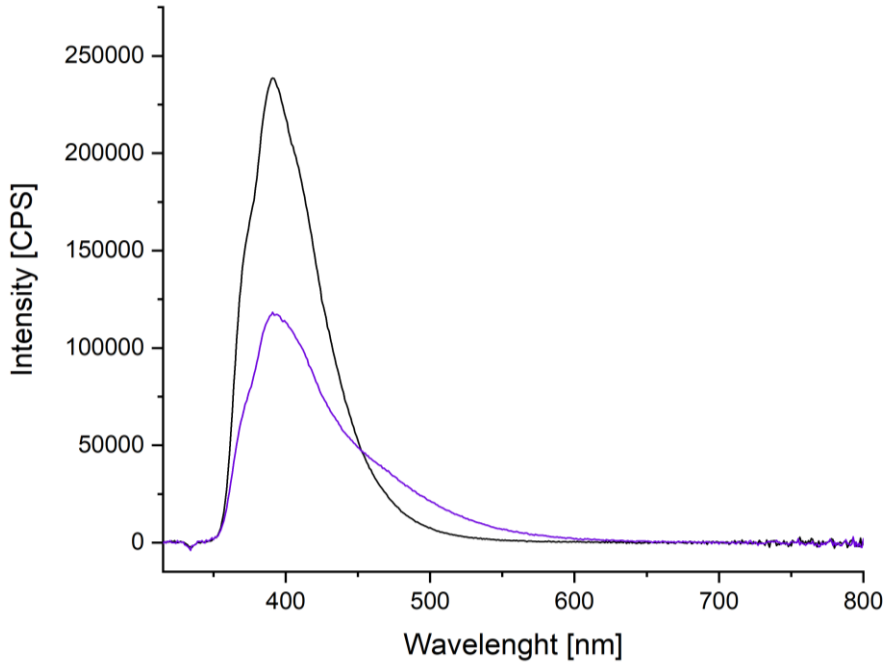

Figure S43. Comparison of the steady-state emission spectra of **GdLt^{s,CF3}** (black, λ_{ex} = 331 nm),[2] **GdLt^{t,CF3}** (purple, λ_{ex} = 330 nm), [**GdL**] = 10 μM.

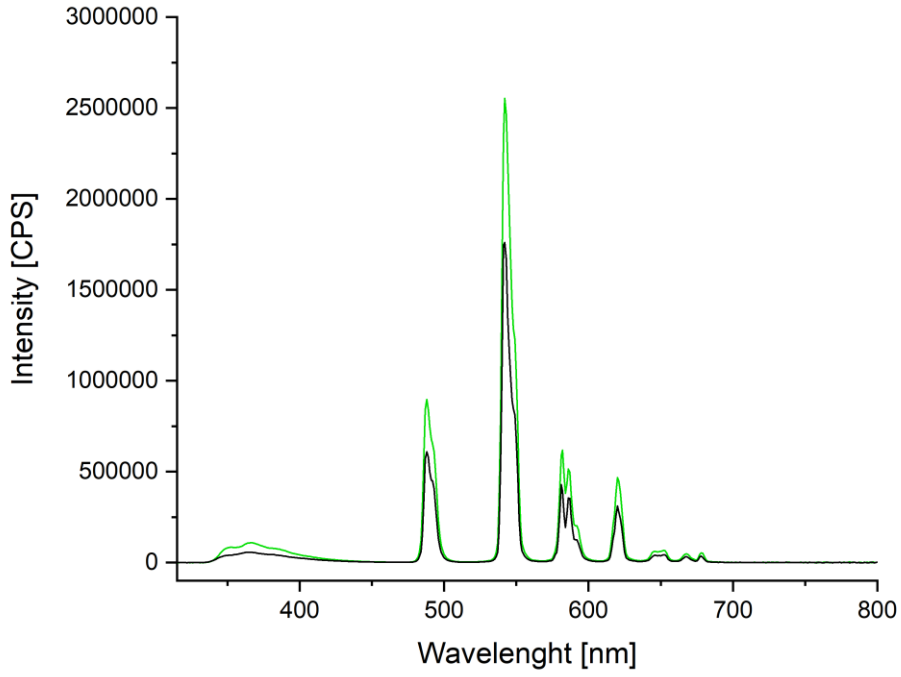

Figure S44. Comparison of the steady-state emission spectra of **TbLt^{s,Me}** (black, λ_{exc} = 328 nm)[2], **TbLt^{t,Me}** (green, λ_{ex} = 325 nm), [**TbL**] = 10 μM.

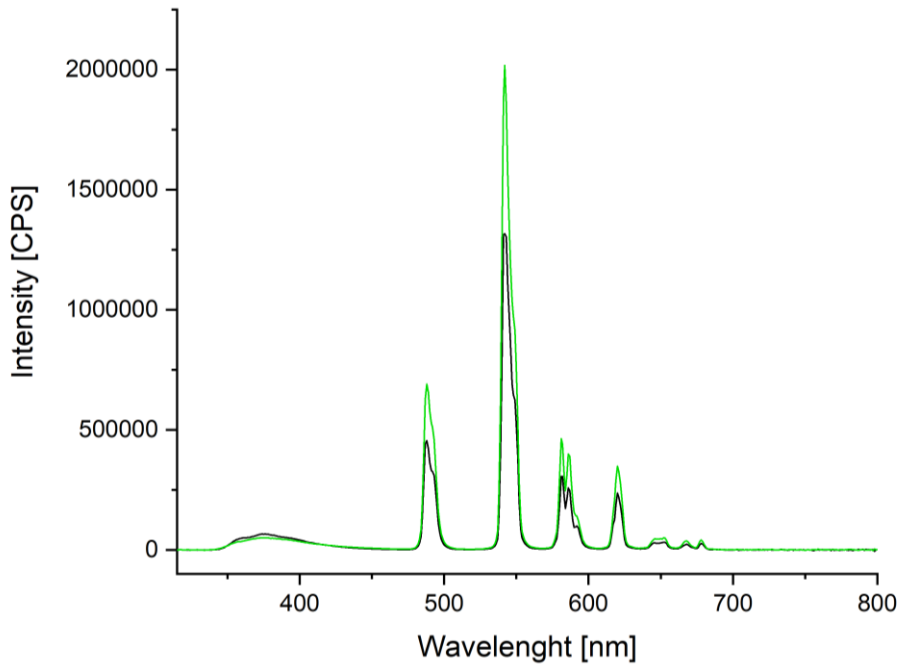

Figure S45. Comparison of the steady-state emission spectra of **TbLt^{s,MOM}** (black, λ_{ex} = 328 nm)[2], **TbLt^{t,MOM}** (green, λ_{ex} = 328 nm), [**TbL**] = 10 μM.

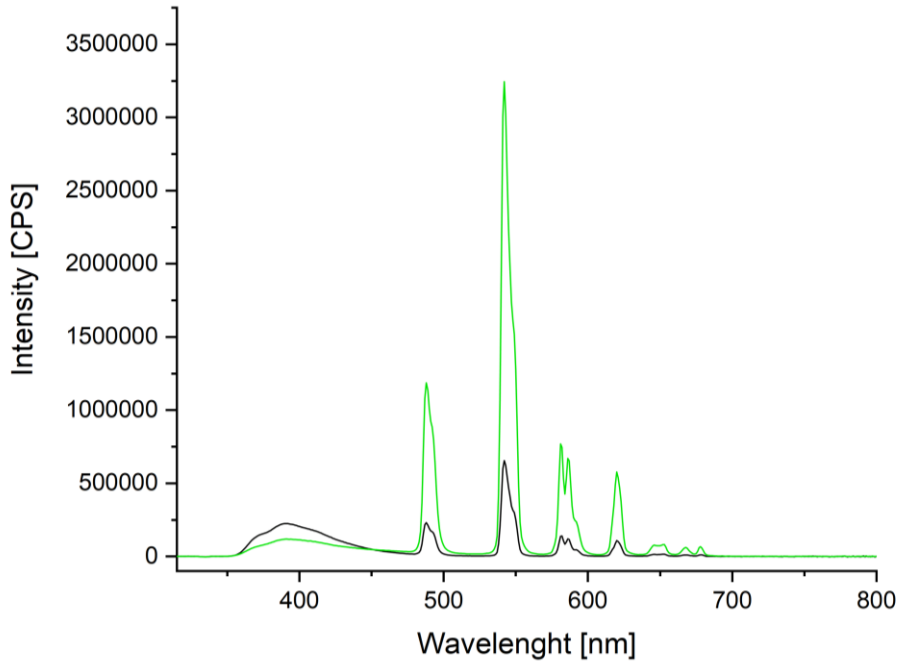

Figure S46. Comparison of the steady-state emission spectra of **TbLt^{s,CF3}** (black, λ_{ex} = 331 nm)[2], **TbLt^{t,CF3}** (green, λ_{ex} = 330 nm), [**TbL**] = 10 μM.

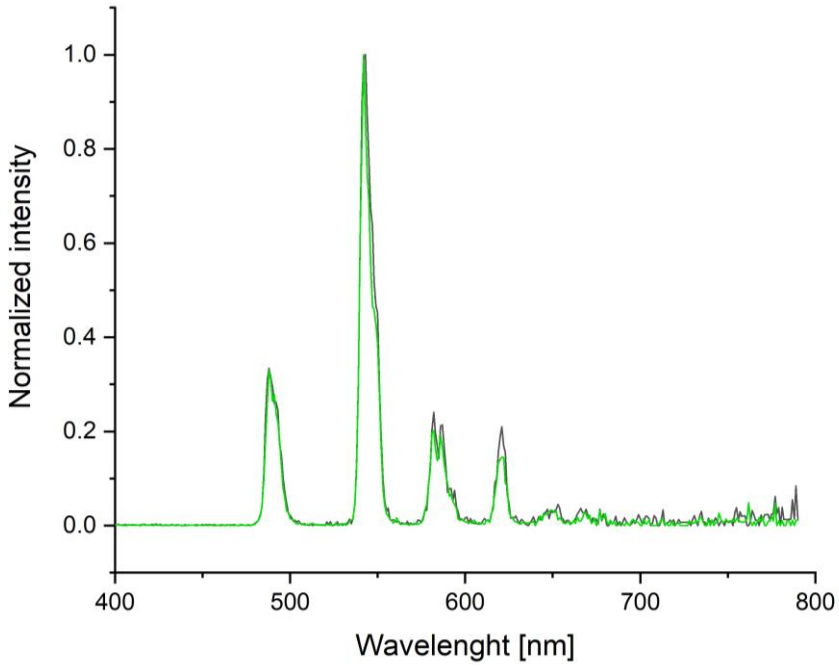

Figure S47. Comparison of the time-resolved emission spectra of **TbLt^{s,Me}** (grey, λ_{ex} = 330 nm)[2] and **TbLt^{t,Me}** (green, λ_{ex} = 325 nm).

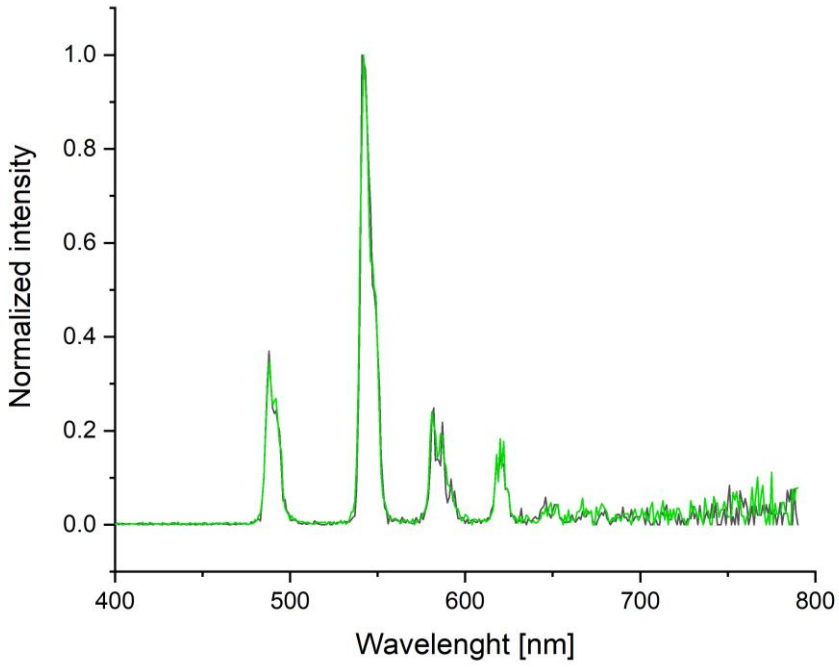

Figure S48. Comparison of the time-resolved emission spectra of **TbLt^{s,MOM}** (grey, λ_{ex} = 328 nm)[2] and **TbLt^{t,MOM}** (green, λ_{ex} = 328 nm).

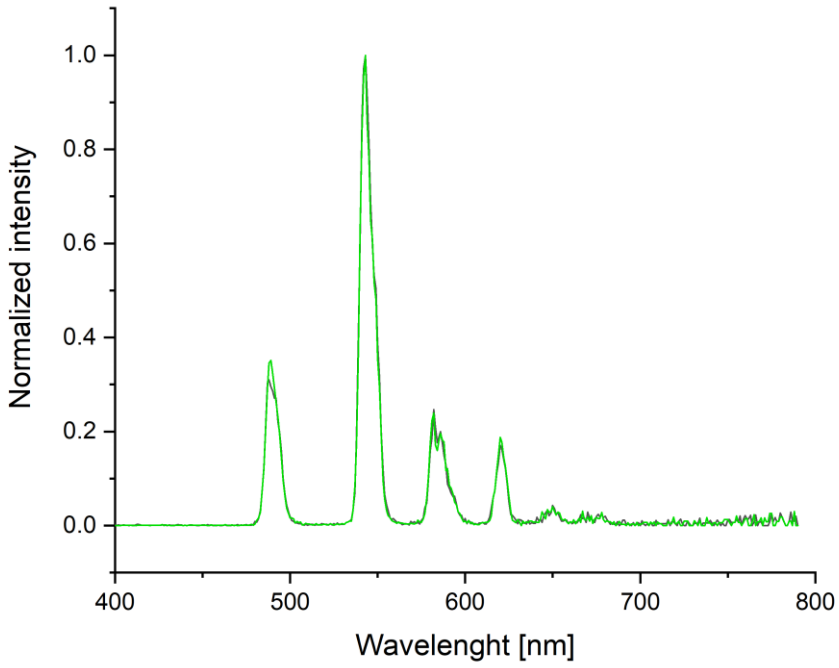

Figure S49. Comparison of the time-resolved emission spectra of **TbLt^{s,CF3}** (grey, λ_{ex} = 331 nm)[2] and **TbLt^{t,CF3}** (green, λ_{ex} = 330 nm).

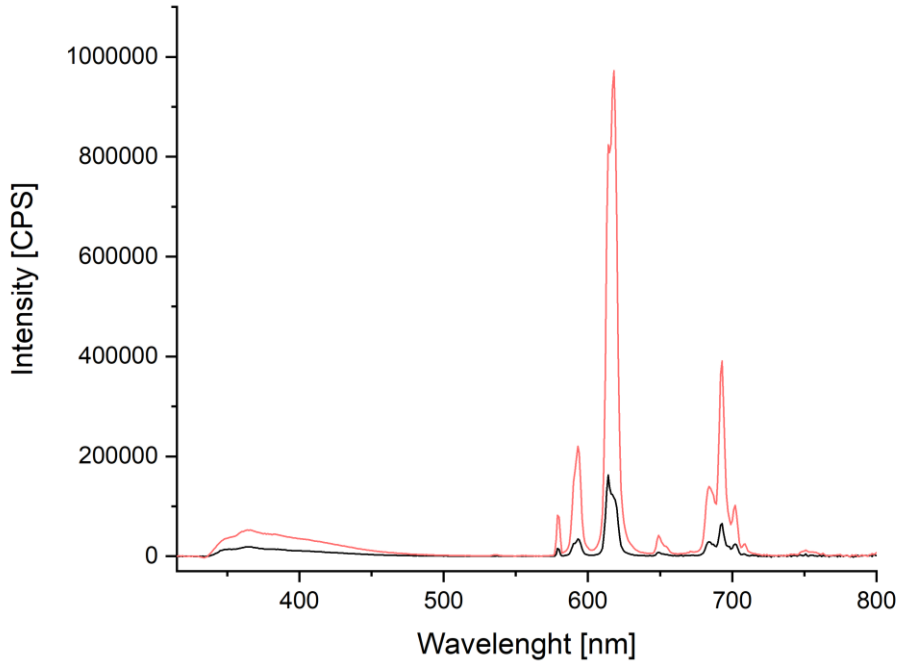

Figure S50. Comparison of the steady-state emission spectra of **EuLt^{s,Me}** (black, λ_{ex} = 328 nm)[2], **EuLt^{t,Me}** (red, λ_{ex} = 325 nm), [**EuL**] = 10 μM.

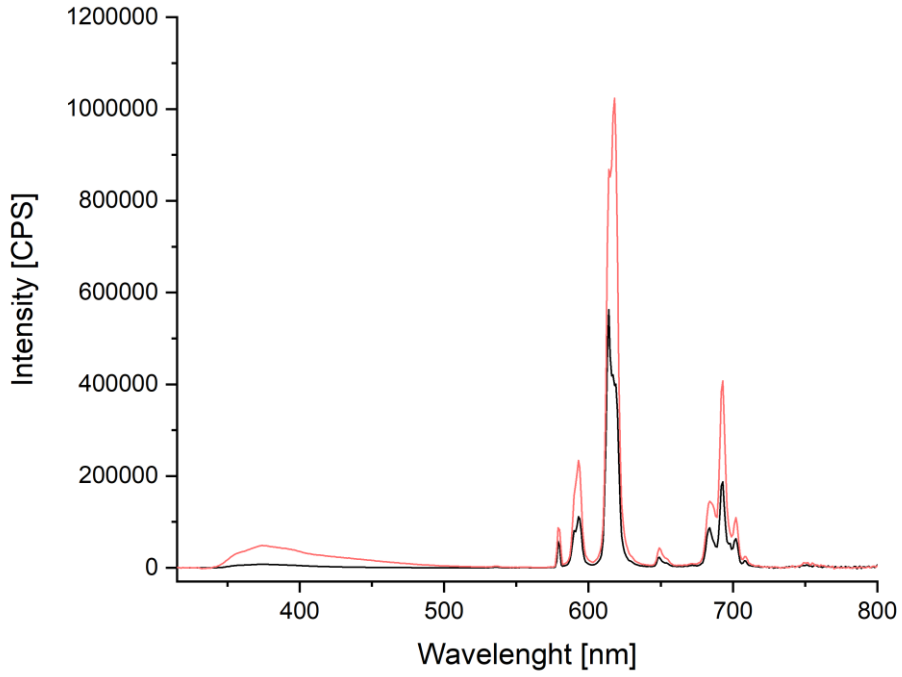

Figure S51. Comparison of the steady-state emission spectra of **EuLt^{s,MOM}** (black, λ_{ex} = 328 nm)[2], **EuLt^{t,MOM}** (red, λ_{ex} = 328 nm), [**EuL**] = 10 μM.

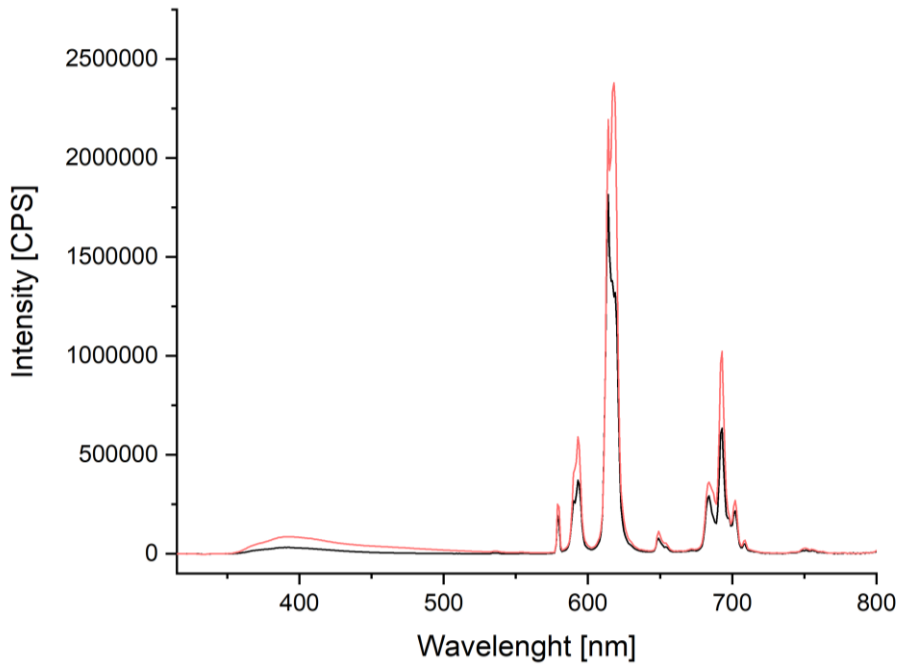

Figure S52. Comparison of the steady-state emission spectra of **EuLt^{s,CF3}** (black, λ_{ex} = 331 nm)[2], **EuLt^{t,CF3}** (red, λ_{ex} = 330 nm), [**EuL**] = 10 μM.

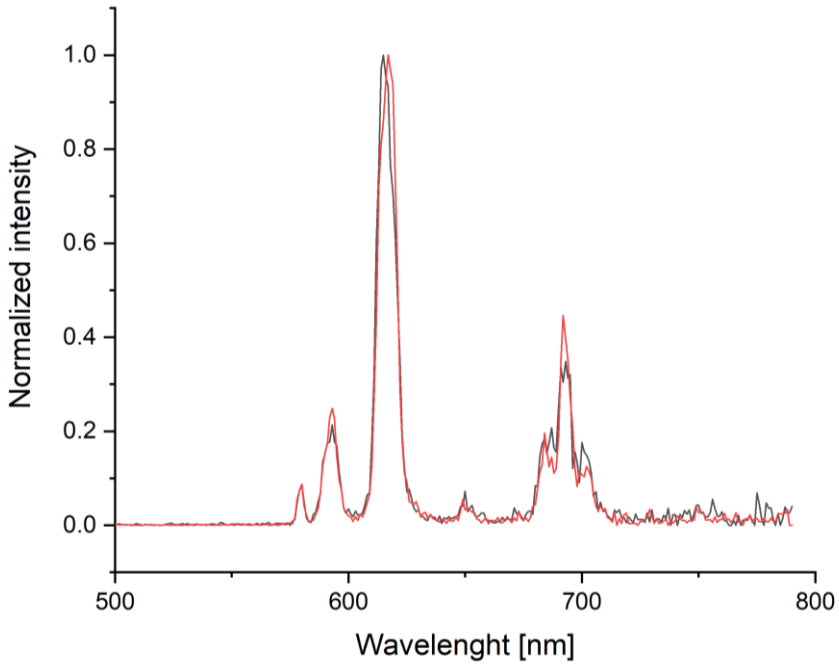

Figure S53. Comparison of the time-resolved emission spectra of **EuLt^{s,Me}** (grey, λ_{ex} = 330 nm)[2] and **EuLt^{t,Me}** (red, λ_{ex} = 325 nm).

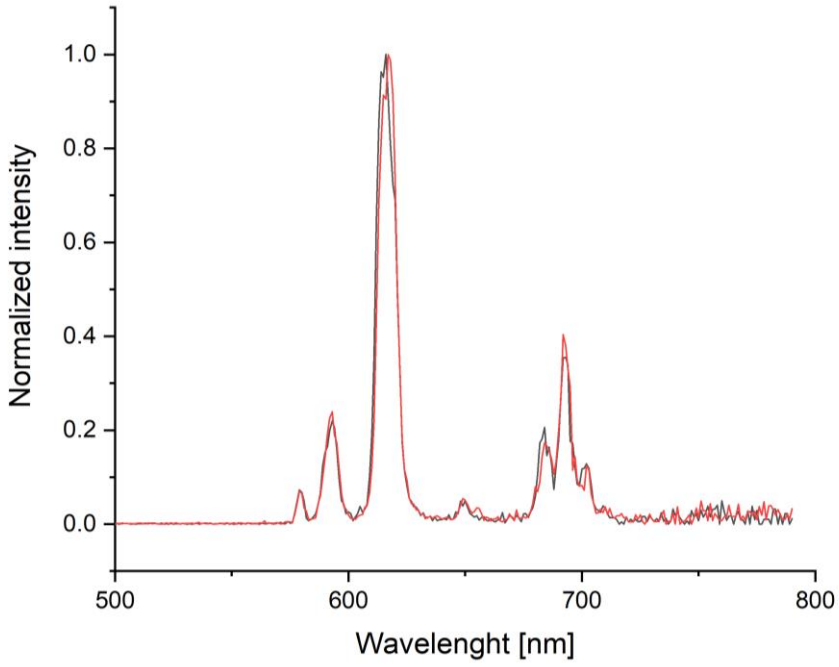

Figure S54. Comparison of the time-resolved emission spectra of **EuLt^{s,MOM}** (grey, λ_{ex} = 328 nm)[2] and **EuLt^{t,MOM}** (red, λ_{ex} = 328 nm).

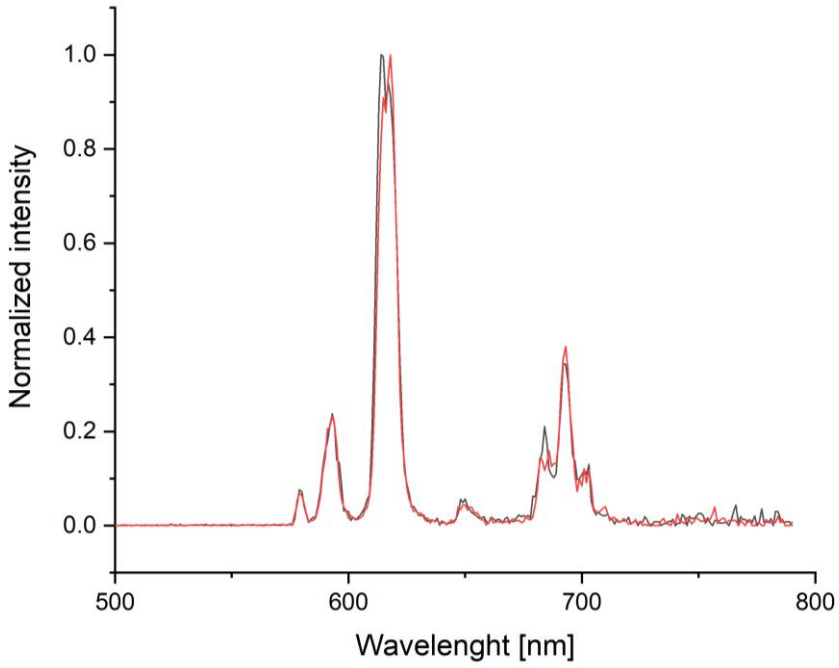

Figure S55. Comparison of the time-resolved emission spectra of **EuLt^{s,CF3}** (grey, λ_{ex} = 331 nm)[2] and **EuLt^{t,CF3}** (red, λ_{ex} = 330 nm).

Photostability studies

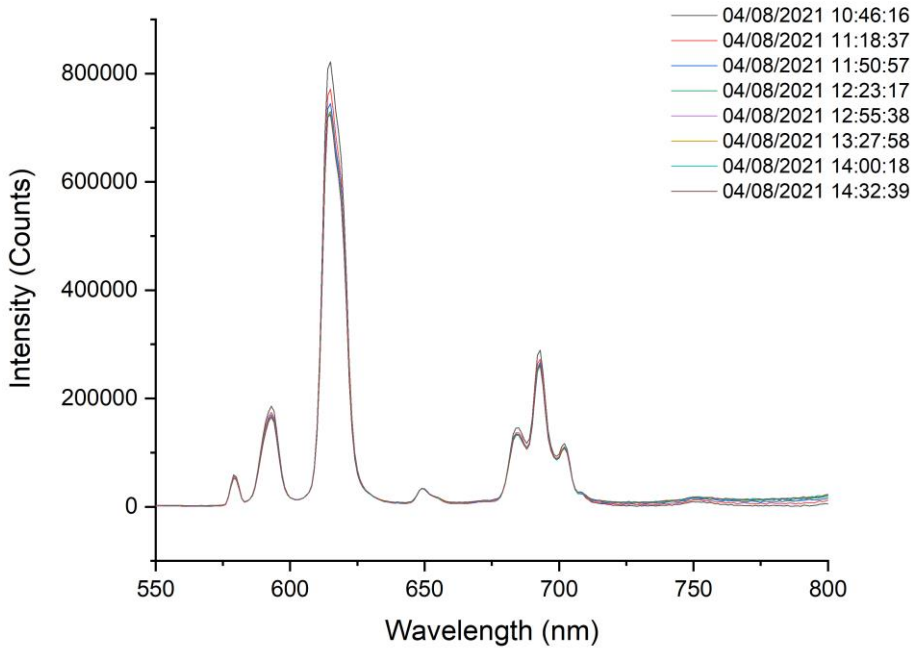

Figure S56. Steady-state emission of **EuLt^{s,Me}** recorded during a 4 h period upon continuous irradiation.

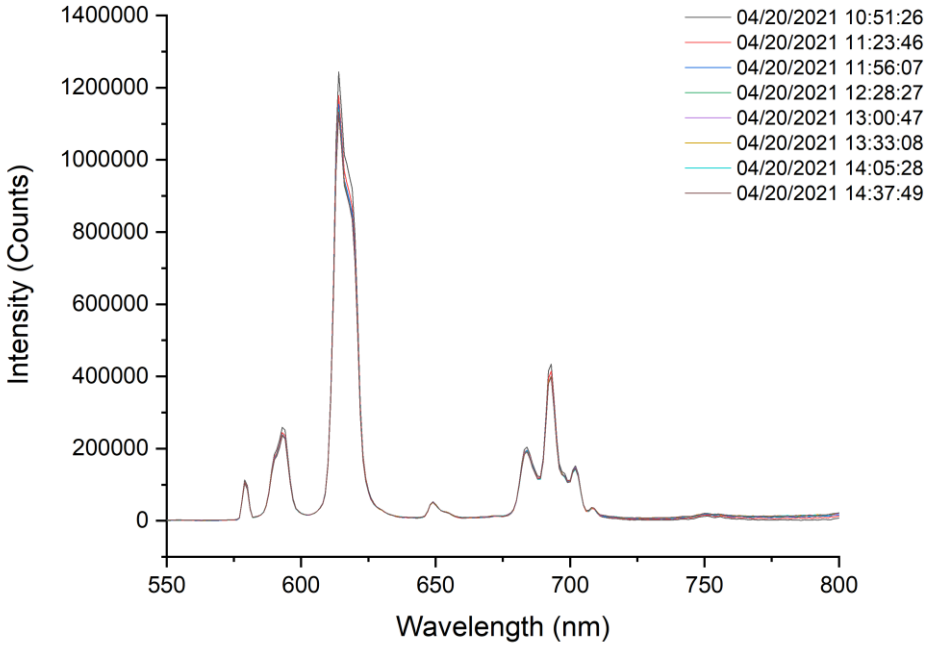

Figure S57. Steady-state emission of **EuLt^{s,MOM}** recorded during a 4 h period upon continuous irradiation.

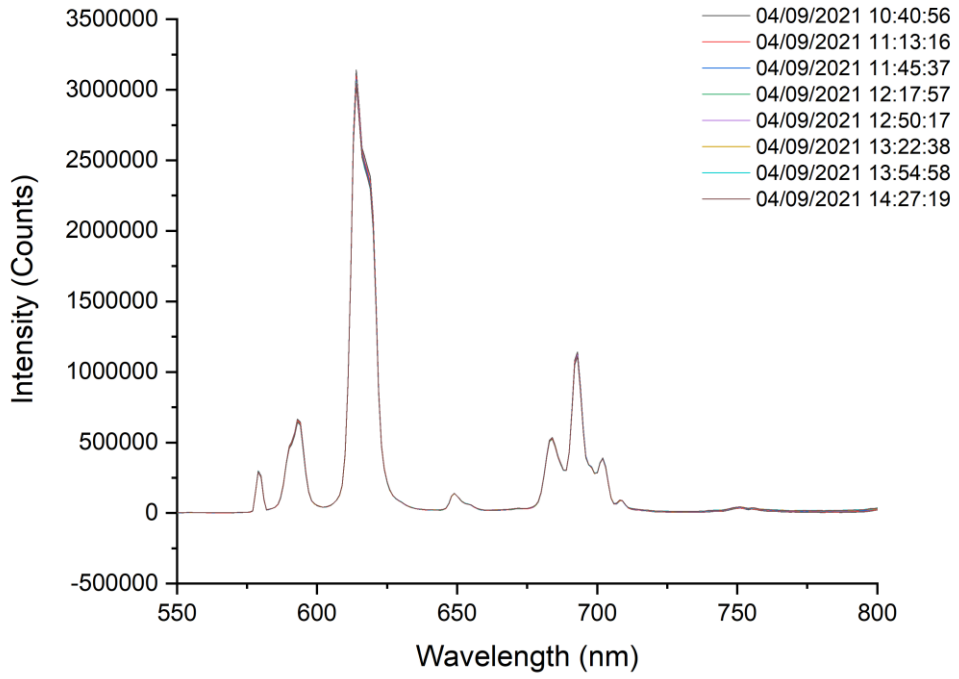

Figure S58. Steady-state emission of **EuLt^{s,CF3}** recorded during a 4 h period upon continuous irradiation.

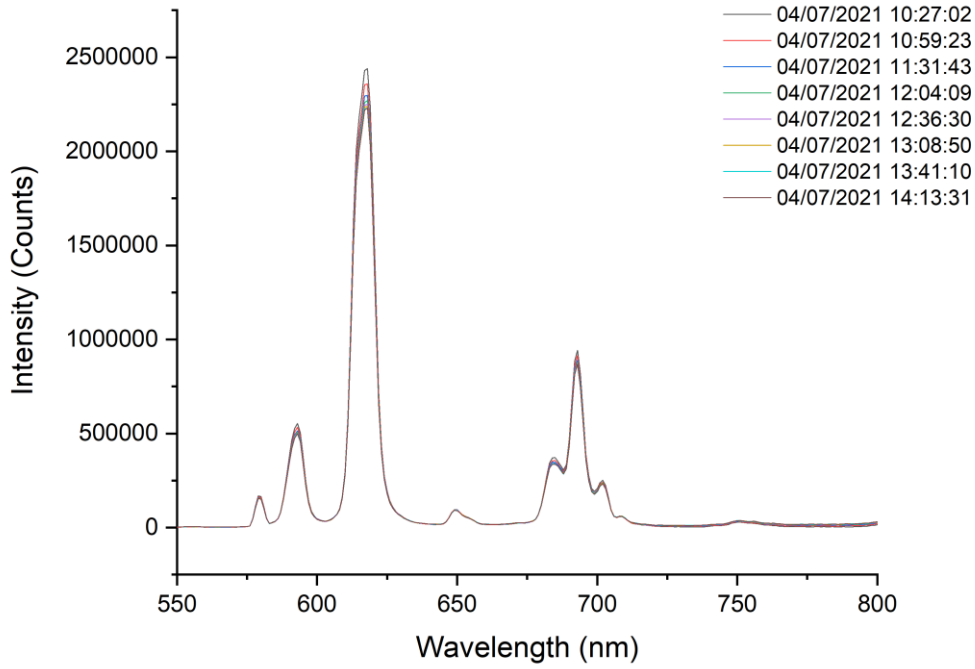

Figure S59. Steady-state emission of **EuLt^{t,Me}** recorded during a 4 h period upon continuous irradiation.

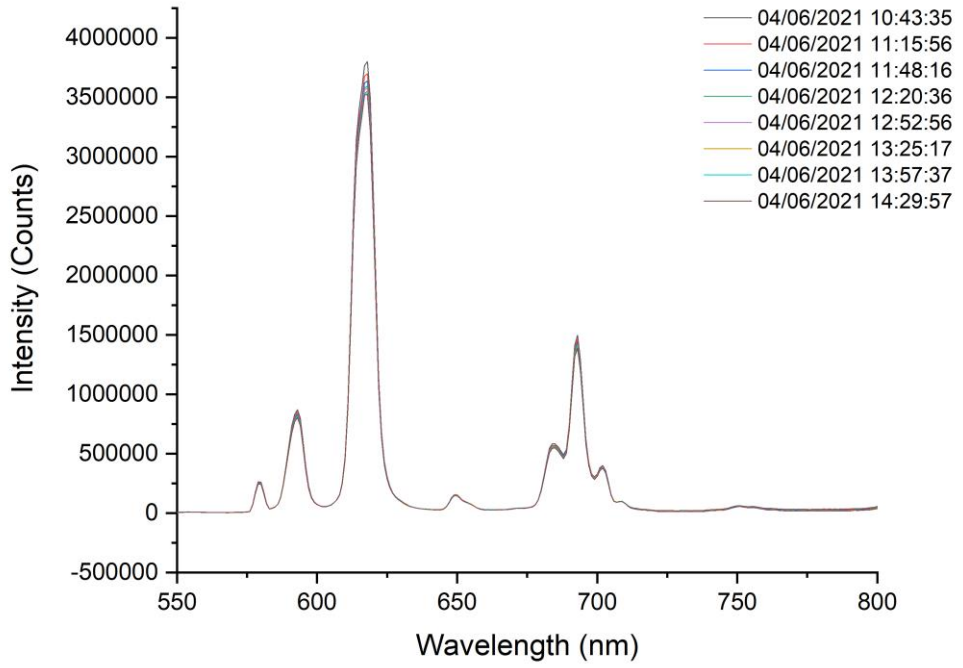

Figure S60. Steady-state emission of **EuLt^{t,MOM}** recorded during a 4 h period upon continuous irradiation.

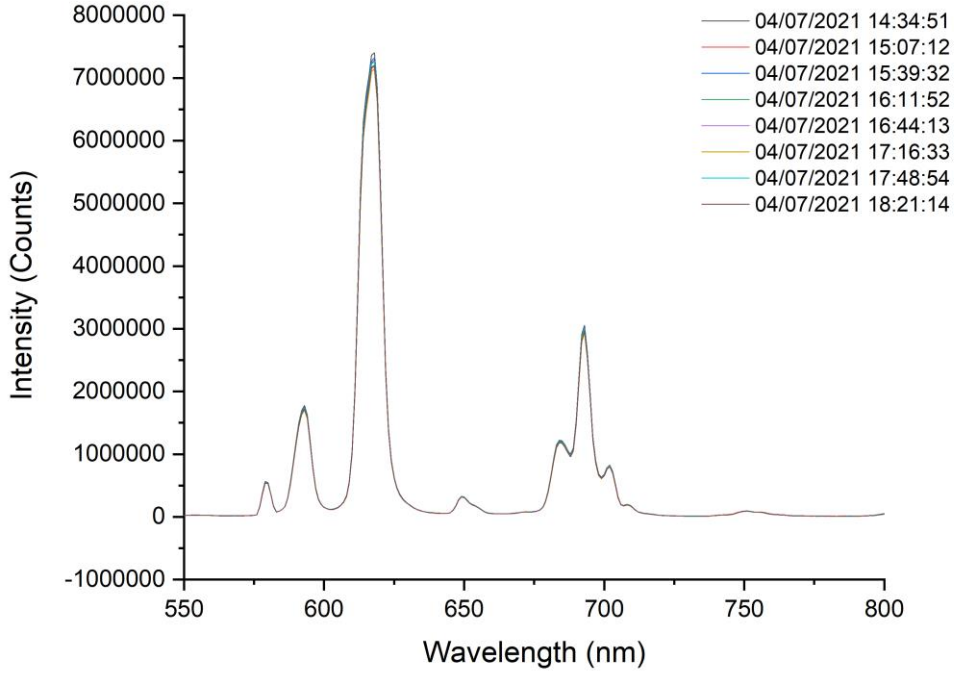

Figure S61. Steady-state emission of **EuLt^{t,CF3}** recorded during a 4 h period upon continuous irradiation.

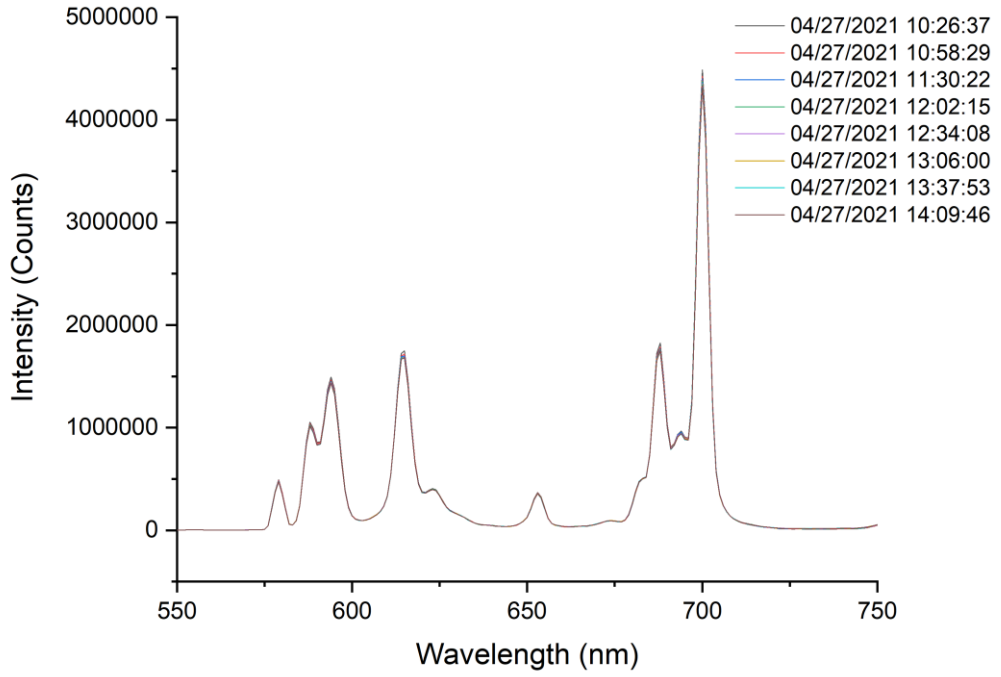

Figure S62. Steady-state emission of **EuLc^{t,Me}** recorded during a 4 h period upon continuous irradiation.

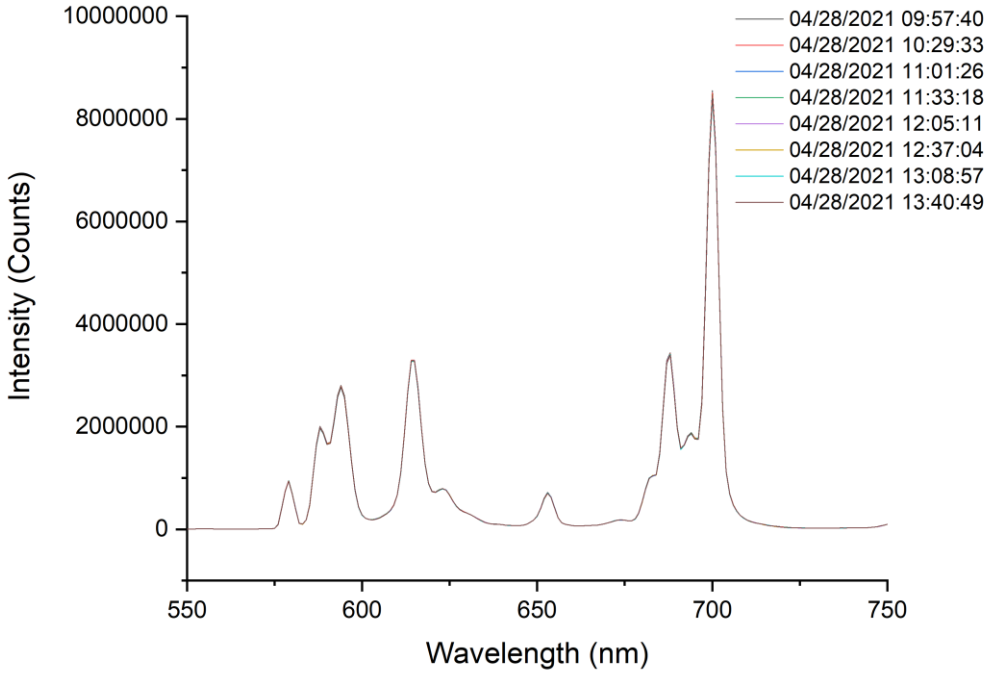

Figure S63. Steady-state emission of **EuLc^{t,MOM}** recorded during a 4 h period upon continuous irradiation.

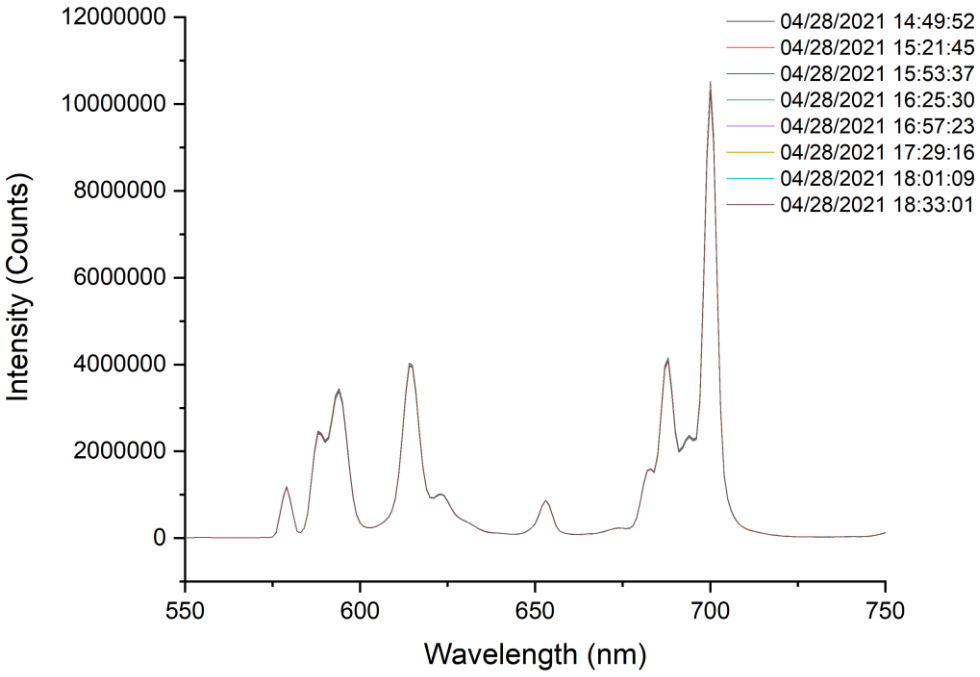

Figure S64. Steady-state emission of **EuLc^{t,CF3}** recorded during a 4 h period upon continuous irradiation.

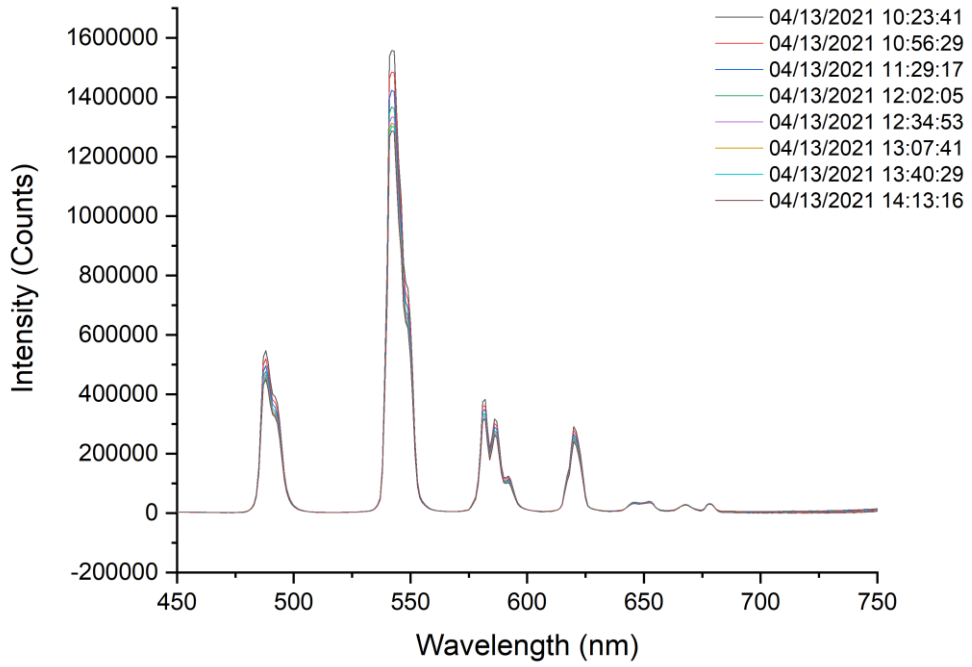

Figure S65. Steady-state emission of **TbLt^{s,Me}** recorded during a 4 h period upon continuous irradiation.

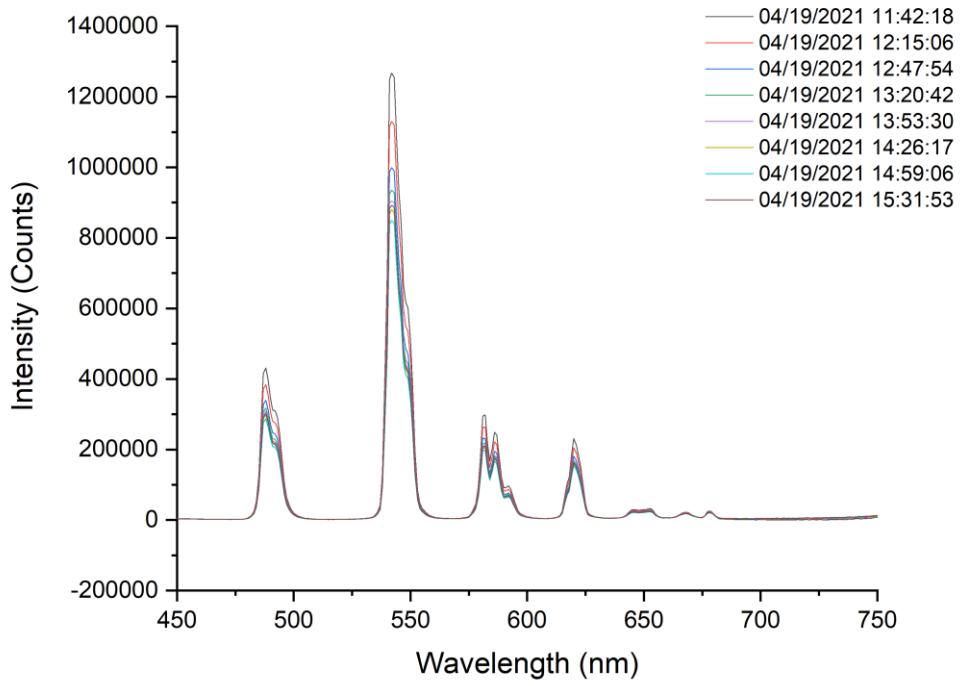

Figure S66. Steady-state emission of **TbLt^{s,MOM}** recorded during a 4 h period upon continuous irradiation.

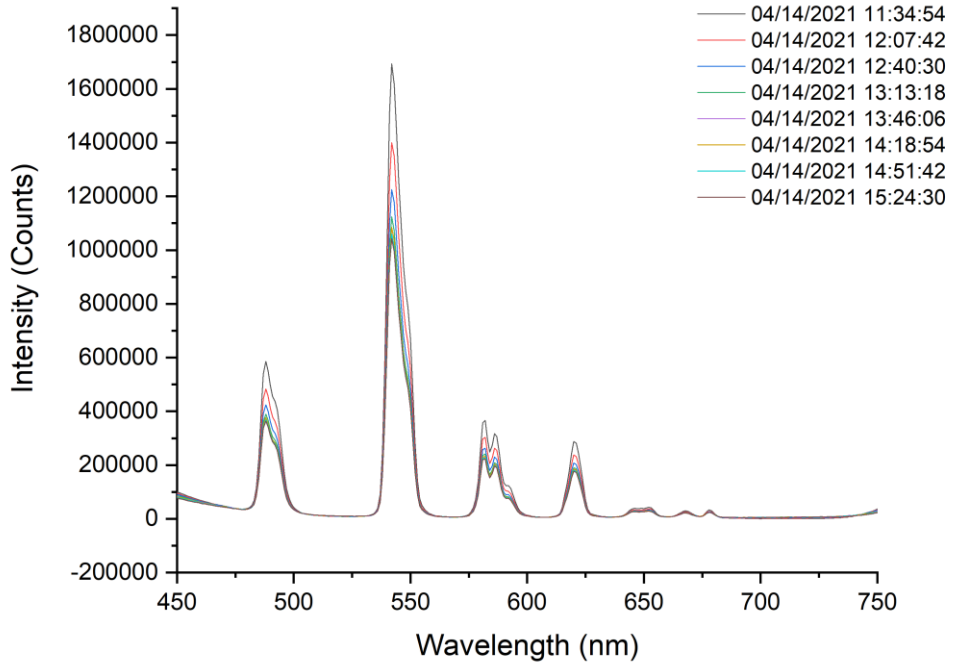

Figure S67. Steady-state emission of **TbLt^{s,CF3}** recorded during a 4 h period upon continuous irradiation.

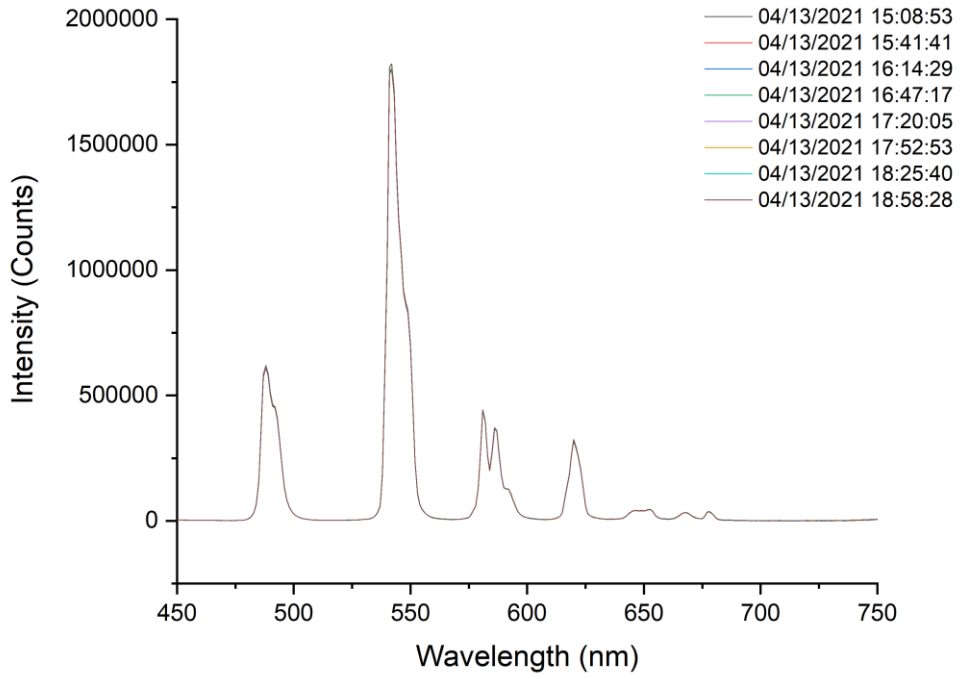

Figure S68. Steady-state emission of **TbLt^{t,Me}** recorded during a 4 h period upon continuous irradiation.

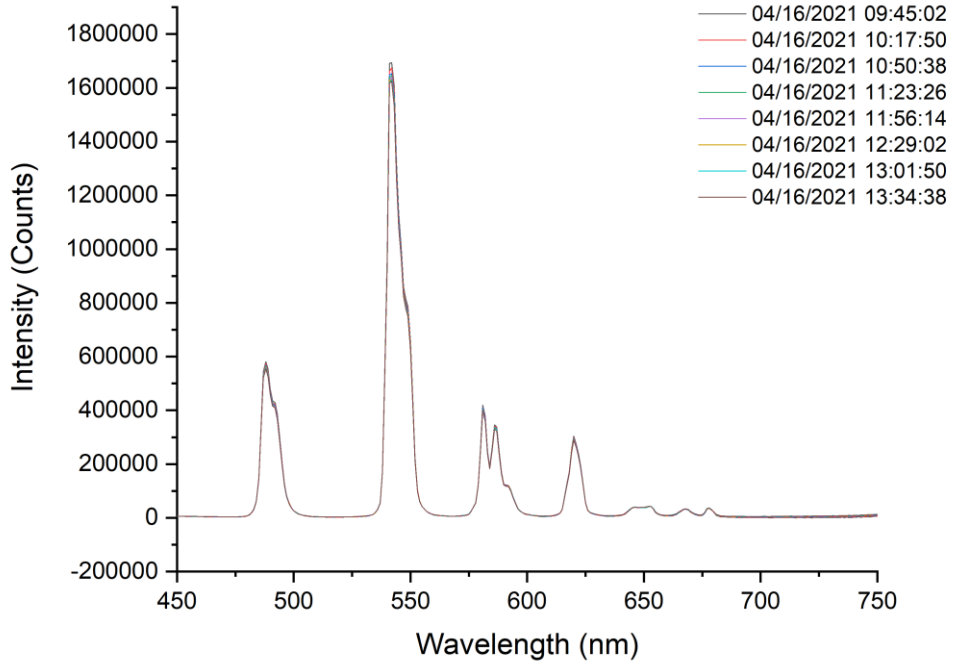

Figure S69. Steady-state emission of **TbLt^{t,MOM}** recorded during a 4 h period upon continuous irradiation.

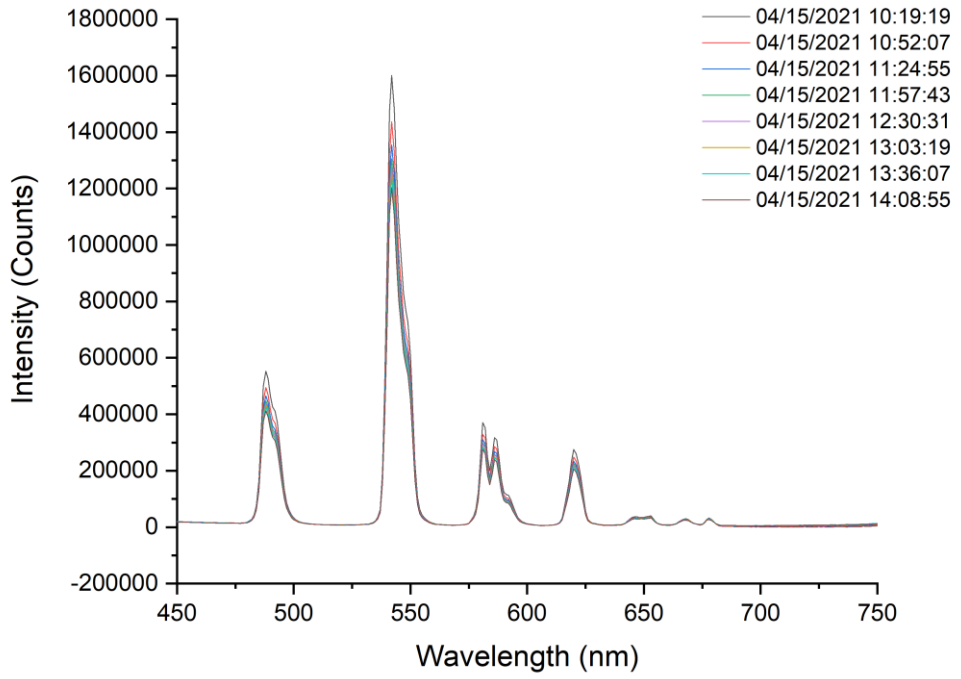

Figure S70. Steady-state emission of **TbLt^{t,CF3}** recorded during a 4 h period upon continuous irradiation.

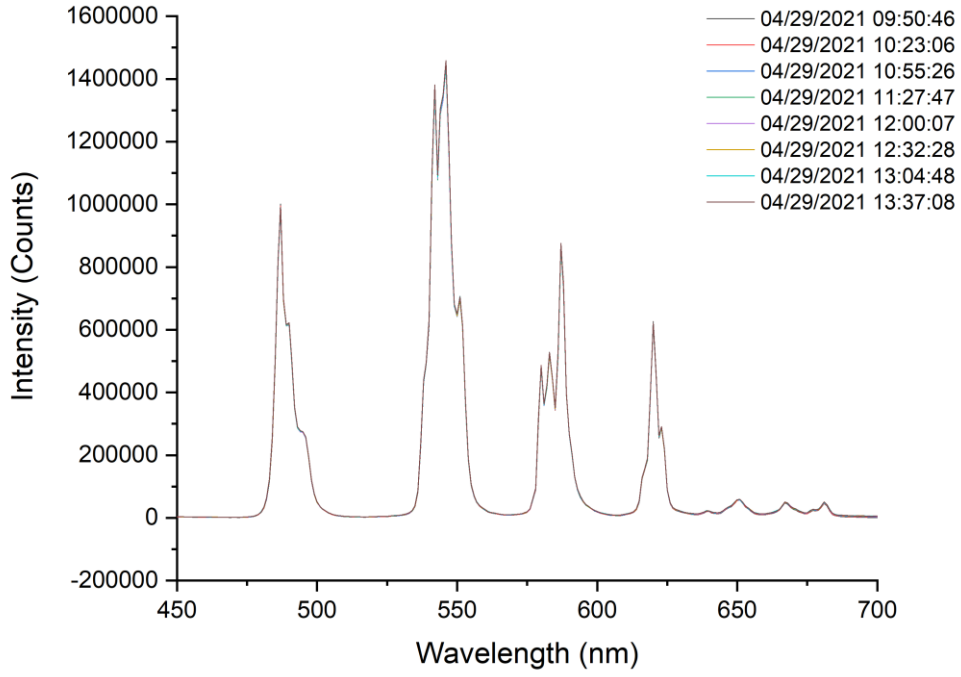

Figure S71. Steady-state emission of **TbLc^{t,Me}** recorded during a 4 h period upon continuous irradiation.

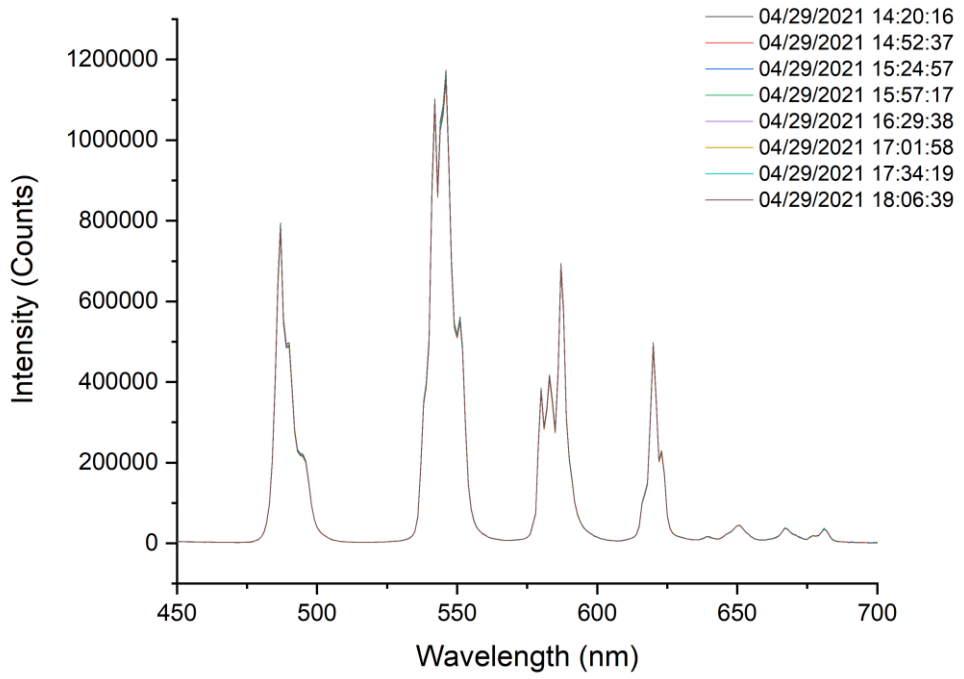

Figure S72. Steady-state emission of **TbLc^{t,MOM}** recorded during a 4 h period upon continuous irradiation.

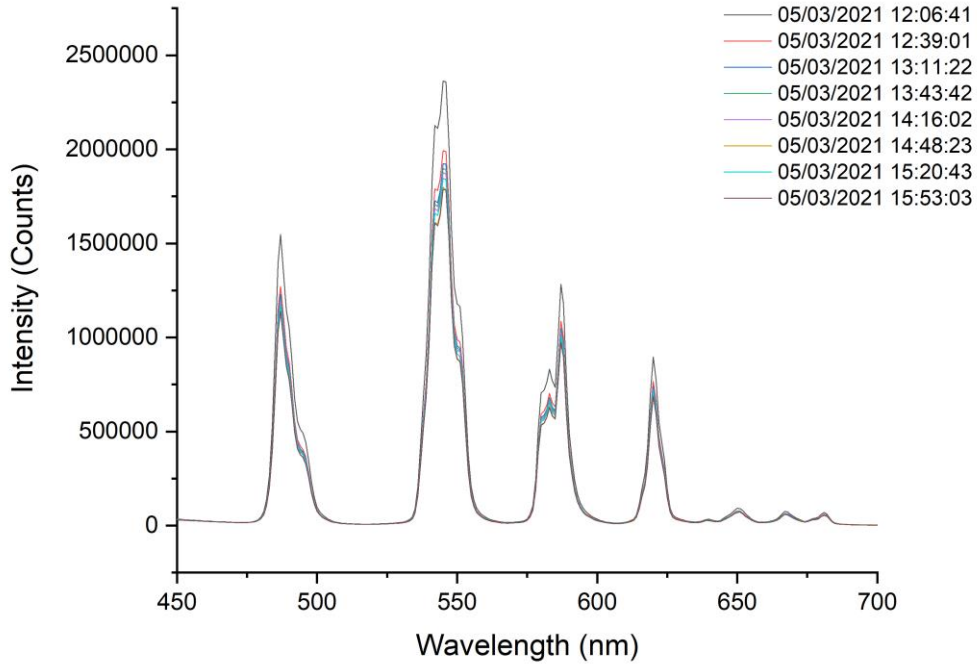

Figure S73. Steady-state emission of **TbLc^{t,CF3}** recorded during a 4 h period upon continuous irradiation.

^{1}H, ^{13}C and ^{19}F NMR spectra

S1a

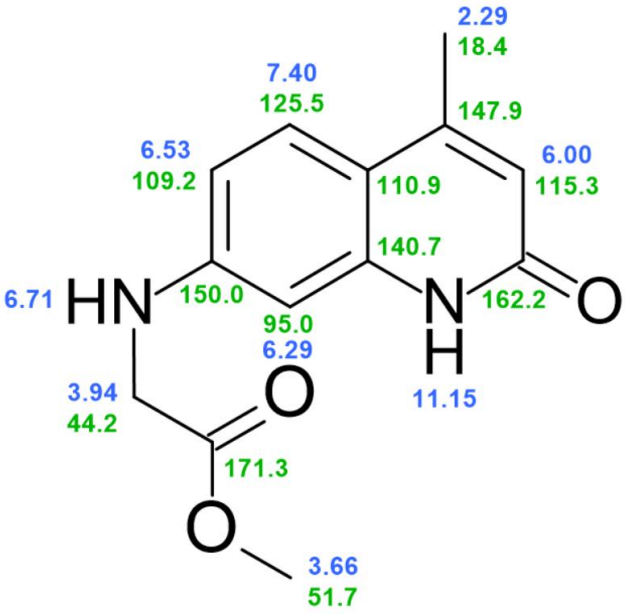

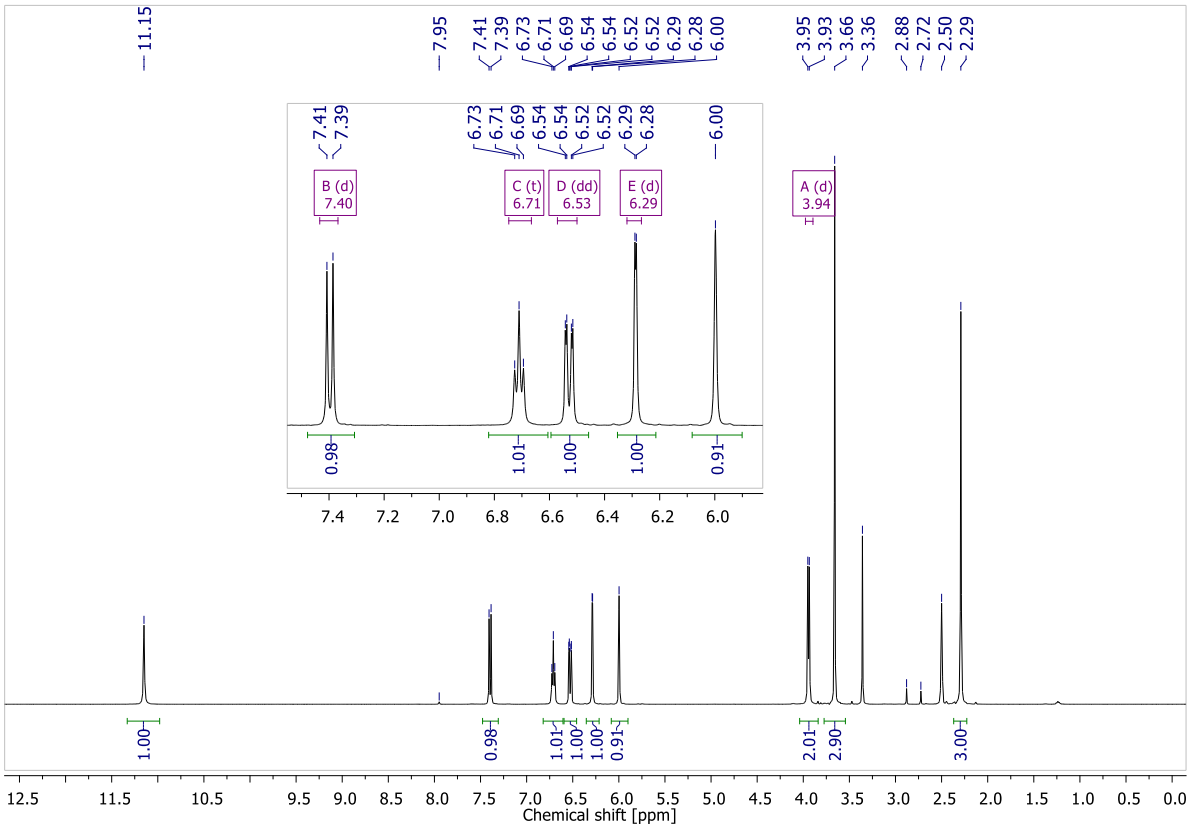

Figure S74. ^{1}H NMR spectrum of **S1a** (400 MHz, DMSO-d_6).

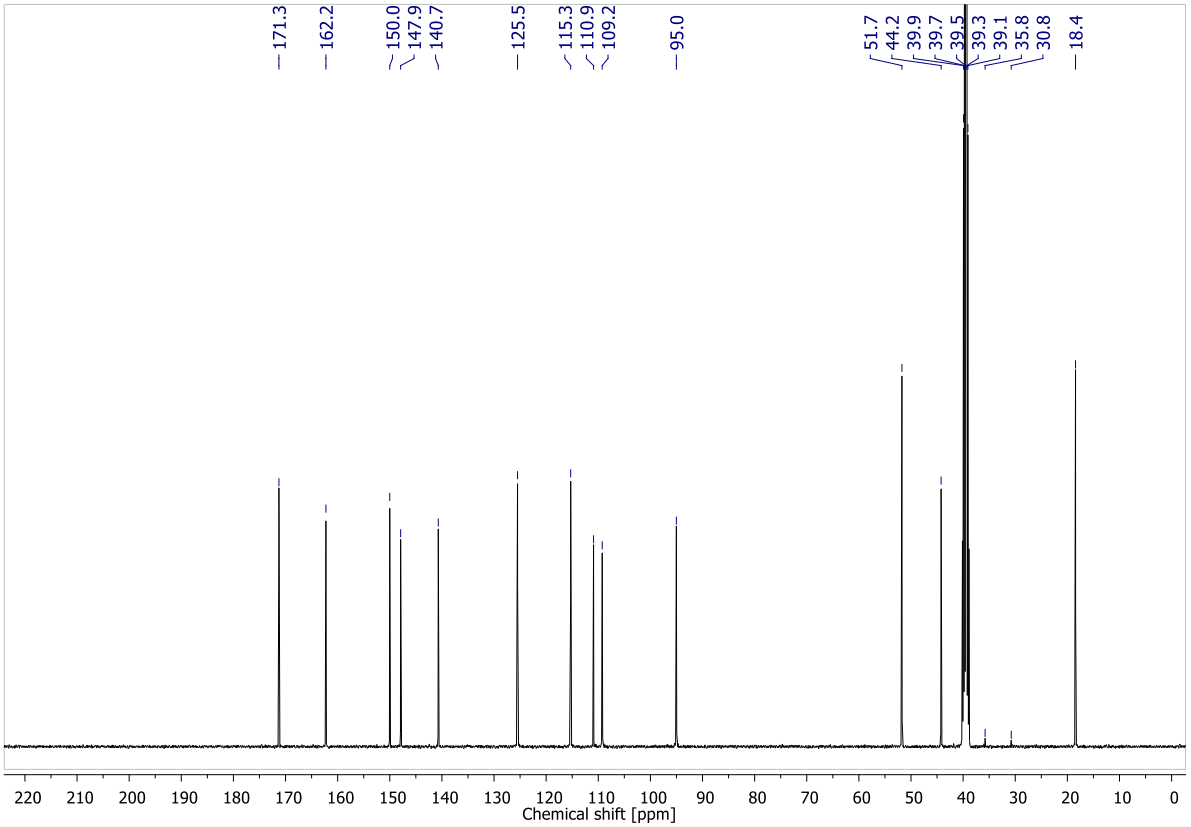

Figure S75. ^{13}C NMR spectrum of **S1a** (101 MHz, DMSO-d_6).

S1b

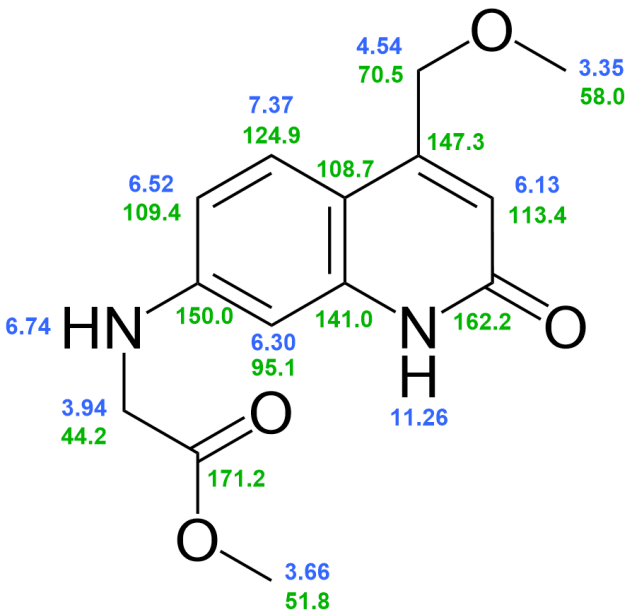

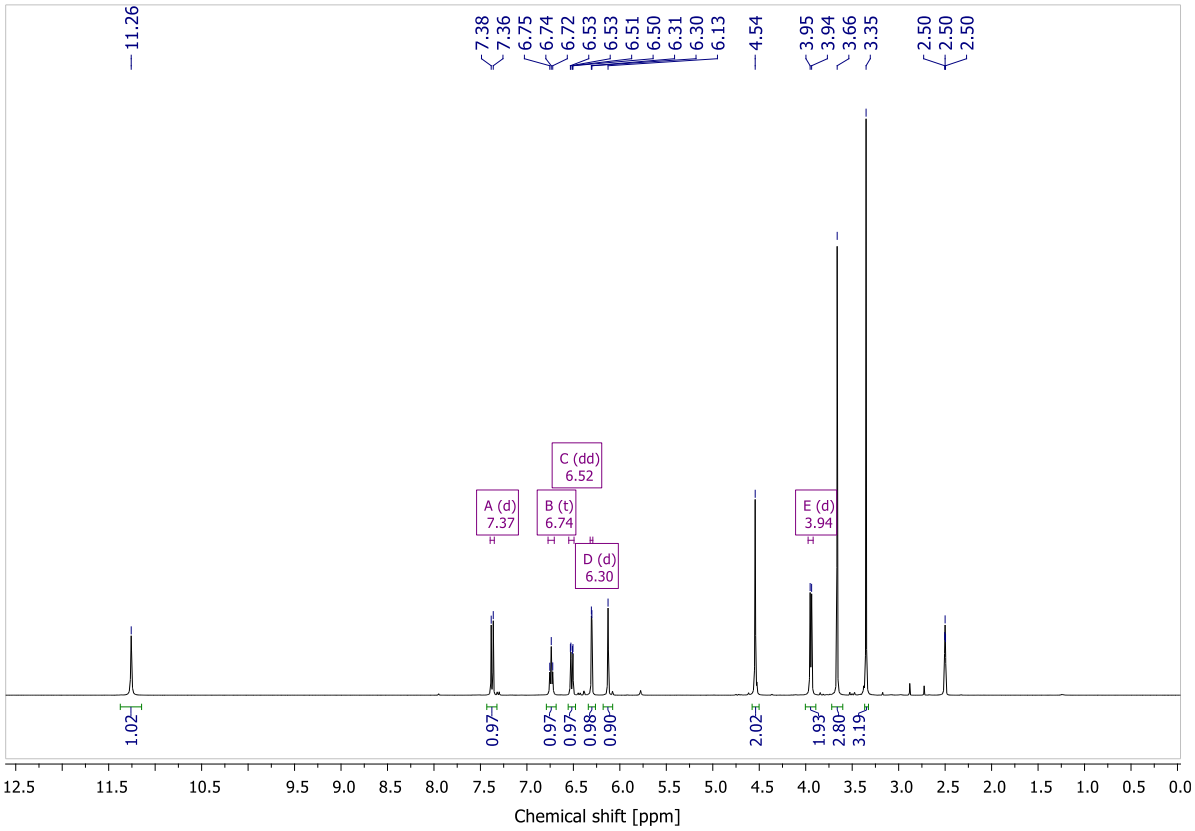

Figure S76. ^{1}H NMR spectrum of **S1b** (400 MHz, DMSO-d_6).

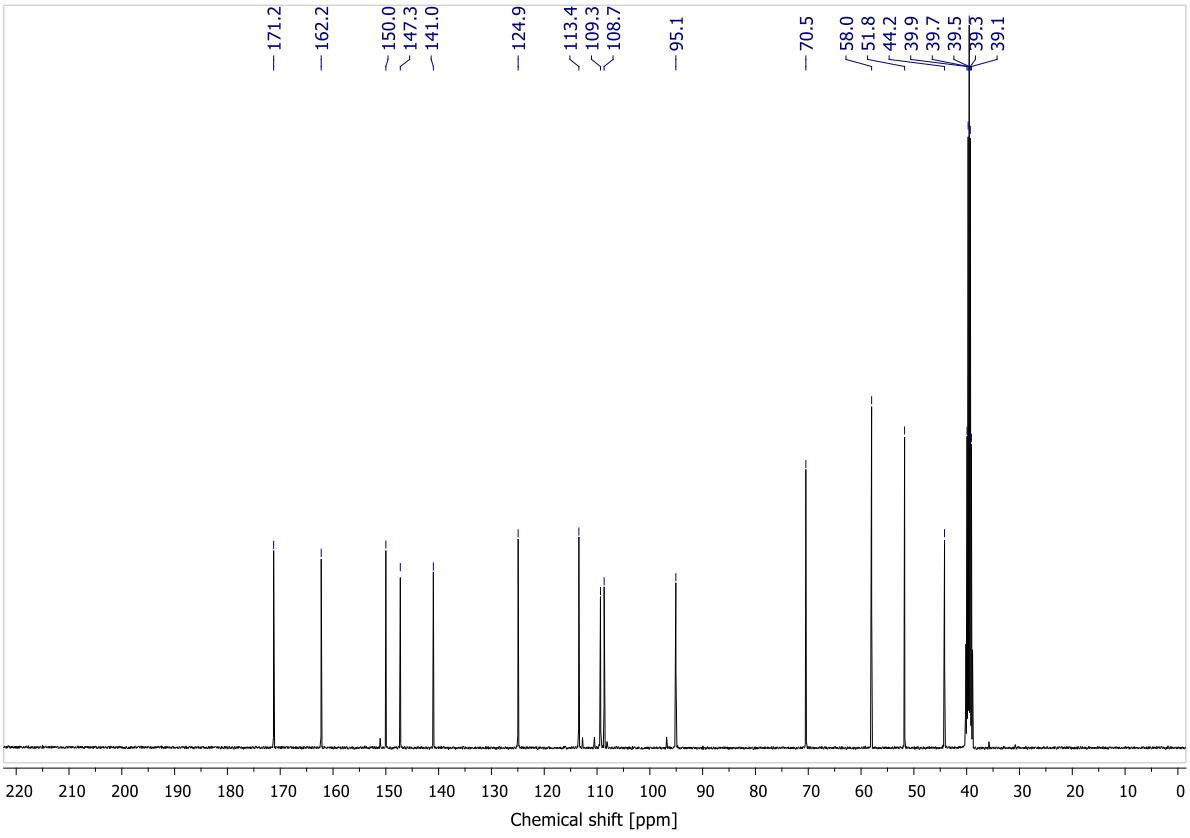

Figure S77. ^{13}C NMR spectrum of **S1b** (101 MHz, DMSO-d_6).

S1c

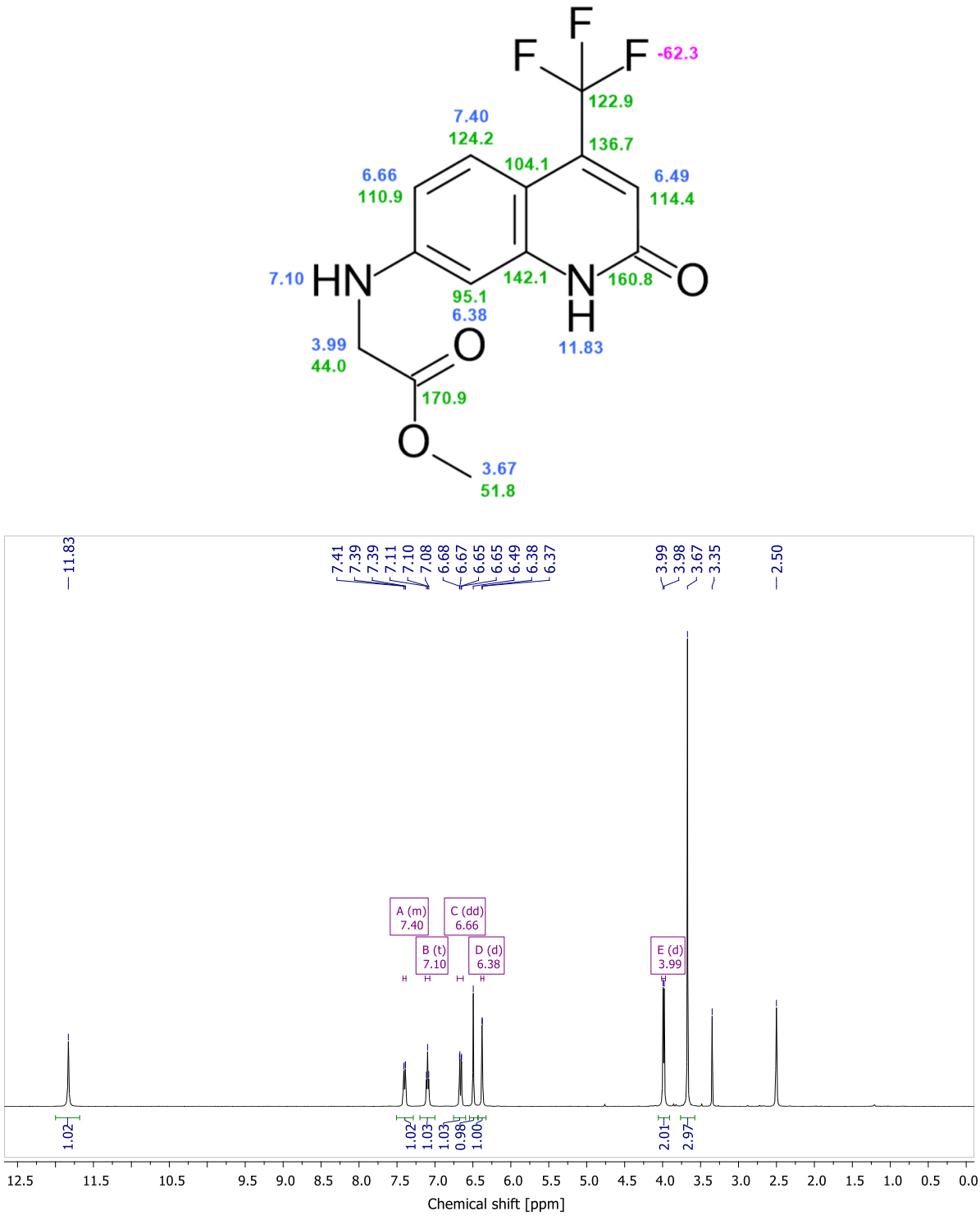

Figure S78. ^{1}H NMR spectrum of **S1c** (400 MHz, DMSO-d_6).

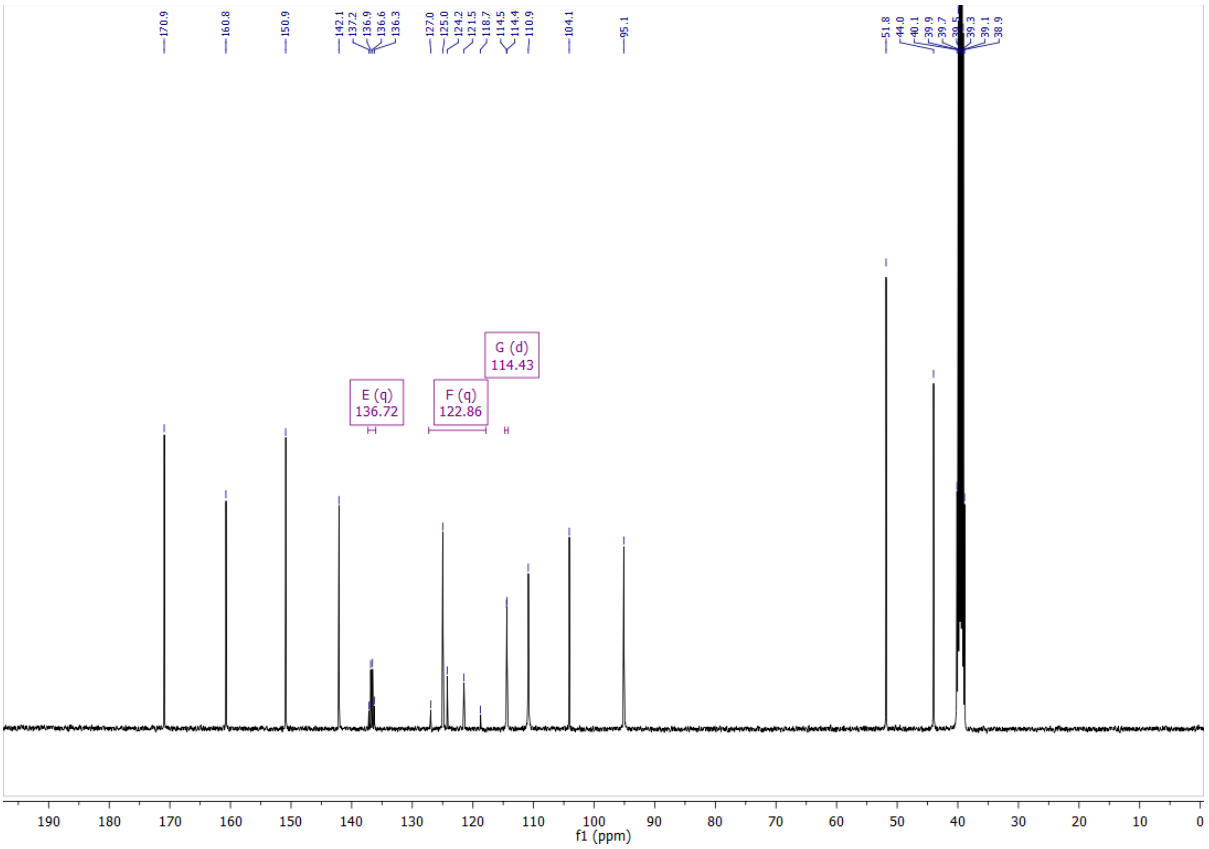

Figure S79. ^{13}C NMR spectrum of **S1c** (101 MHz, DMSO-d_6).

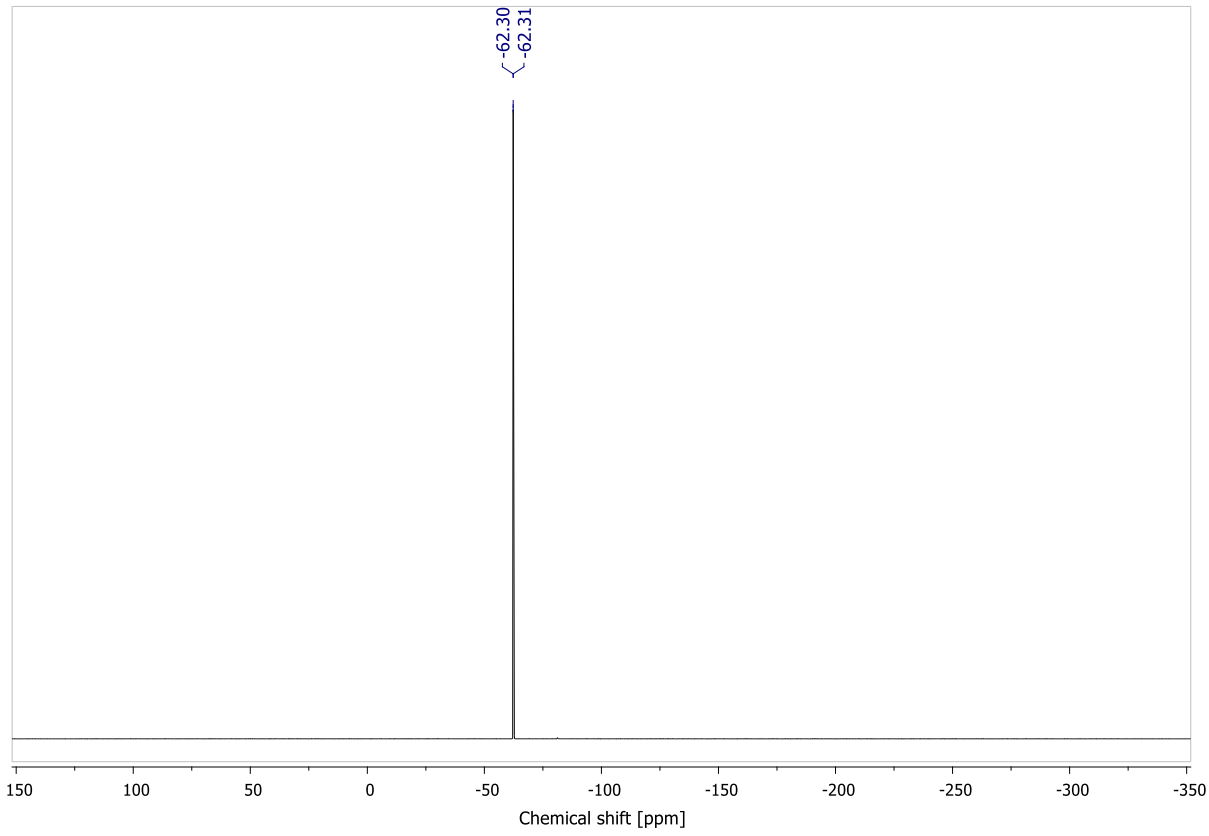

Figure S80. ^{19}F NMR spectrum of **S1c** (376 MHz, DMSO-d_6).

5a

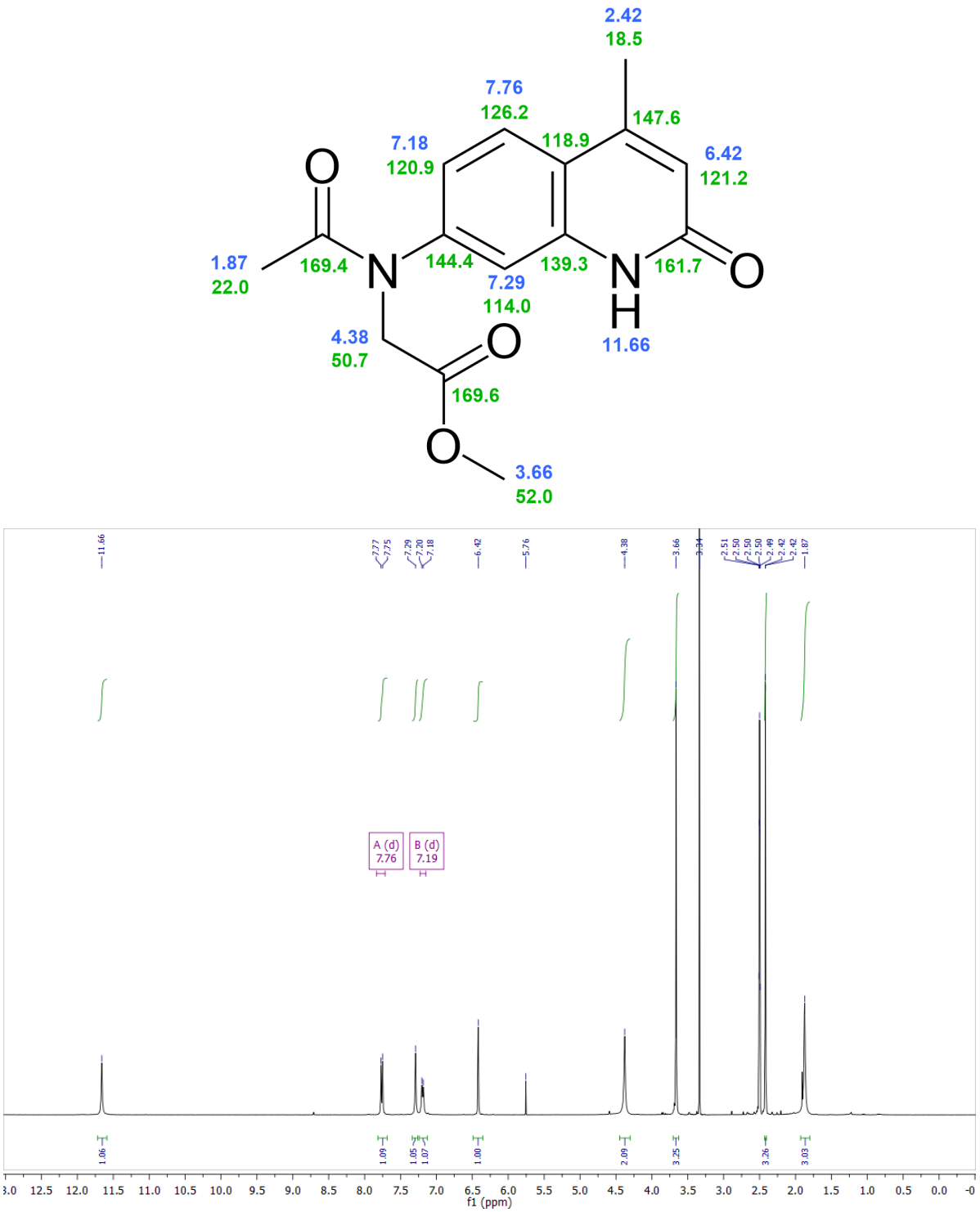

Figure S81. ^{1}H NMR spectrum of **5a** (400 MHz, DMSO-d_6).

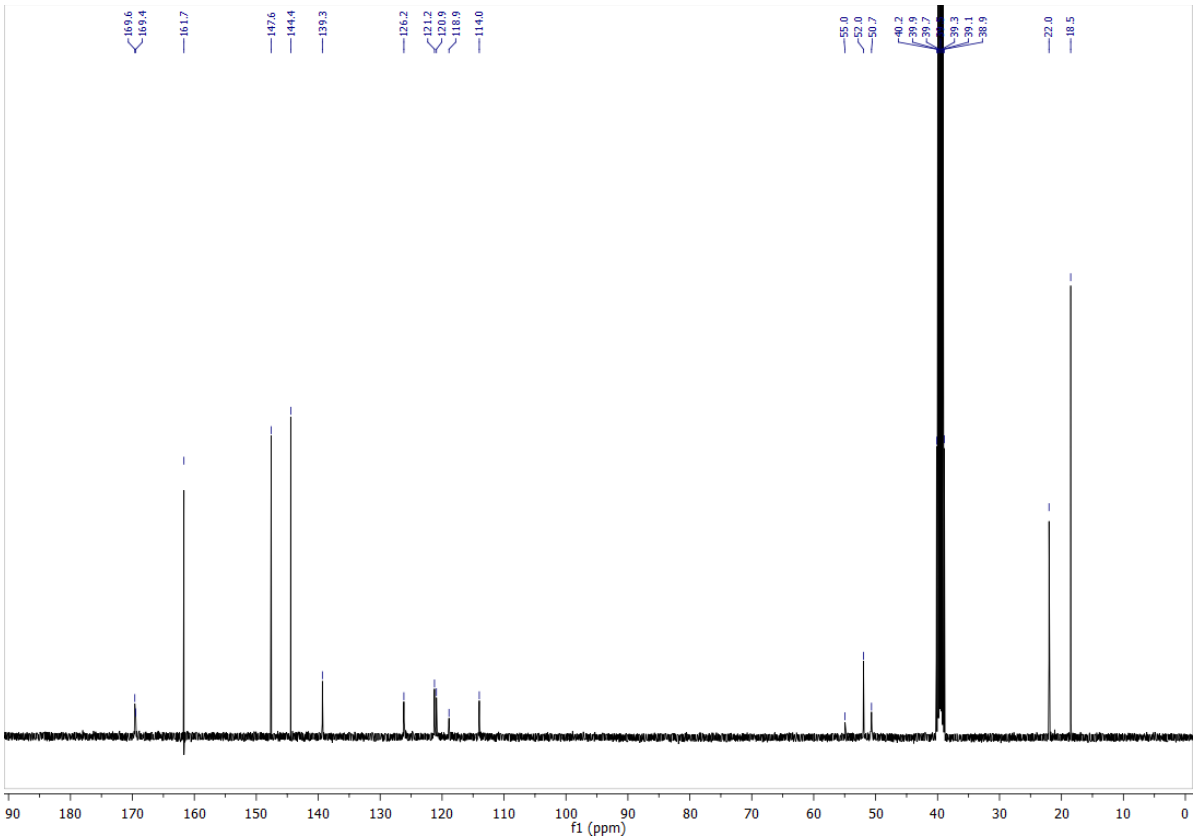

Figure S82. ^{13}C NMR spectrum of **5a** (101 MHz, DMSO-d_6).

5b

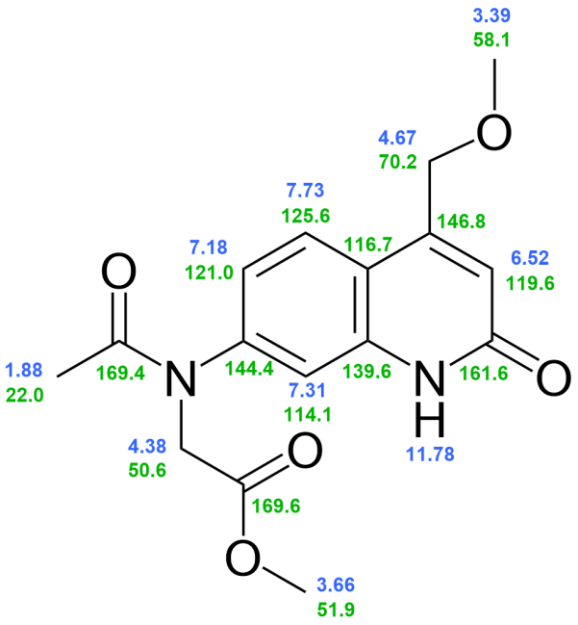

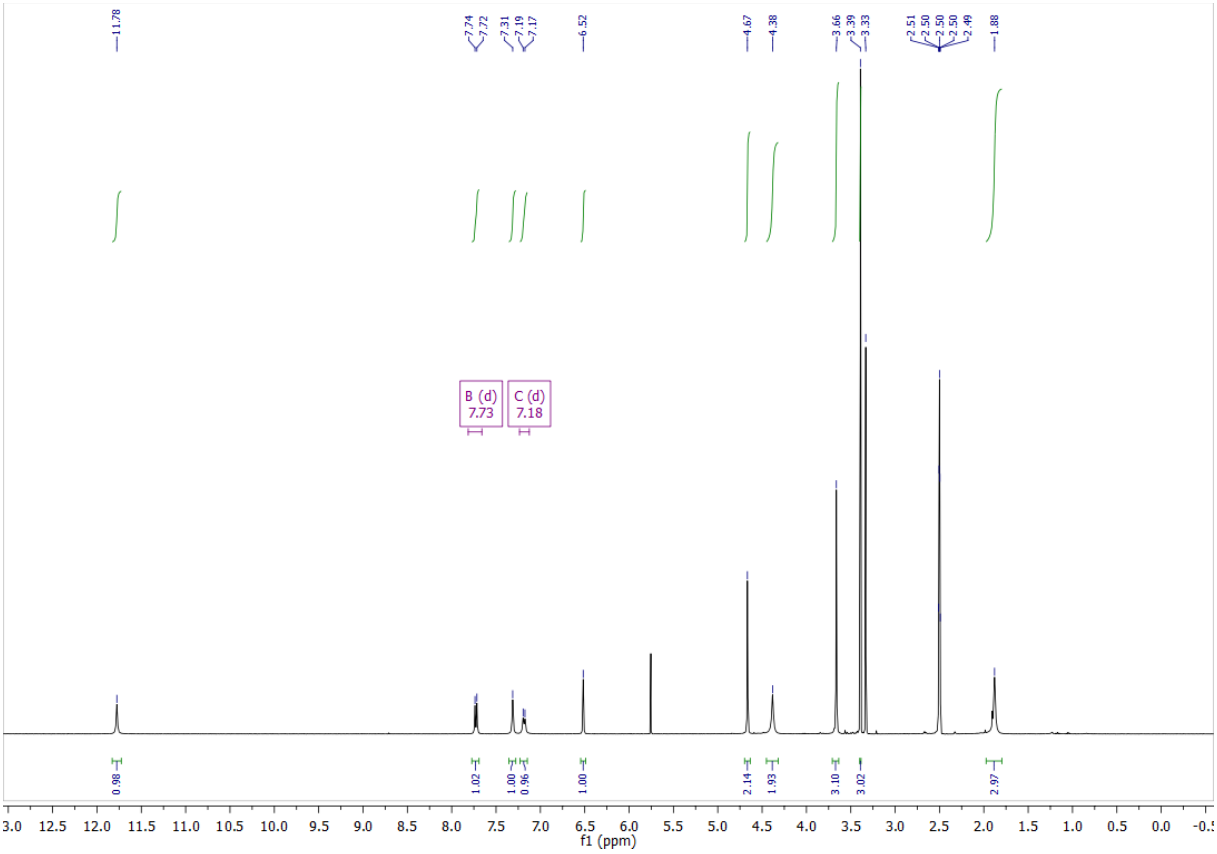

Figure S83. [1]H NMR spectrum of **5b** (400 MHz, DMSO-d_6).

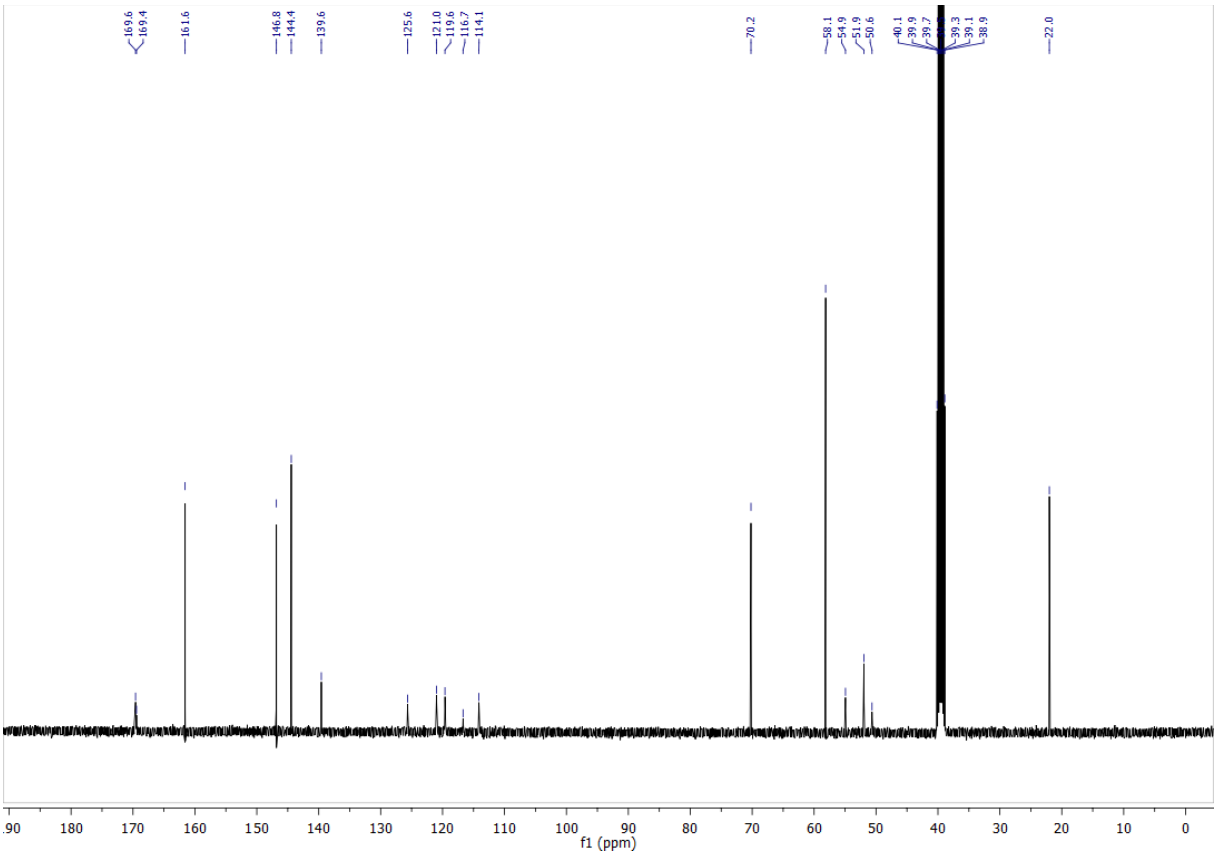

Figure S84. [13]C NMR spectrum of **5b** (101 MHz, DMSO-d_6).

5c

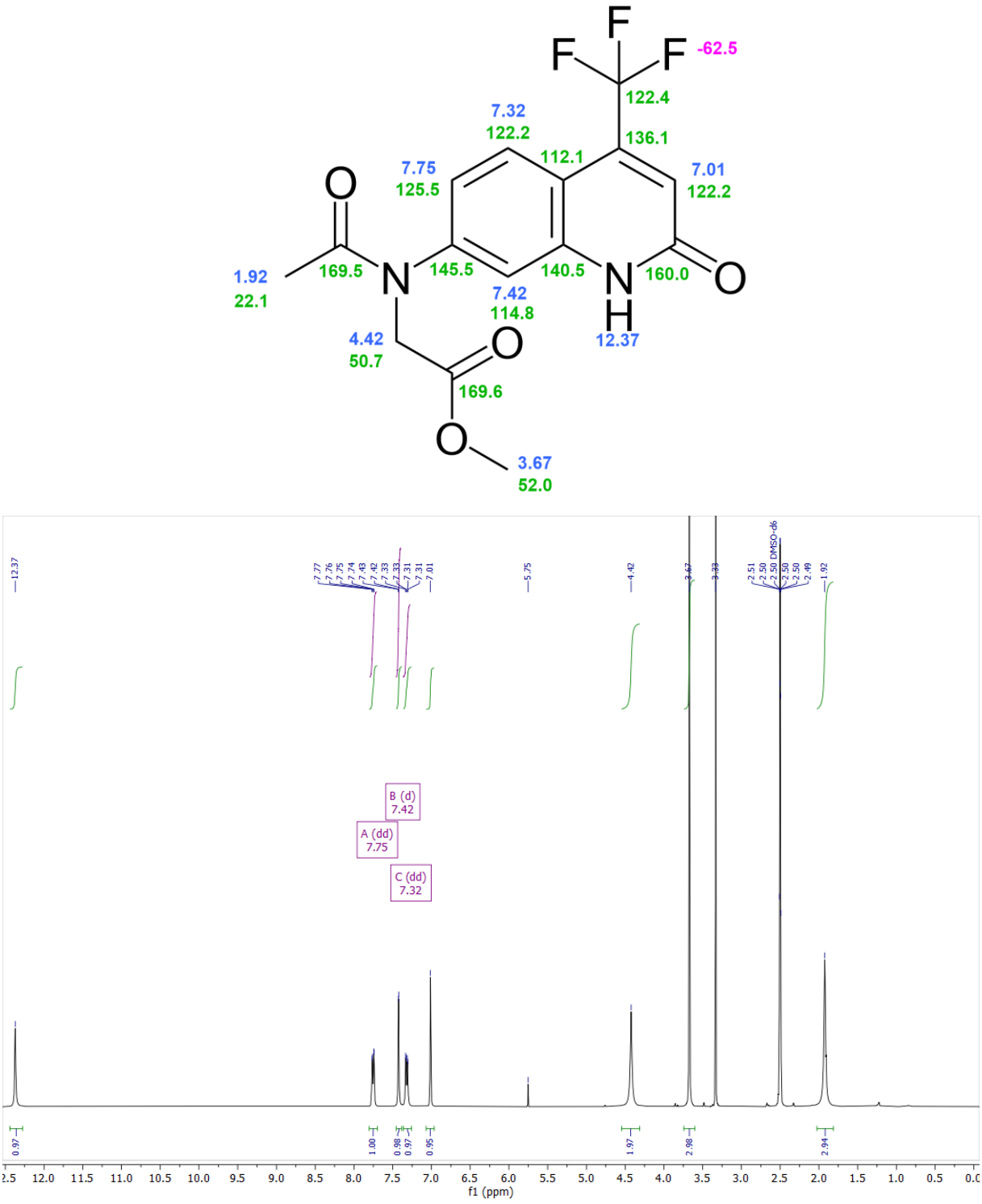

Figure S85. ^{1}H NMR spectrum of **5c** (400 MHz, DMSO-d_6).

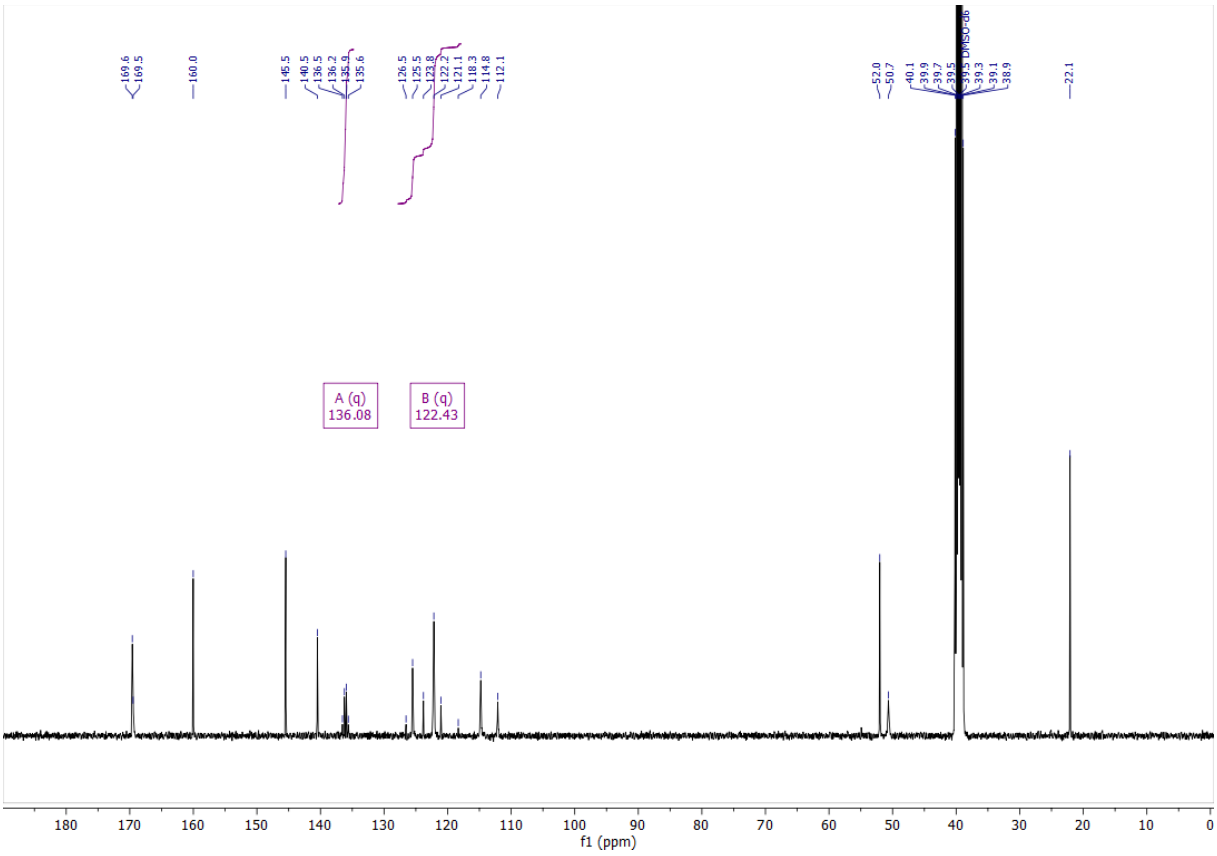

Figure S86. ^{13}C NMR spectrum of **5c** (101 MHz, DMSO-d_6).

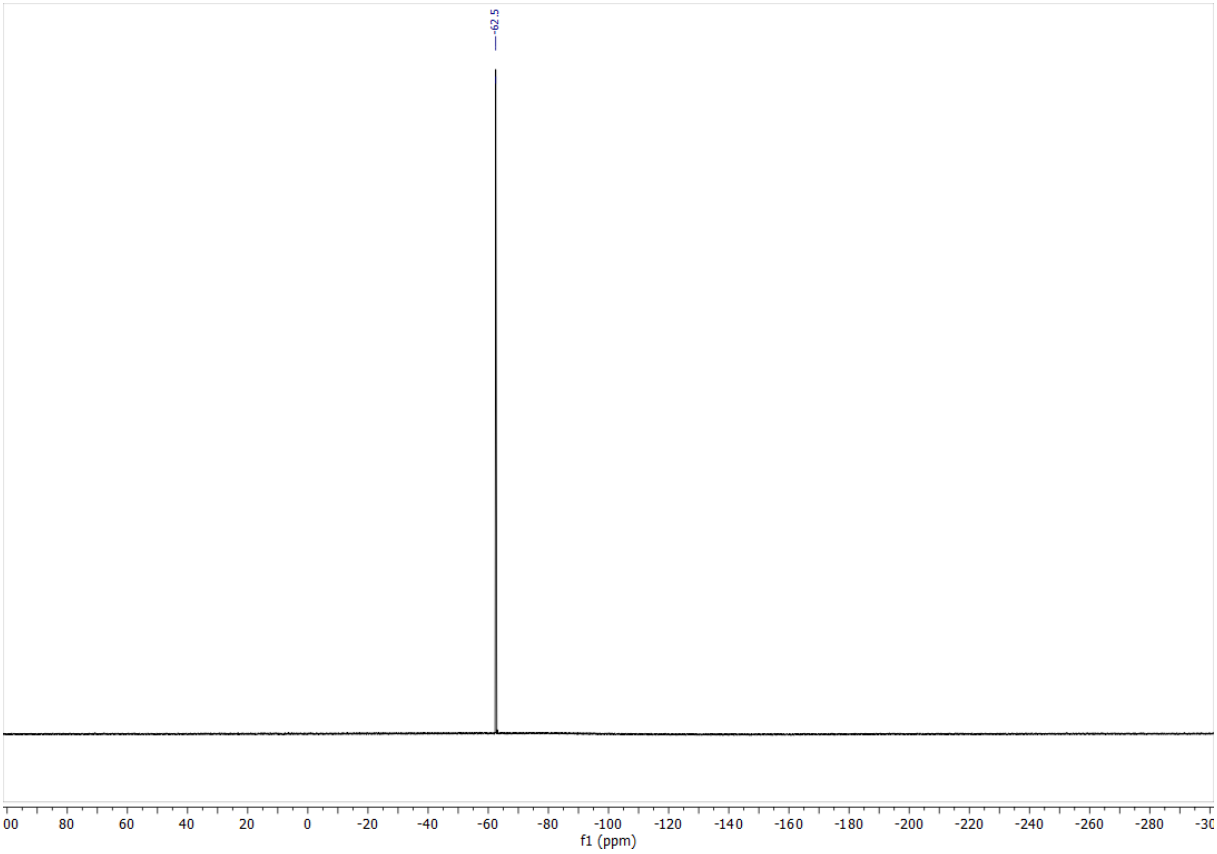

Figure S87. ^{19}F NMR spectrum of 5**c** (376 MHz, DMSO-d_6).

2a

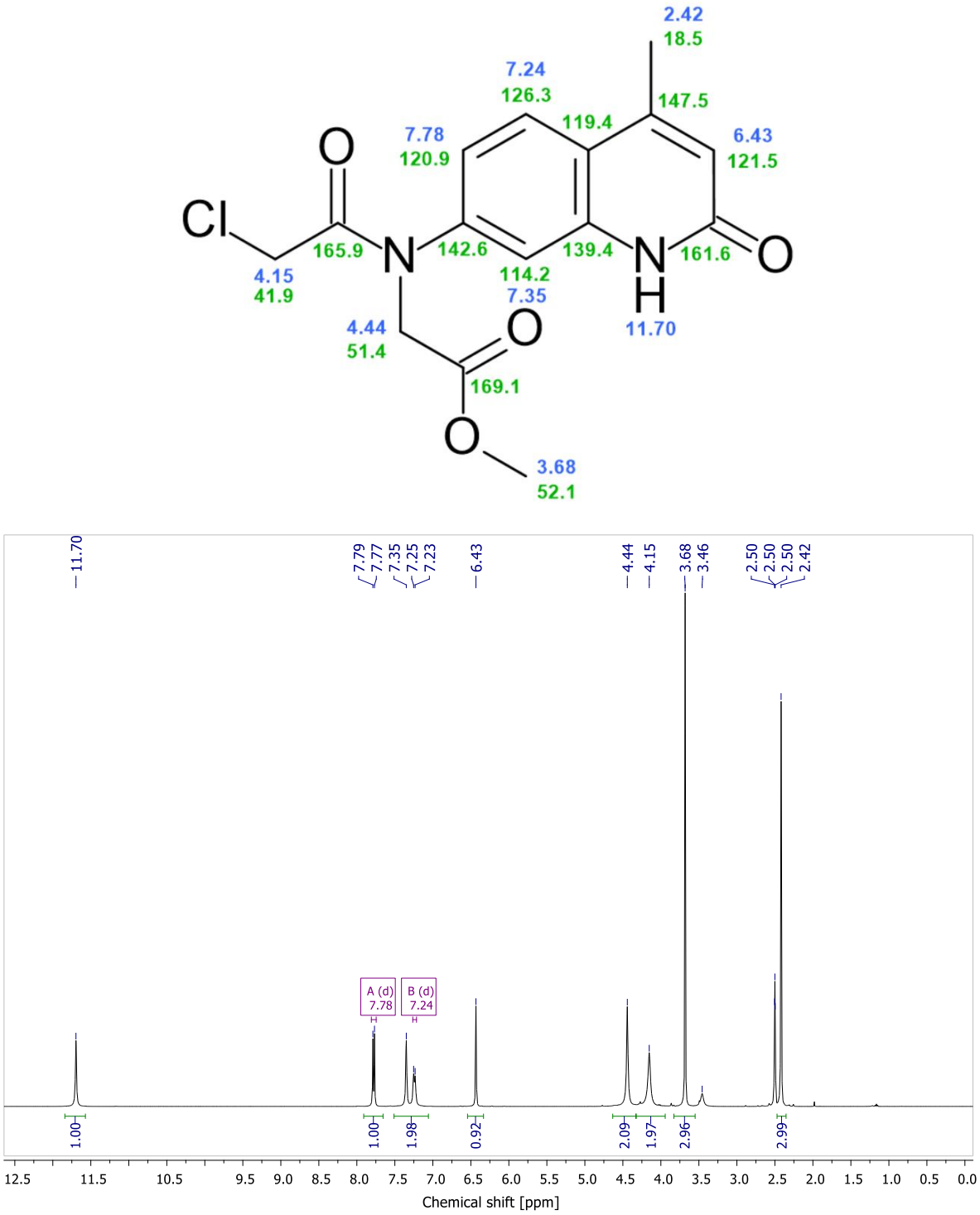

Figure S88. ^{1}H NMR spectrum of **2a** (400 MHz, DMSO-d_6).

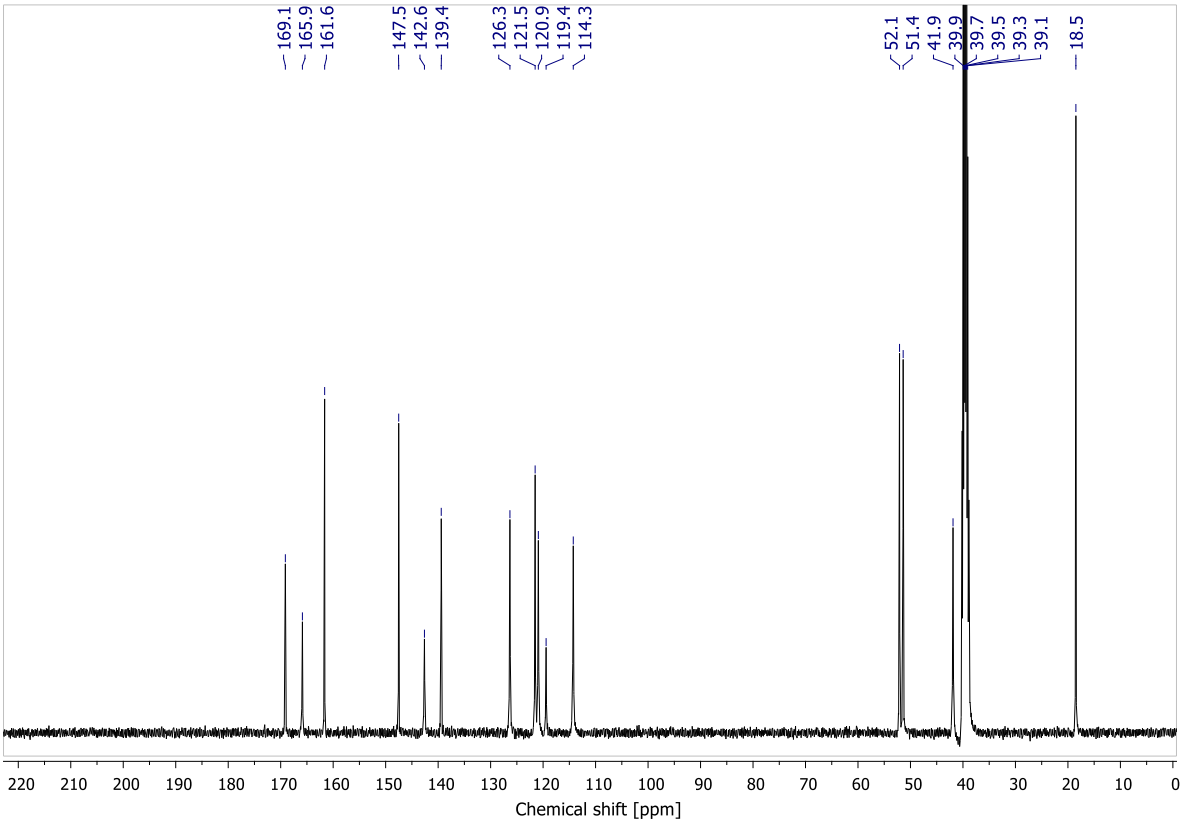

Figure S89. ^{13}C NMR spectrum of **2a** (101 MHz, DMSO-d_6).

2b

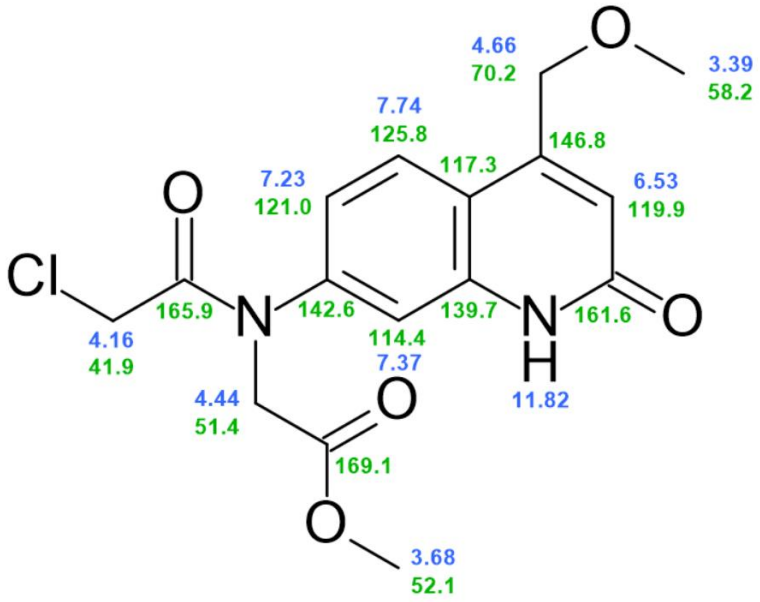

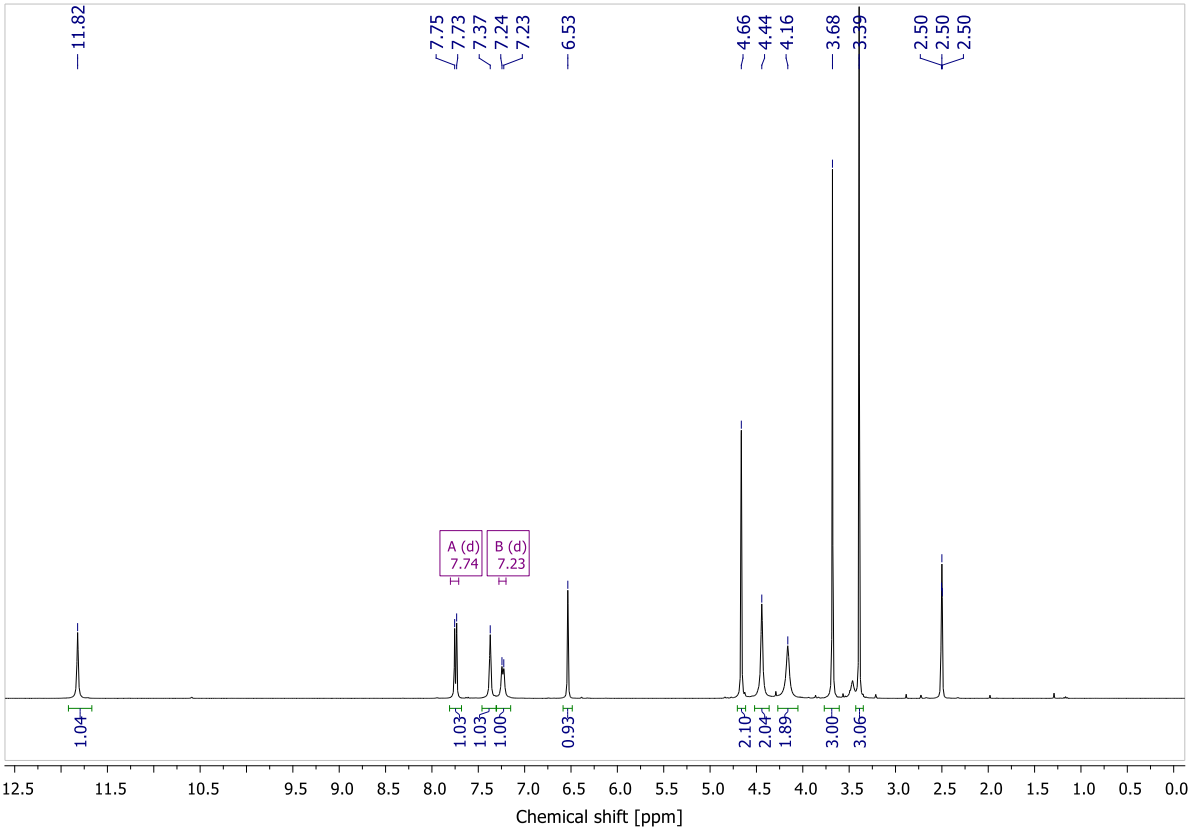

Figure S90. ^{1}H NMR spectrum of **2b** (400 MHz, DMSO-d_6).

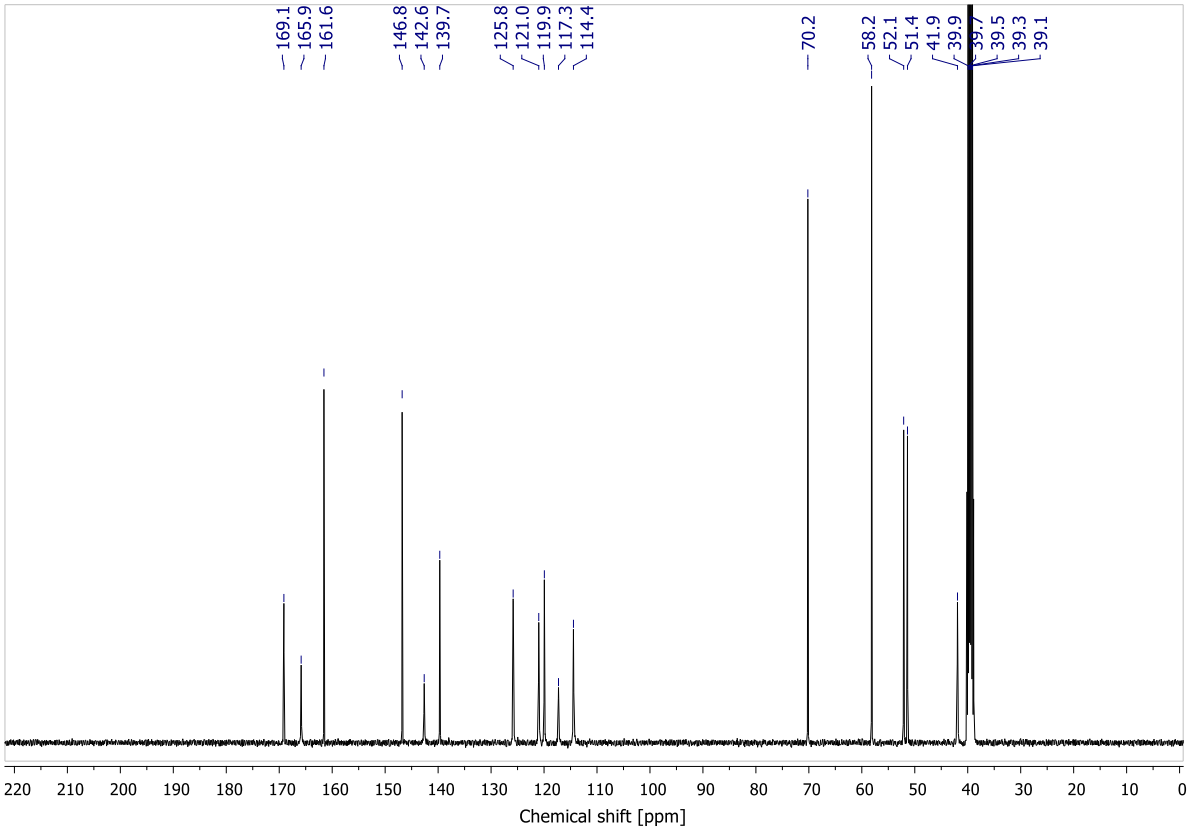

Figure S91. ^{13}C NMR spectrum of **2b** (101 MHz, DMSO-d_6).

2c

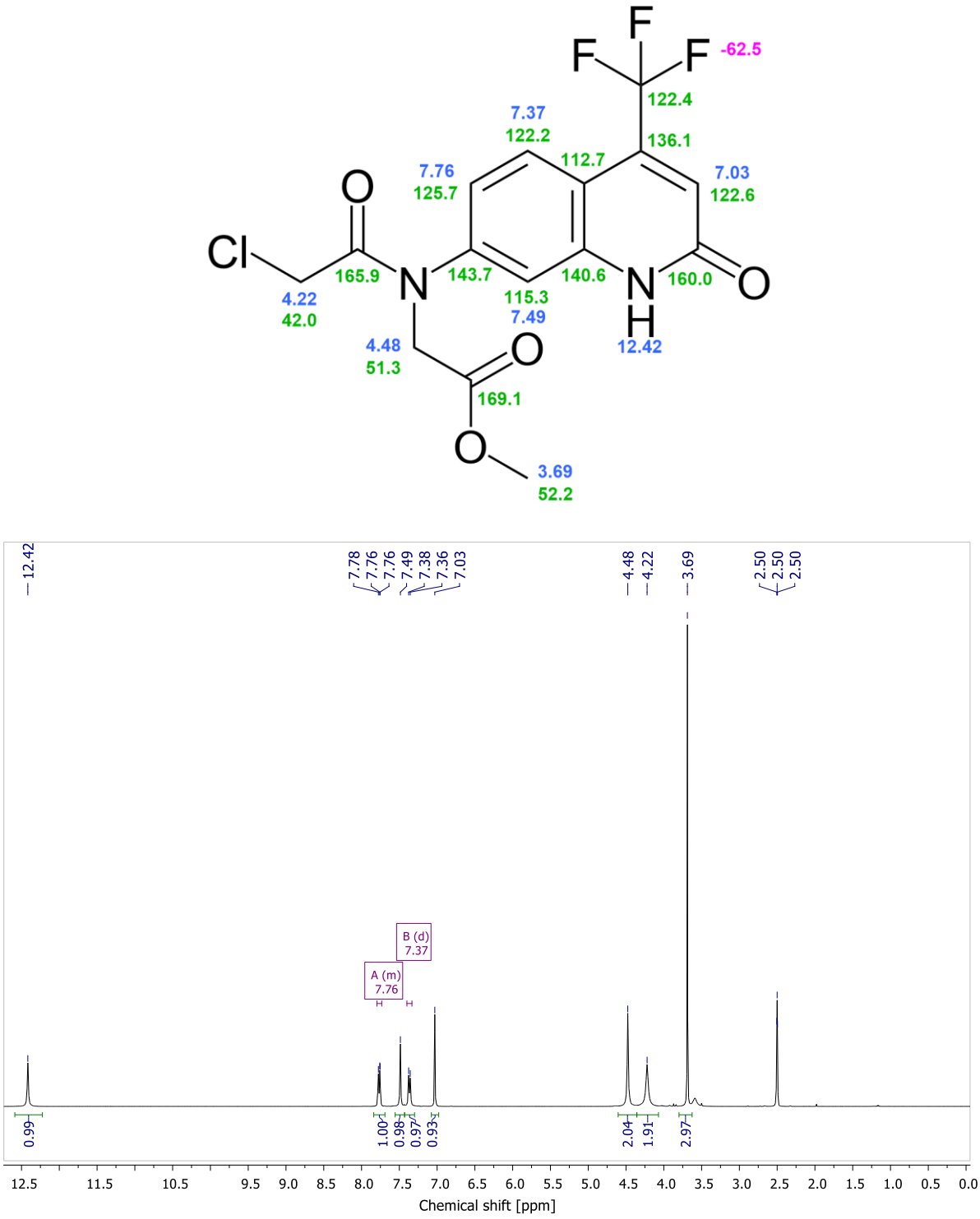

Figure S92. ^{1}H NMR spectrum of **2c** (400 MHz, DMSO-d_6).

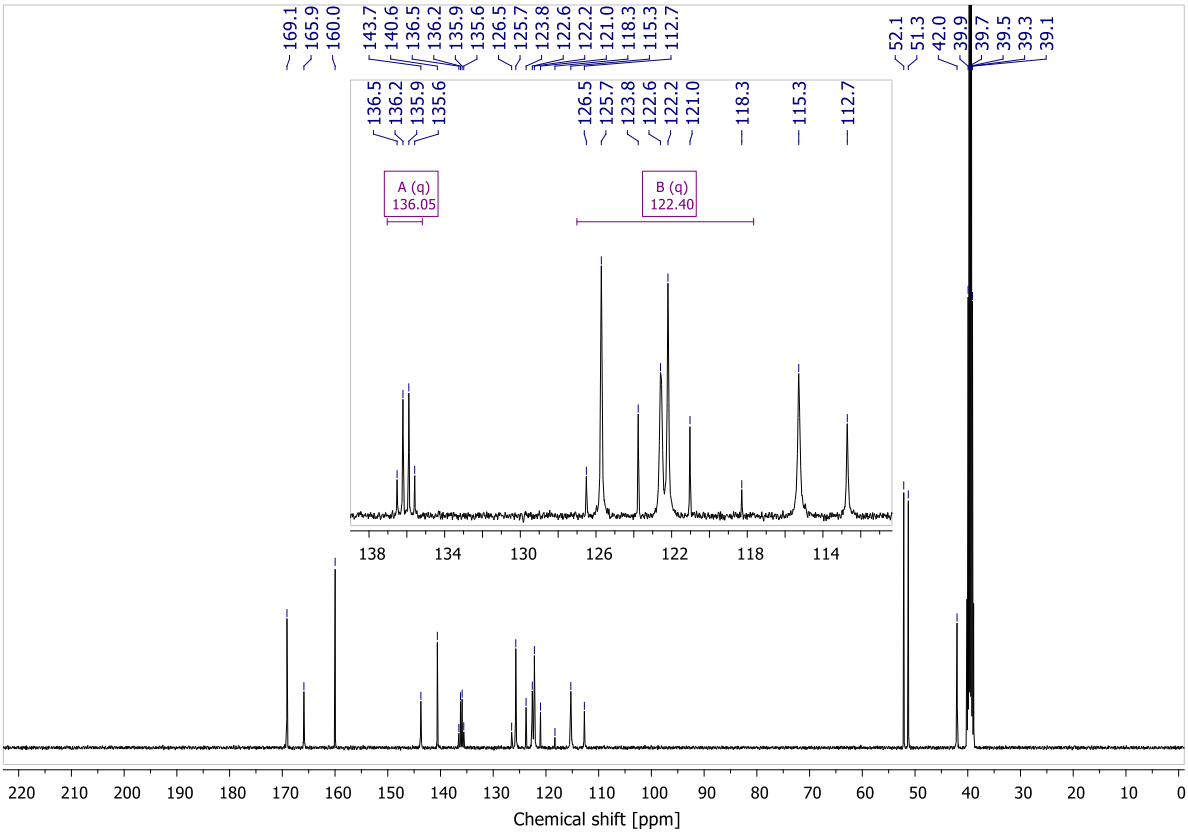

Figure S93. ^{13}C NMR spectrum of **2c** (101 MHz, DMSO-d_6).

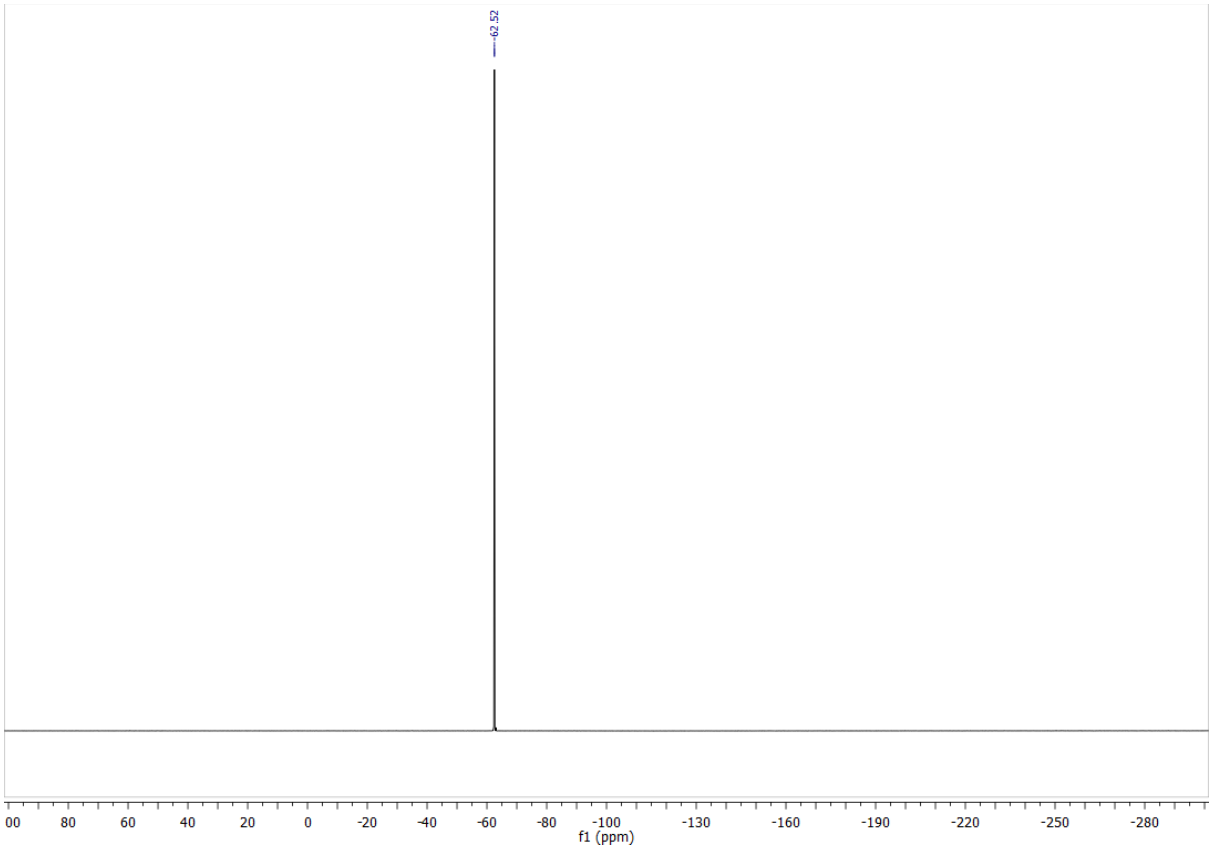

Figure S94. ^{19}F NMR spectrum of **2c** (376 MHz, DMSO-d_6).

4a

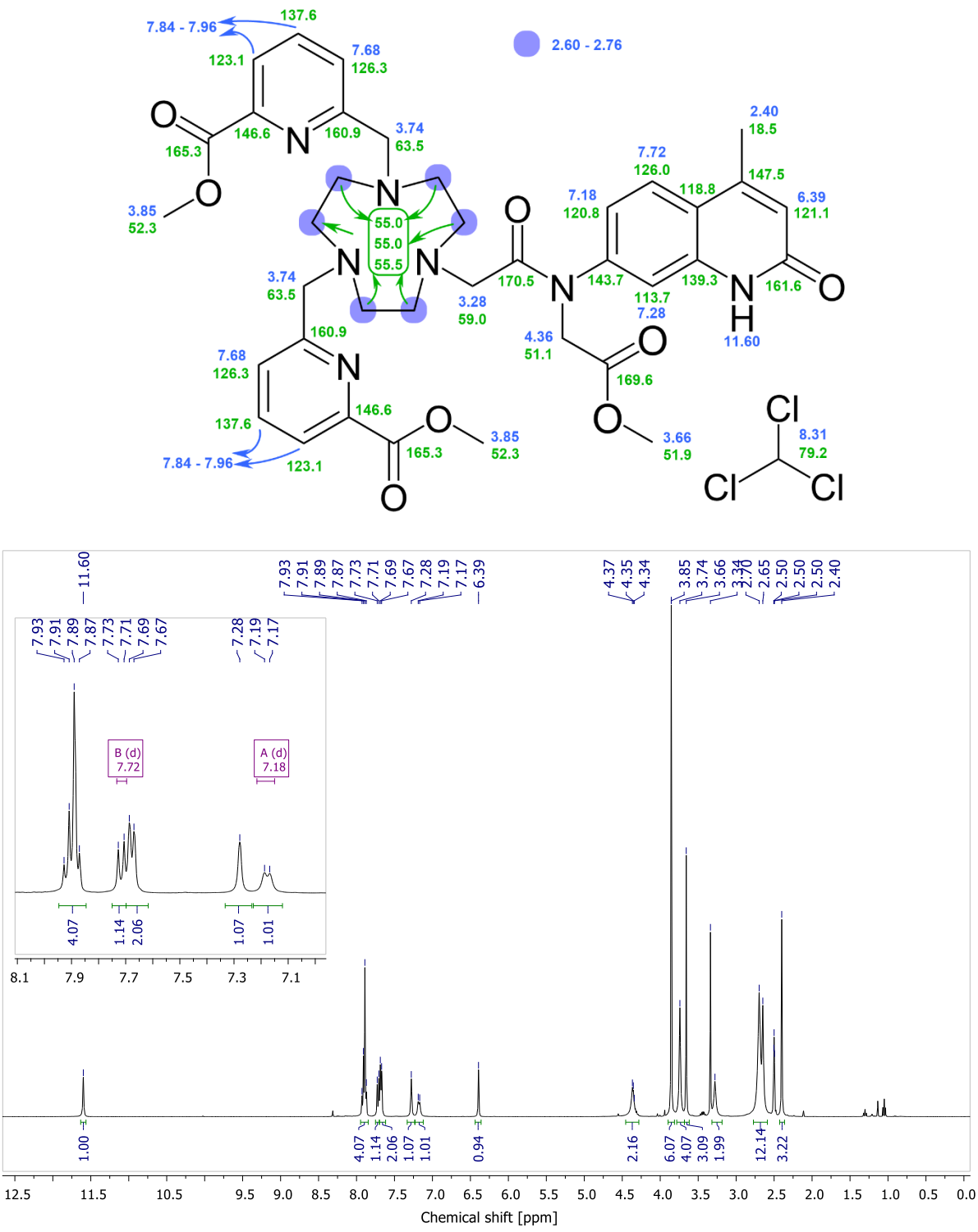

Figure S95. ^{1}H NMR spectrum of **4a** (400 MHz, DMSO-d_6).

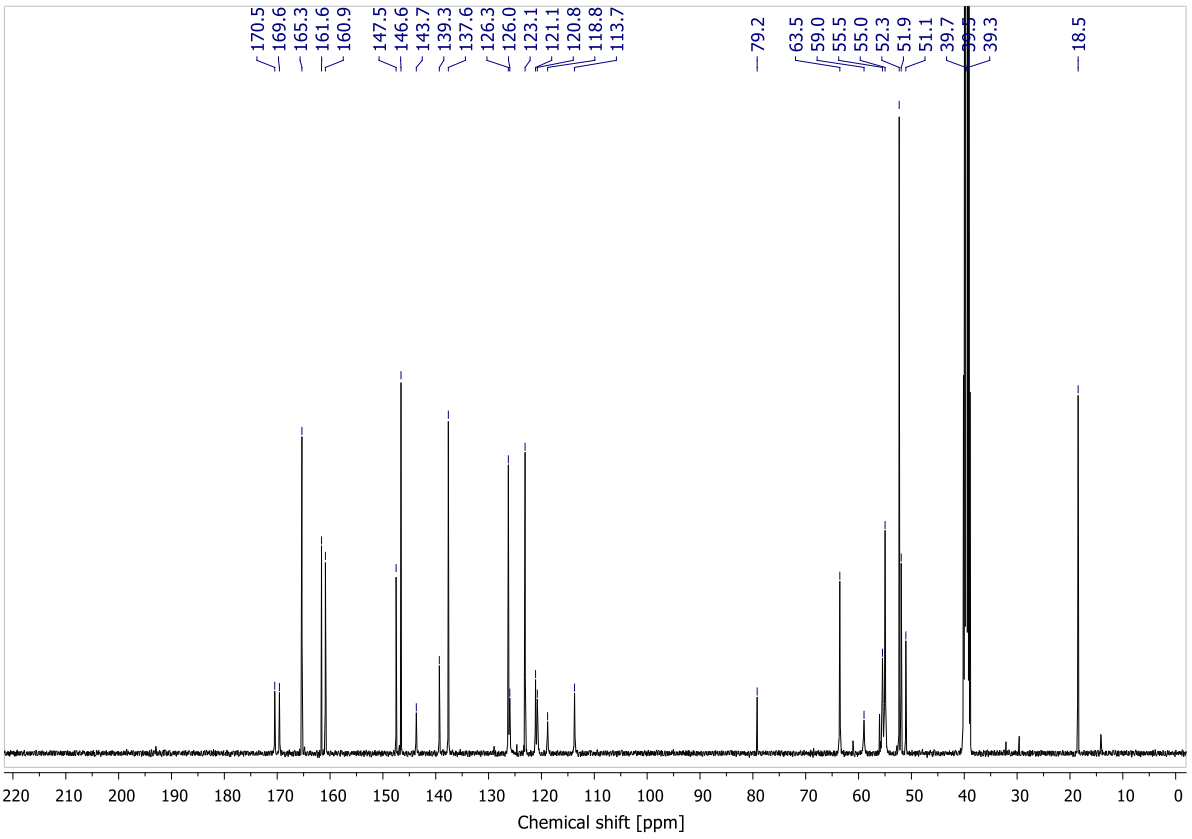

Figure S96. ^{13}C NMR spectrum of **4a** (101 MHz, DMSO-d_6).

4b

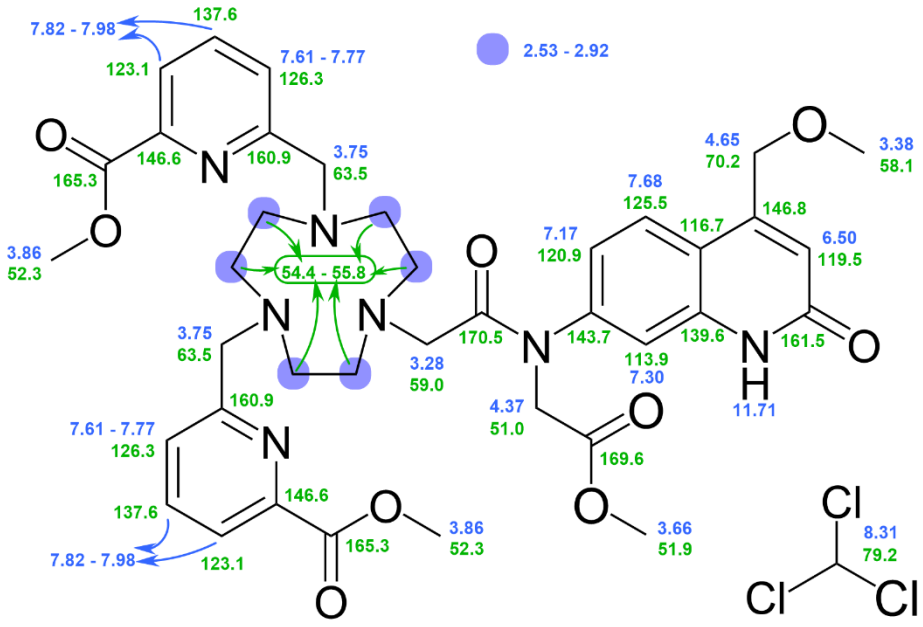

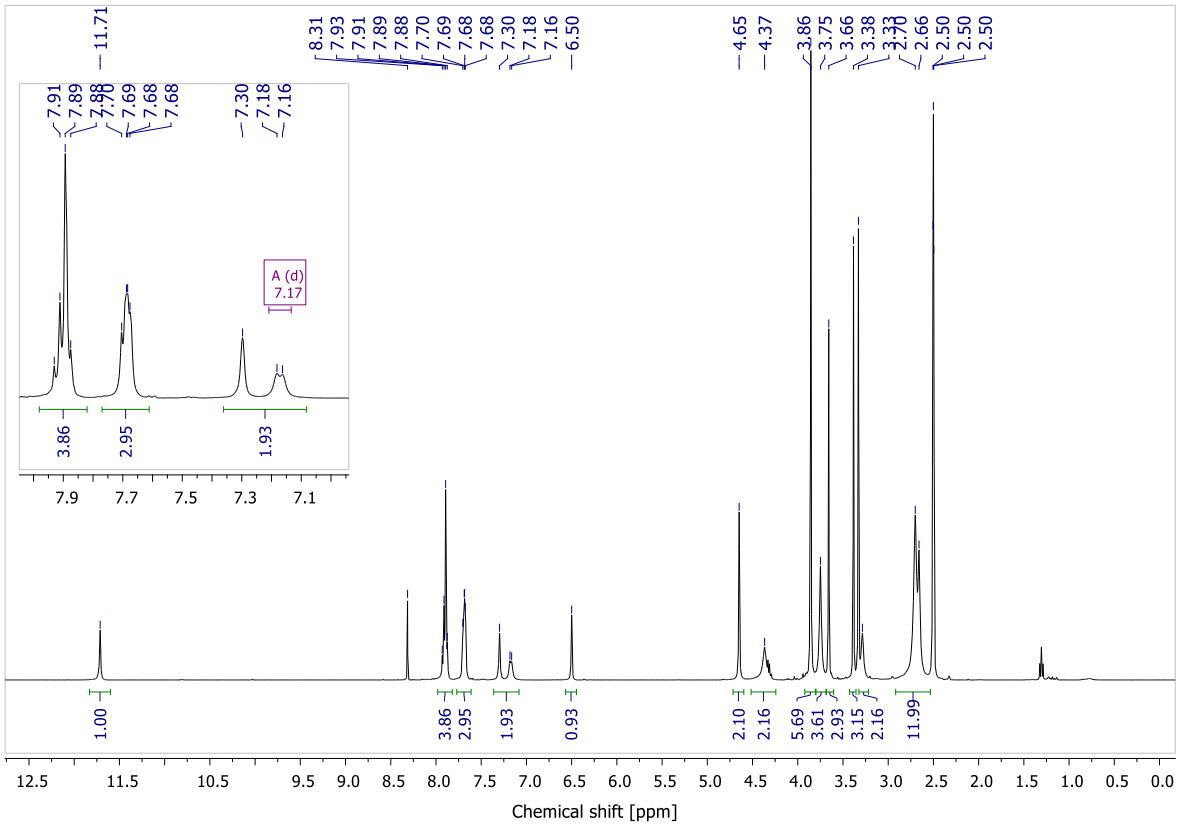

Figure S97. ^{1}H NMR spectrum of **4b** (400 MHz, DMSO-d_6).

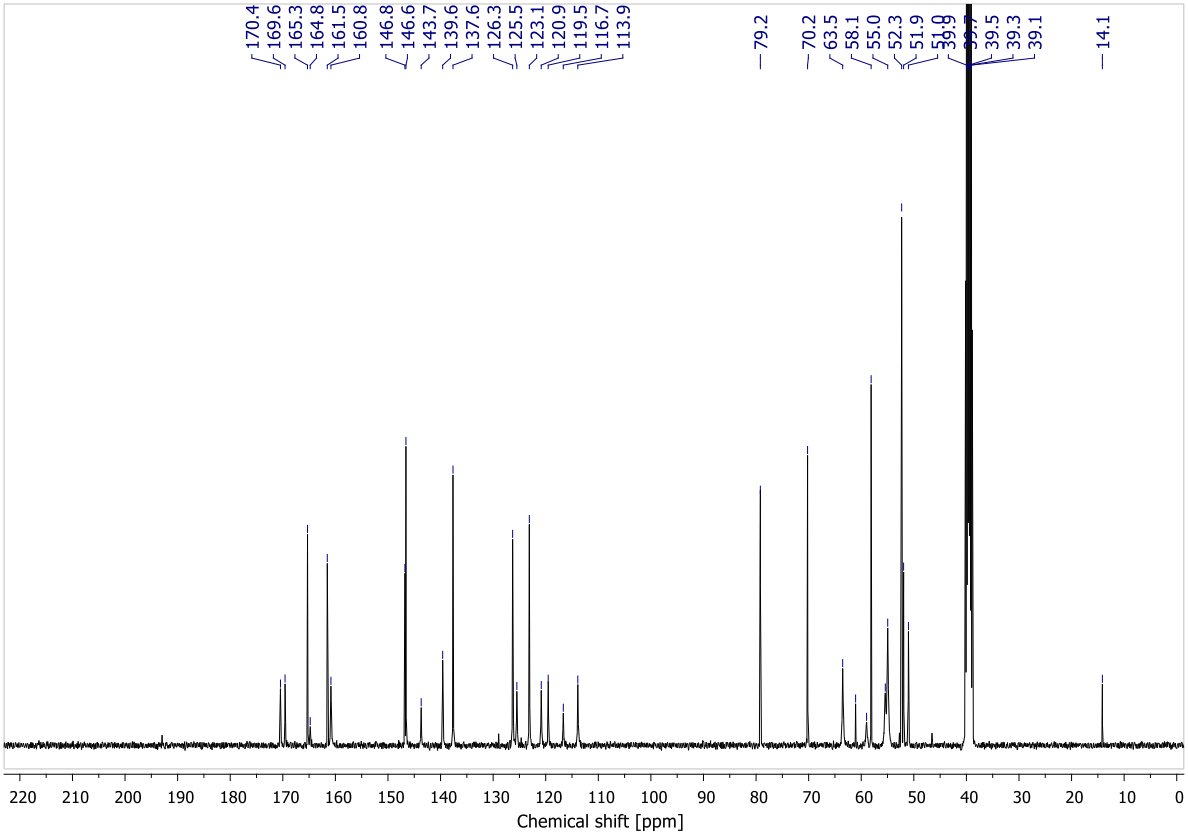

Figure S98. ^{13}C NMR spectrum of **4b** (101 MHz, DMSO-d_6).

4c

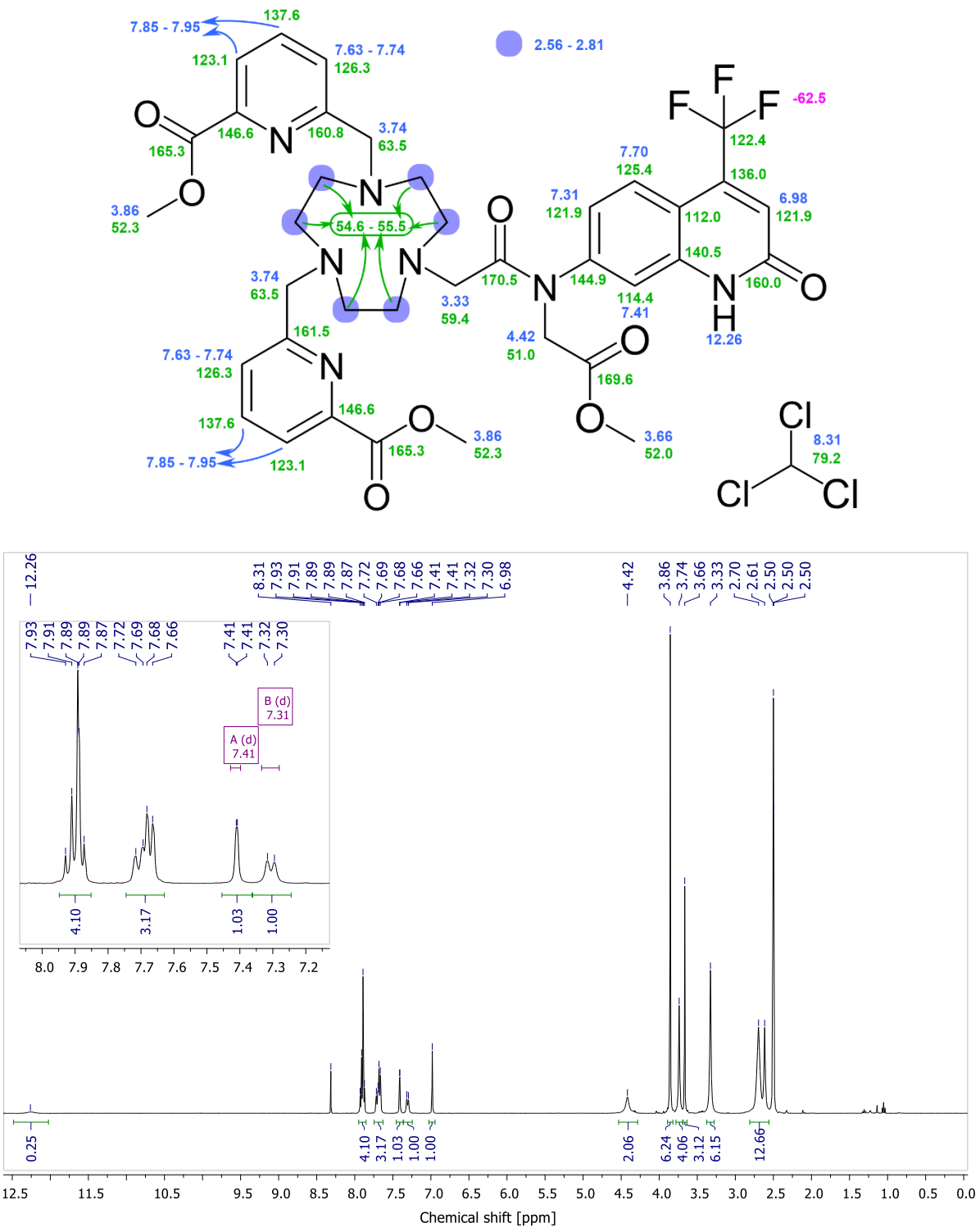

Figure S99. ^{1}H NMR spectrum of **4c** (400 MHz, DMSO-d_6).

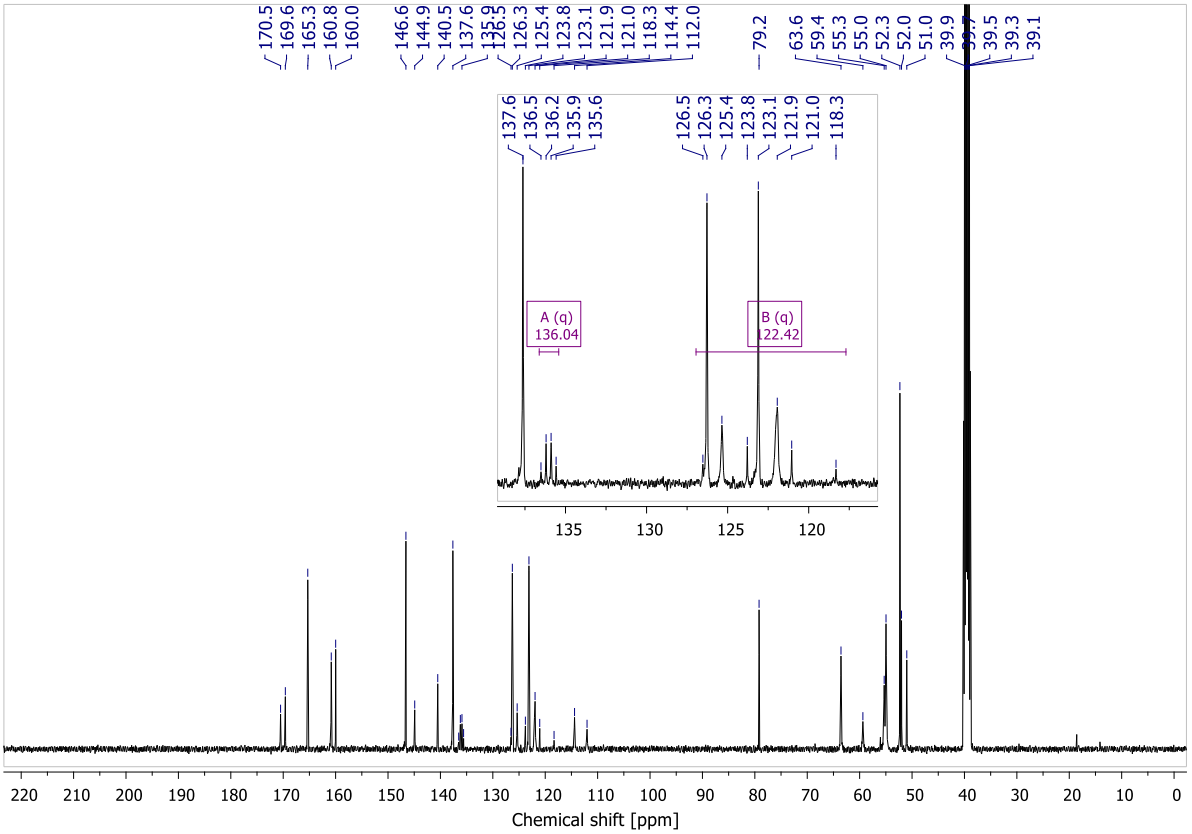

Figure S100. ^{13}C NMR spectrum of **4c** (101 MHz, DMSO-d_6).

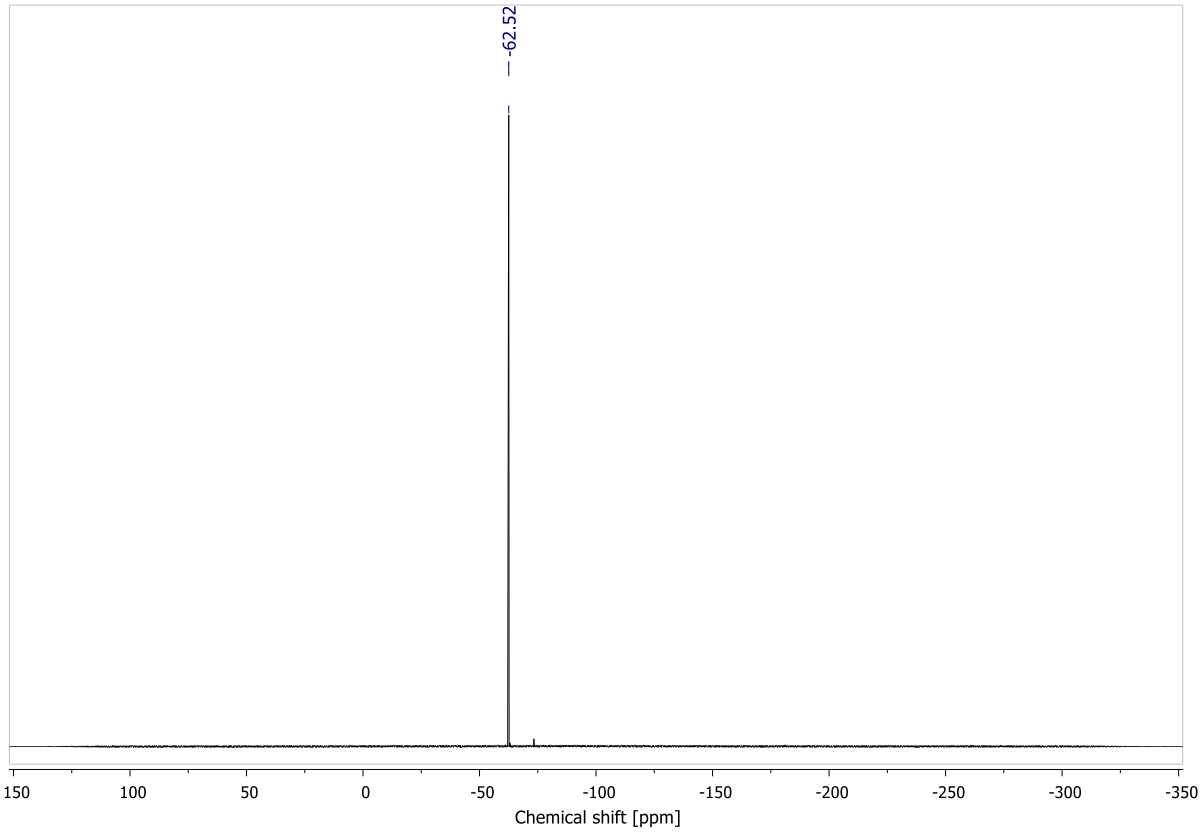

Figure S101. ^{19}F NMR spectrum of **4c** (376 MHz, DMSO-d_6).

Lt^{t,Me}

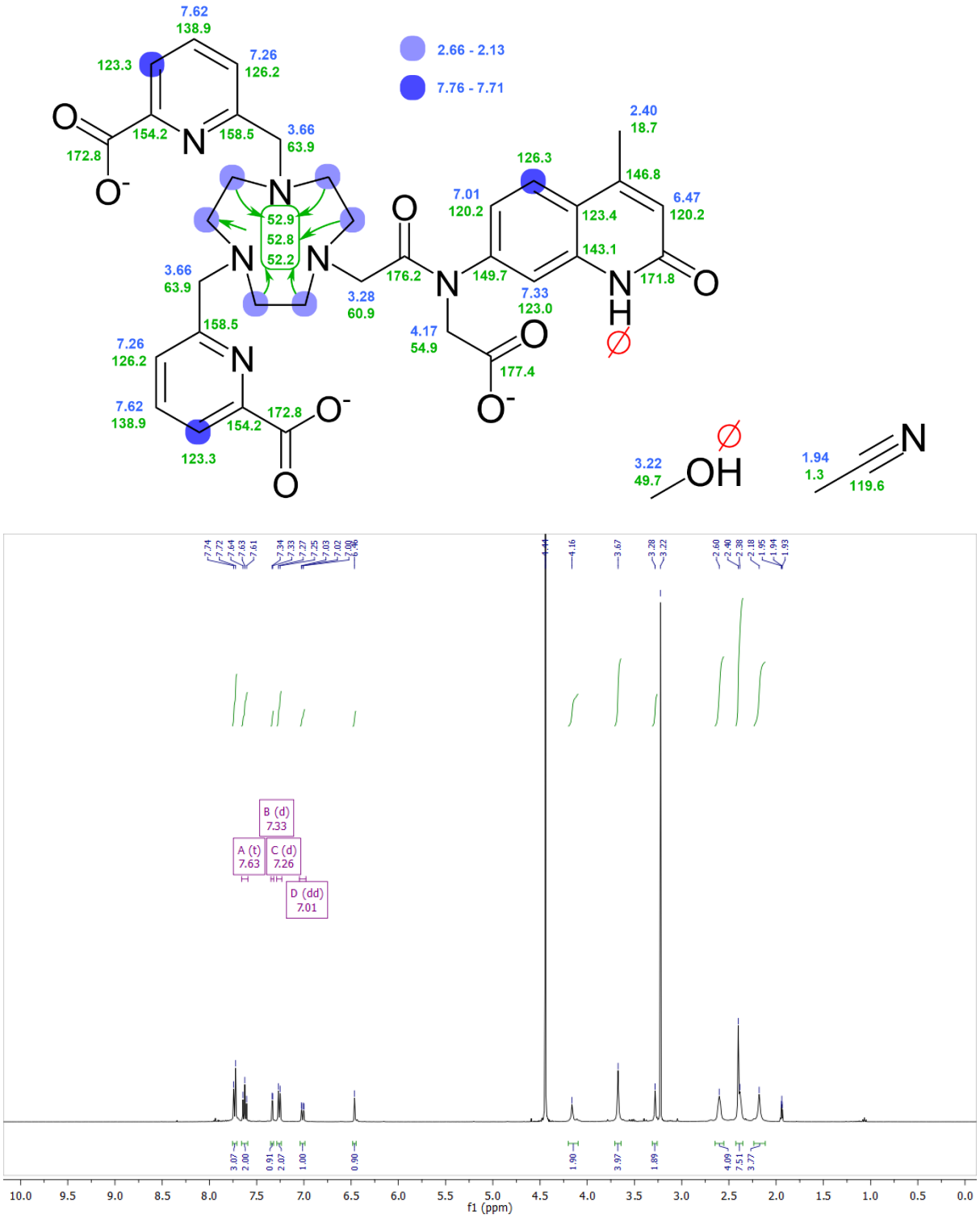

Figure S102. ^{1}H NMR spectrum of **Lt^{t,Me}** (400 MHz, CD_3CN:D2O (1:1)).

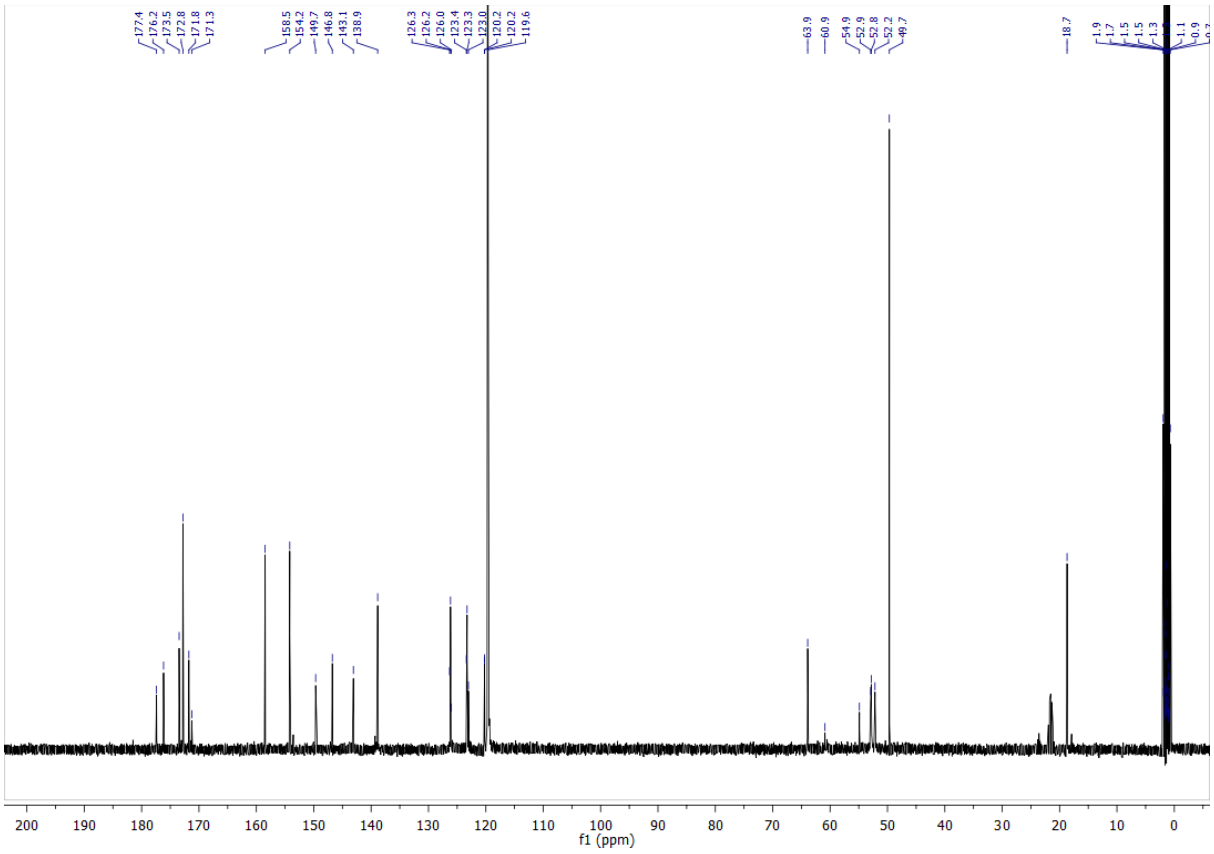

Figure S103. ^{13}C NMR spectrum of **Lt^{t,Me}** (101 MHz, CD_3CN:D2O (1:1)).

Lt^{t,MOM}

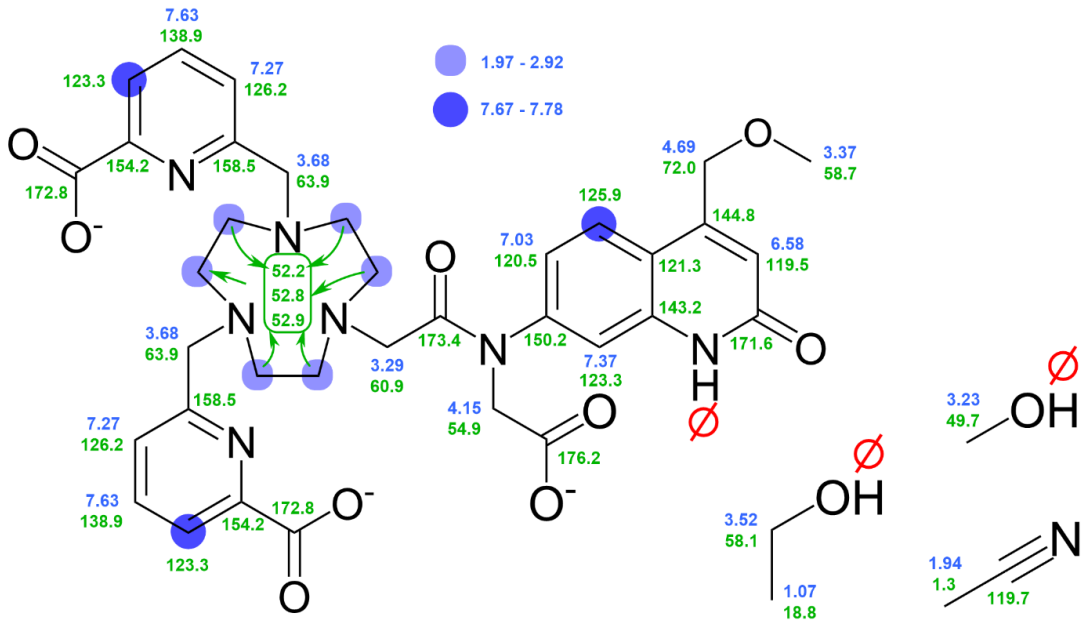

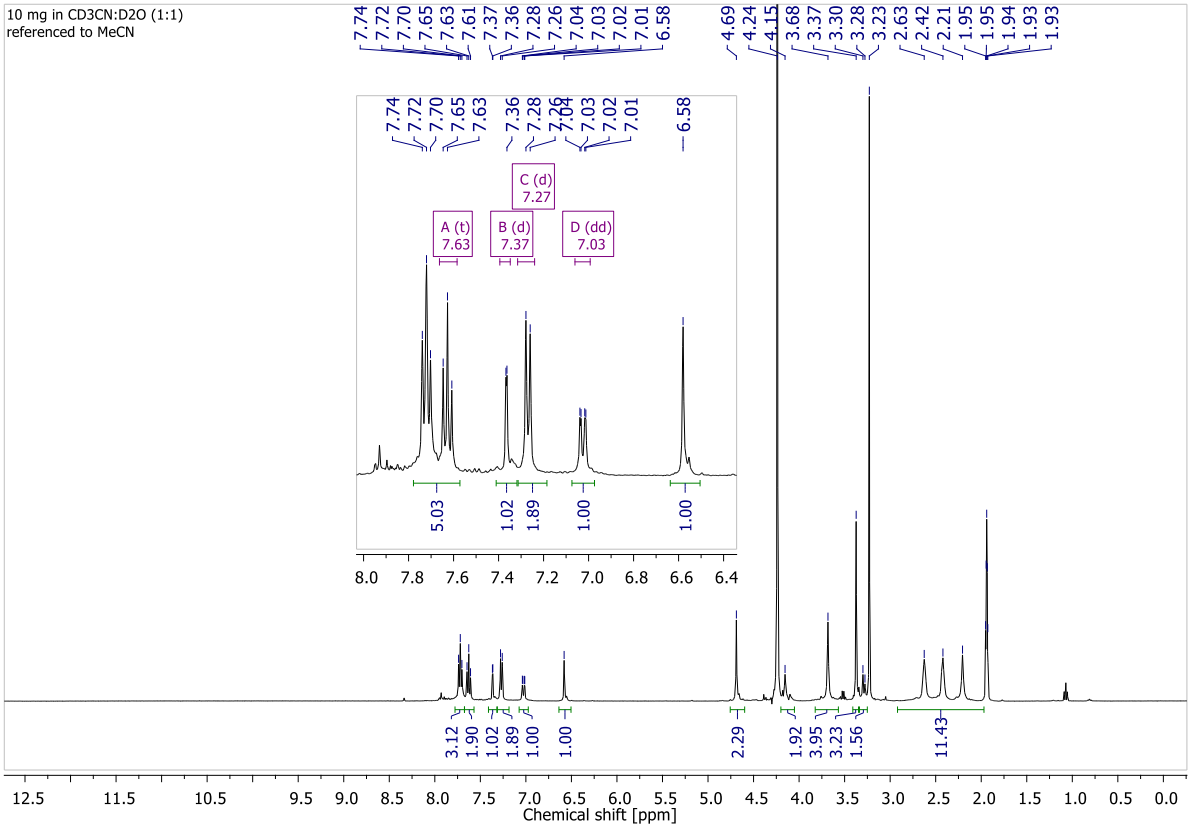

Figure S104. ^{1}H NMR spectrum of **Lt^{t,MOM}** (400 MHz, CD_3CN:D2O (1:1)).

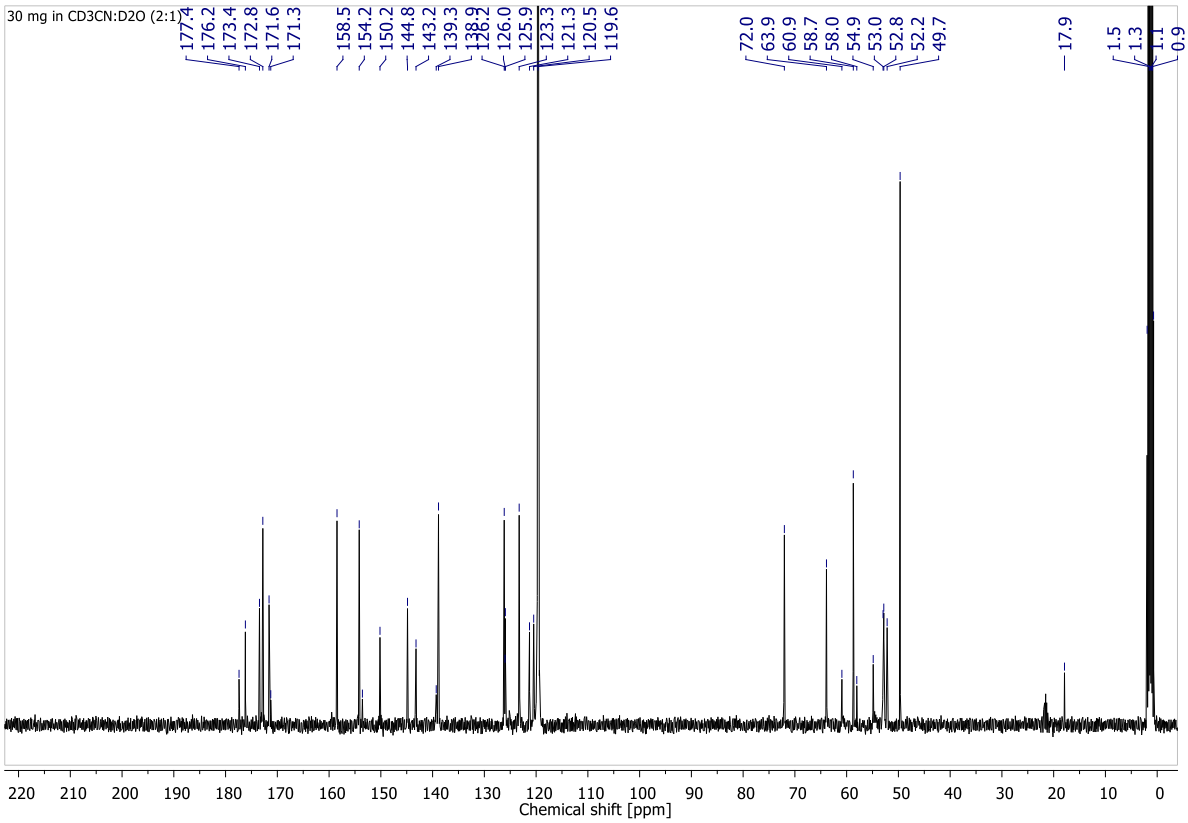

Figure S105. ^{13}C NMR spectrum of **Lt^{t,MOM}** (101 MHz, CD_3CN:D2O (1:1)).

Lt^{t,CF3}

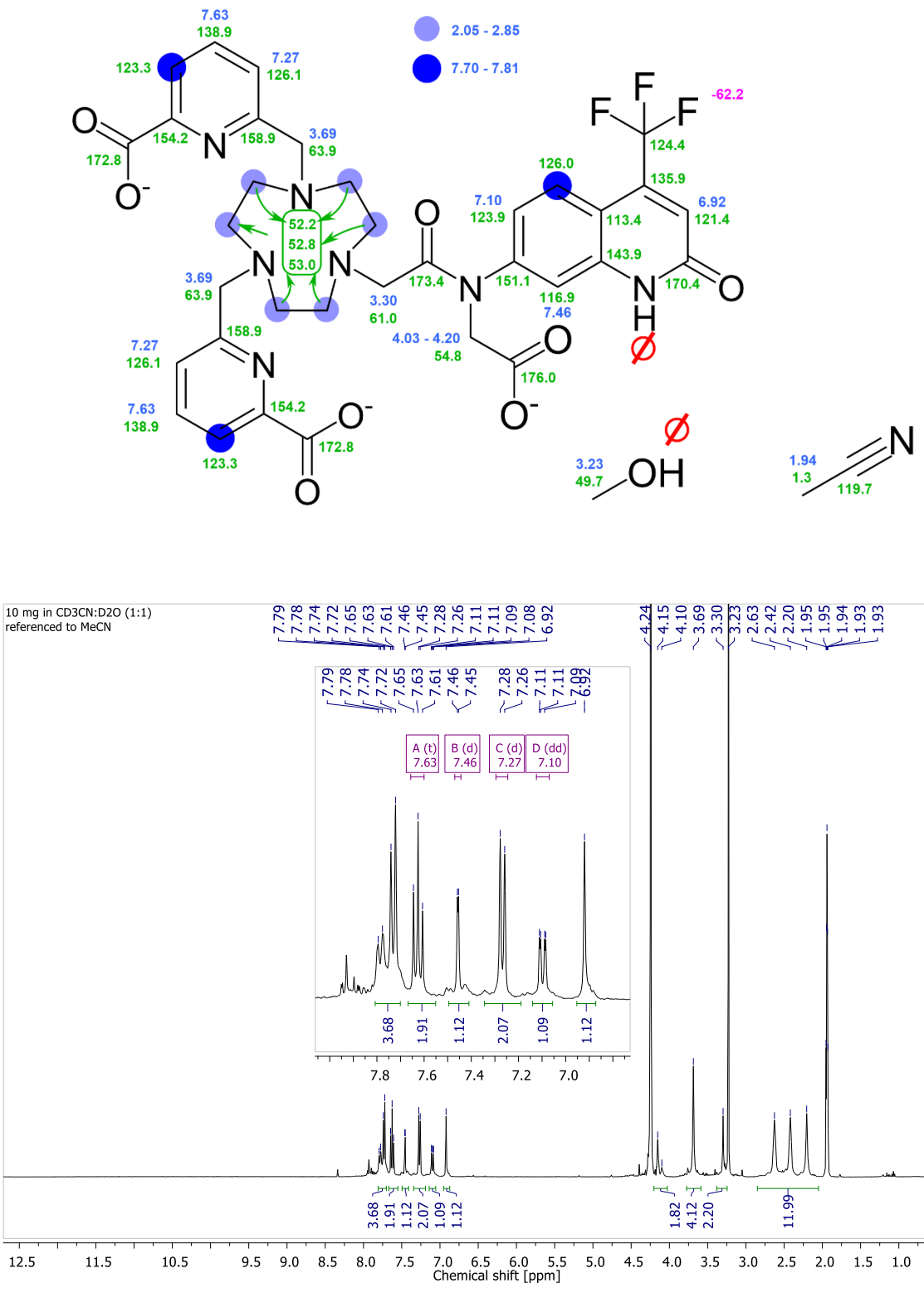

Figure S106. ^{1}H NMR spectrum of **Lt^{t,CF3}** (400 MHz, CD_3CN:D2O (1:1)).

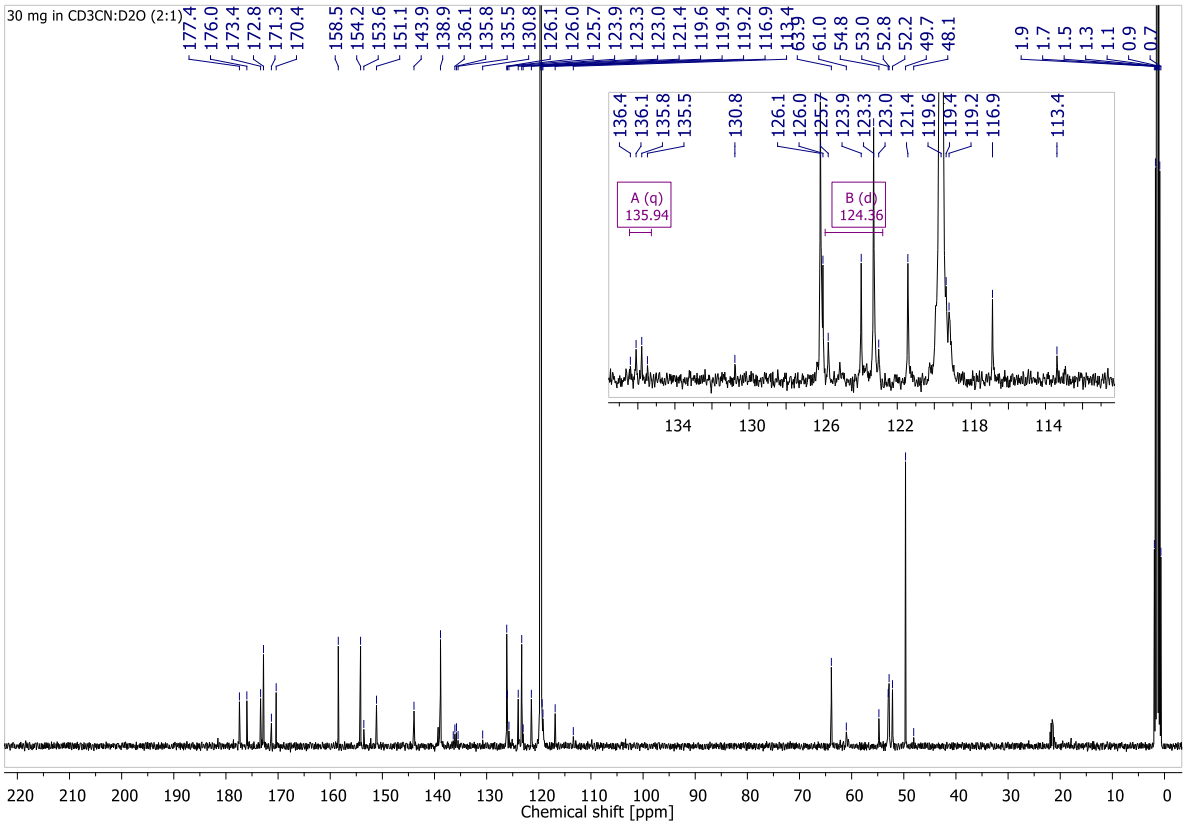

Figure S107. ^{13}C NMR spectrum of **Lt^{t,CF3}** (101 MHz, CD_3CN:D2O (1:1)).

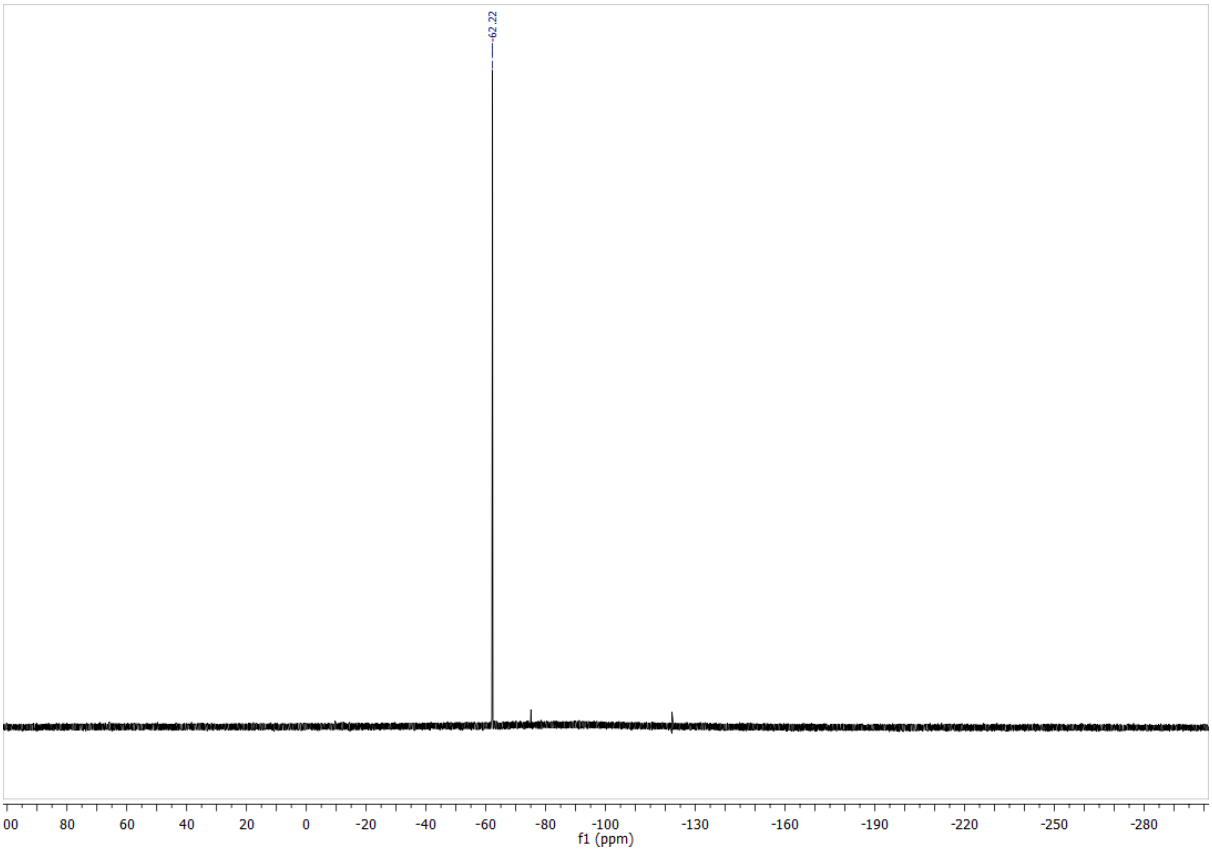

Figure S108. ^{19}F NMR spectrum of **Lt^{t,CF3}** (376 MHz, CD_3CN:D2O (1:1)).

References

1. Kovacs, D.; Lu, X.; Mészáros, L. S.; Ott, M.; Andres, J.; Borbas, K. E., Photophysics of coumarin and carbostyril-sensitized luminescent lanthanide complexes: Implications for complex design in multiplex detection. *J. Am. Chem. Soc.* **2017,** *139*(16), 5756−5767.
2. Kovacs, D.; Kocsi, D.; Wells, J. A. L.; Kiraev, S. R.; Borbas, K. E., Electron transfer pathways in photoexcited lanthanide(III) complexes of picolinate ligands. *Dalton Trans.* **2021,** *50*(12), 4244−4254.
3. Suzuki, K.; Kobayashi, A.; Kaneko, S.; Takehira, K.; Yoshihara, T.; Ishida, H.; Shiina, Y.; Oishi, S.; Tobita, S., Reevaluation of absolute luminescence quantum yields of standard solutions using a spectrometer with an integrating sphere and a back-thinned CCD detector. *Phys. Chem. Chem. Phys.* **2009,** *11*(42), 9850−9860.
4. Harvey, A. H.; Gallagher, J. S.; Sengers, J. M. H. L., Revised formulation for the refractive index of water and steam as a function of wavelength, temperature and density. *J. Phys. Chem. Ref. Data* **1998,** *27*(4), 761−774.
5. Supkowski, R. M.; Horrocks, W. D., Jr., On the determination of the number of water molecules, *q*, coordinated to europium(III) ions in solution from luminescence decay lifetimes. *Inorg. Chim. Acta* **2002,** *340*, 44−48.
6. Beeby, A.; Clarkson, I. M.; Dickins, R. S.; Faulkner, S.; Parker, D.; Royle, L.; de, S. A. S.; Williams, J. A. G.; Woods, M., Non-radiative deactivation of the excited states of europium, terbium and ytterbium complexes by proximate energy-matched OH, NH and CH oscillators: an improved luminescence method for establishing solution hydration states. *J. Chem. Soc., Perkin Trans. 2* **1999**, 493−504.
7. Kovacs, D.; Kiraev, S. R.; Phipps, D.; Orthaber, A.; Borbas, K. E., Eu(III) and Tb(III) complexes of octa- and nonadentate macrocyclic ligands carrying azide, alkyne, and ester reactive groups. *Inorg Chem* **2020,** *59*(1), 106−117.